THE UNIVERSITY OF MICHIGAN

COLLEGE OF ENGINEERING
Department of Mechanical Engineering

Progress Report No. 5

THE EFFECT OF DIRECTED MIXTURE MOTION ON THE FLAME KERNEL DEVELOPMENT IN A CONSTANT VOLUME BOMB

David E. Cole

ORA Project 05057

under contract with:

ENGINEERING STAFF, G. M. TECHNICAL CENTER
GENERAL MOTORS CORPORATION
WARREN, MICHIGAN

administered through:

OFFICE OF RESEARCH ADMINISTRATION ANN ARBOR

May 1966

This report was also a dissertation submitted in partial fulfillment of the requirements for the degree of Doctor of Philosophy in The University of Michigan, 1966.

TABLE OF CONTENTS

TABLE OF CONTENTS (Continued)

TABLE OF CONTENTS (Concluded)

LIST OF TABLES

LIST OF FIGURES

LIST OF FIGURES (Continued)

LIST OF FIGURES (Continued)

LIST OF FIGURES (Concluded)

NOMENCLATURE

English

A_f = Flame front area

A_N = Nozzle exit area

C = Capacitance

C_P = Constant pressure specific heat

C_V = Constant volume specific heat

d = Jet nozzle width—narrow dimension

dP/dt = Rate of pressure rise

E = Voltage drop

i_{HW} = Hot wire current

K_C = Ratio of specific heat

L = length

M = Mean

$\dot{m}$ = Mass rate of combustion = $\rho_m A_f V_f$

$\dot{m}_A$ = Mass flow rate of air

N = Number of occurrences

P = Pressure

P_f = Partial pressure of fuel

P_t = Total pressure of mixture

Q = transistor

r = Radius of flame kernel

R = Gas constant

R_x = Resistance

R_{HW} = Resistance of hot wire

S = Switch

T = Temperature of mixture

t = Time

t_p = Time of schlieren photograph after ignition

V = Velocity

V_F = Velocity of the flame relative to mixture

V_J = Peak profile velocity for a given mixture jet nozzle at a given mixture flow rate

V_S = Apparent flame velocity--spatial velocity

$V_{B_3B_4}$ = Voltage drop across hot-wire bridge circuit

W_M = Velocity profile width measure at median velocity

X = Variable

x = Coordinate of long dimension in jet nozzle exit plane

y = Coordinate of short dimension in jet nozzle exit plane

z = Distance from jet nozzle exit to the spark gap

Greek Symbols

Δ = Difference

η = Ratio of actual air to stoichiometric air

μ_m = Viscosity of the mixture

π_A = Percent increase in flame front area

$$\frac{(A_f)_{V_J} - (A_f)_{V_J=0}}{(A_f)_{V_J=0}} \times 100$$

π_M = Percent increase in mass rate of combustion

$$\frac{(\dot{m})_{V_J} - (\dot{m})_{V_J=0}}{(\dot{m})_{V_J=0}} \times 100$$

π_P = Percent increase in rate of pressure rise

$$\frac{(dP/dt)_{V_J} - (dP/dt)_{V_J=0}}{(dP/dt)_{V_J=0}} \times 100$$

ρ_m = Density of the mixture

ρ_{air} = Density of air

σ = Standard deviation

Σ = Summation

ϕ = Equivalence ratio

Ω = Ohms

Abbreviations

a-c = Alternating current

ASA = Film speed designation

°C = Degrees centigrade

cm = Centimeter

cps = Cycles per second

d-c = Direct current

°F = Degrees Fahrenheit

F/A = Fuel-air ratio

ft = Feet

ft/sec, fps = Feet per second

H.W. = Hot wire

HY = Henry

in. = Inch

°K = Degrees Kelvin

KV = Kilo volt

lb. = Pound

MA = Milliamperes

mm = Millimeters

MFD. = Microfarad

m sec. = Millisecond

Pot = Potentiometer

psi = Pounds per square inch

°R = Degrees Rankin

V = Volt

W = Watt

Wd. = Width

" = Inch

= Number

μf = Micro farad

ABSTRACT

This investigation was undertaken to provide a partial explanation for the influence of random mixture motion on cycle-to-cycle pressure rate variation in constant volume engine combustion.

A jet of stoichiometric propane-air mixture was directed on the initial flame kernel in a constant volume bomb, which was charged initially with an identical mixture to atmospheric pressure and ambient temperature. Three different jet nozzles with exit widths of .026, .066, and .156 inch controlled the scale of mixture motion. The long dimension of the nozzle exit was essentially constant at approximately .9 inch. Jet velocities of 0,1,3,5, and 7 fps were used.

The pressure rate was recorded and schlieren photographs taken of the combustion front early in its development. Flame front area was measured from these photographs. The mass rate of combustion was calculated using this area, a mixture density based on isentropic compression of the unburned mixture and a relative flame velocity obtained from the literature.

The pressure rate for the jet-influenced combustion was compared to the pressure rate for combustion in a quiescent mixture. The flame front area and combustion rate were correlated with the pressure rate.

The primary conclusions were:

1. Pressure rate increased approximately linearly with mixture jet velocity.

2. The width of the mixture jet had an effect on pressure rate. A jet profile width slightly greater than the spark gap caused the greatest pressure rate.

CHAPTER I

INTRODUCTION

A. PURPOSE

The purpose of this thesis project was to determine the effect of mixture motion on the early development of the flame kernel and the resulting rate of pressure rise in a spark-ignited constant volume bomb. This experimental study was prompted by the undesirable and largely unexplained cycle-to-cycle pressure variation which exists in spark-ignited engines. The results of this study clearly show that perturbations of the flame front area caused by mixture motion could be an important contribution to this engine problem.

B. GENERAL

Engineers and scientists have sought to improve the combustion process in the spark-ignited internal combustion engine since its inception in the late nineteenth century. Although many aspects of spark-ignited combustion have been examined in detail, particular emphasis has been placed on the improvement of thermal efficiency through the increase of compression ratio and modification of the combustion chamber shape.

One problem currently of major significance is the cycle-to-cycle variation in pressure and rate of pressure rise observed in all spark-ignition engine cylinders If cyclic variation were eliminated, the engine could be operated at the best economy fuel/air ratio and still produce a smooth, steady power output. It would be possible to minimize engine roughness, decrease octane requirement and increase com-

pression ratio, thus greatly improving the efficiency with which fuel is utilized by the engine.[8]

Of particular interest at the present time are the exhaust emissions from the Otto cycle engine. The necessity to enrich the fuel-air mixture ratio to avoid vehicle surge (engine torque variations caused by cyclic variation in each cylinder and variation in cyclinder-to-cylinder fuel/air distribution) and other problems associated with lean mixture operation increase the hydrocarbon emissions significantly.

The combustion in a reciprocating engine is exceedingly difficult to evaluate and explain due to the many and transient variables involved. This is particularly true of cycle-to-cycle pressure variations. Several experiments have been performed in Otto cycle engines to study this problem.[3,8,9,11] Among the more important factors influencing this variation are:

1. air/fuel ratio variation
2. type of fuel
3. ignition problems
4. turbulent mixture motion

The first three factors have been examined in detail for their influence on cycle-to-cycle variation in cylinder pressure.

There is general agreement that random turbulence has an effect on cycle-to-cycle variation but quantitative experiments have not been performed to evaluate this effect from the standpoint of scale and intensity of turbulence because no technique has been found which is suitable.

C. HYPOTHESIS

A hypothesis was proposed relating the rate of change of the flame front area and rate of pressure rise to the scale and intensity of a

jet of mixture impinging upon a developing flame kernel. The scale was taken as a measure of the size of the jet relative to the diameter of the developing flame kernel and the intensity was taken to be proportional to the velocity of the jet.

The hypothesis was: A mixture motion (motion induced by the mixture-jet) of proper scale and intensity increases the flame area and hence, the mass rate of combustion. Mixture motion rather than turbulence is used to describe the movement induced in the combustion chamber since the classical definition of turbulence implies homogeneity and statistical randomness which are not characteristic of the motion under consideration.

D. DESCRIPTION OF EXPERIMENT

The physical combustion process in a constant volume cylindrical bomb with central spark-ignition, shown in Figure 1, was studied to determine the influence of scale and intensity of mixture motion on the early flame development. The apparatus provided a measurable, controllable, reproducible and geometrically simple combustion process which served as a first order simulation of the more complex, turbulent combustion process in a spark-ignition engine.

The combustion bomb was approximately the same size and shape as the conventional spark-ignited engine combustion chamber. In contrast to the turbulent conditions in the engine combustion chamber, a simple, two-dimensional mixture-jet of a given scale and intensity produced the only relevant motion in the bomb prior to ignition. The mixture-jet had the characteristics of a single eddy of very large scale relative to the flame front thickness. This jet, which in every case

had a Reynolds number less than 700 and thus was laminar, persisted through the initial development of the flame kernel.

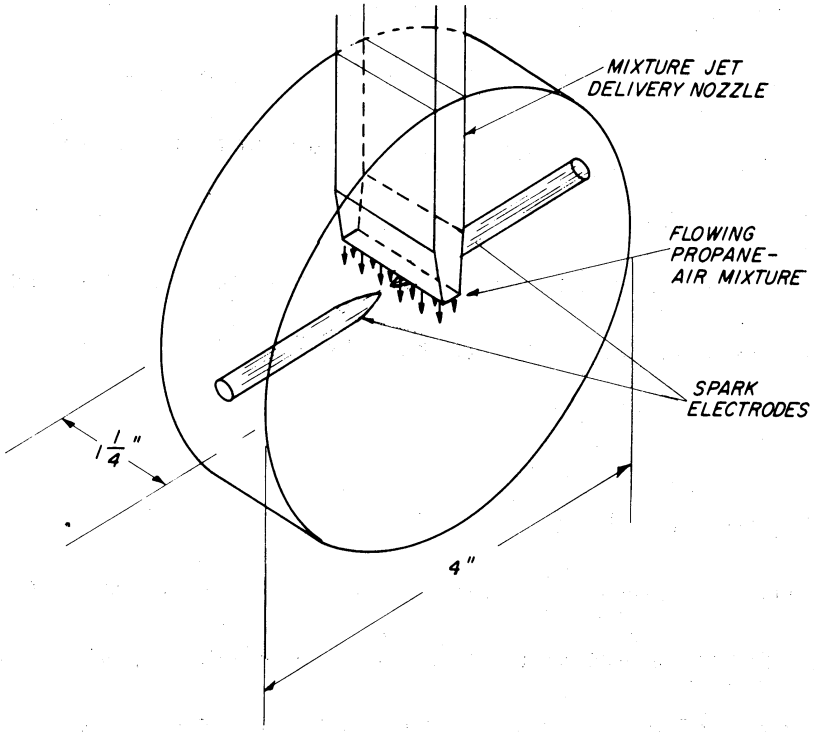

Figure 1. Constant volume bomb.

It was hypothesized that the mixture-jet would affect the physical combustion process only through a flame area change and would not directly affect the flame velocity, which would remain the laminar flame velocity.

To generate the disturbance the mixture-jet was directed at the spark-gap, as shown in Figure 1, by one of three rectangular nozzles, differing only in the smaller exit dimension, thus determining the scale of the mixture motion. The mixture velocity from each nozzle was varied to provide a range of mixture-jet intensities. Hot wire anemometer techniques were used to measure the scale and intensity of the motion prior to ignition.

Schlieren photographs of the distorted flame, taken after a fixed time interval following ignition, were used to evaluate visually the effect of mixture motion on the flame kernel area. The measured rate of pressure rise was used as a measure of the mass rate of combustion. Flame area development and pressure rate in a quiescent mixture were used as a reference for comparison.

CHAPTER II

LITERATURE SURVEY

Literature was not found which was specifically associated with the subject of directed mixture motion on the flame development during combustion in a constant volume bomb.

Two general areas were surveyed which were related to the research problem. These areas were:

A. The effect of engine operating factors on flame propagation and cycle-to-cycle pressure variation in a spark-ignition engine.

B. The influence of turbulence on constant pressure, steady flow combustion.

A. ENGINE STUDIES

In the literature surveyed there was general agreement that the cycle-to-cycle variation in pressure or rate of pressure rise is a direct result of the variation in burning rate and hence, variation in the rate of energy release from cycle-to-cycle. The benefits of eliminating or minimizing this variability could amount to a 2-20% increase in power or efficiency according to Soltau,[11] Curry,[3] Vichnievsky,[15] and Patterson.[8]

The various engine operating characteristics which were discussed in the literature as affecting cycle-to-cycle variation in combustion rate and pressure were:

1. spark (number of sources, timing, energy and duration)
2. air/fuel ratio
3. fuel composition and method of delivery into the engine

4. temperature (initial charge and engine coolant)
5. mass of the charge per cycle
6. compression ratio changes
7. exhaust gas dilution of the charge
8. oil contamination of the charge
9. turbulence and mixture motion as a function of engine speed, intake charge motion and combustion chamber design.

Soltau[11] investigated cycle-to-cycle pressure variation in a Renault research engine. A number of factors studied had no apparent effect on the combustion rate variation. These factors included variation in ignition timing, spark energy, lubricating oil in the combustion chamber and method used to deliver fuel to the combustion chamber. The use of several simultaneous ignition sources provided much more repeatable combustion. Air/fuel ratio also had a significant effect on cycle-to-cycle behavior with the minimum cyclic variation occurring at an air/fuel ratio of 13:1. Combustion with a fast burning fuel such as propane showed less variation than with a slower burning fuel such as isooctane. An increase in the exhaust dilution of the intake charge increased the cycle-to-cycle pressure variation, the variation being more significant than that resulting from a decrease in compression ratio. The increased turbulence caused by an increase in the "squish" area of the combustion chamber decreased the pressure fluctuations.

Curry[3] performed a 3-dimensional study of flame propagation in a Waukesha CFR spark-ignition engine. Using ion gaps Curry found that the ignition process and the formation of the initial flame kernel were repeatable from cycle-to-cycle. The greatest variation in flame propagation rate occurred in the early development of the flame kernel, and was therefore primarily responsible for the overall cycle-to-cycle

variation. It was observed that variations of 25 percent from the average time for both complete combustion and maximum pressure were not uncommon during normal combustion.

Rothrock and Spencer[9] examined combustion in a N.A.C.A. combustion apparatus, which was basically a single cylinder engine, with shrouds on the inlet valves to control the mixture motion. The spark timing, mixture strength and the amount of charge per cycle were held constant from cycle-to-cycle. The minimum cycle-to-cycle pressure variation was observed with the inlet mixture directed at the spark-gap. An increase in the velocity of directed motion past the spark-gap caused an increase in the combustion rate of the same magnitude as that caused by increasing the engine speed.

Vichnievsky[15] studied combustion in a C.F.R. spark-ignition engine. The standard deviation of pressure from a mean pressure curve was measured over several hundred engine cycles for several fuels which had different burning velocities and for several engine speeds. It was concluded that a fast burning fuel decreased the percent cycle-to-cycle pressure variation and that the absolute magnitude of the variation decreased with increase in engine speed.

Kumagai, Sahai and Kumura[6] used ultrasonics to induce a fine-grained turbulence in a spark-ignition engine combustion chamber. A ragged flame front and a small increase in flame speed resulted. They concluded that the increased flame front area caused by wrinkling of the flame and/or the increased heat transfer and diffusion of active particles from the burned to the unburned mixture caused the higher flame speed.

Taylor and Taylor[14] suggested that the apparent velocity of a flame in a constant volume combustion chamber was the sum of 1) the burning velocity, and 2) the rate at which the flame is pushed through the chamber by expansion of the burned gases (transport velocity). The apparent flame velocity was found to increase with increasing turbulence. They believed this was caused by vortexes in the charge which break up the flame front giving it greater contact area with the unburned mixture. The most significant effect of turbulence on the flame front was observed when the scale of the vortexes was small in comparison to the diameter of the flame kernel. Turbulence effects on the initial flame kernel were believed to be negligible.

Marvin, Wharton and Roeder[7] studied several aspects of flame speed in a spark-ignition engine. Flame speed was found to decrease when the air/fuel ratio was changed from the maximum power air/fuel ratio and also when the exhaust residual was increased. The observed increase in flame speed with an increase in engine speed was believed to be a function of small scale turbulence which affected the structure and depth of the reaction zone. It was also found that the flame speed was practically independent of pressure and was increased by an increase in the initial charge temperature. They expressed the opinion that bomb experiments were the best method to study flame propagation under imposed special conditions.

Agnew[1] studied cycle-to-cycle variation in combustion rate by observing variations in flame speed in a single cylinder spark-ignition engine equipped with an ionization gap. Any factor that increased the burning rate was found to decrease the percent cyclic variation. Flame speed was observed to increase slightly with an increase in initial mix-

ture and coolant temperatures and significantly with an increase in engine speed, spark advance, and air flow. The use of two ignition sources decreased the time for complete combustion. The flame speed increased with an increase in fuel/air ratio until a maximum was attained at the best power fuel/air ratio. A subsequent increase in fuel/air ratio caused a decrease in flame speed. No operating variable except engine speed and therefore turbulence had a significant effect on the absolute magnitude of cycle-to-cycle combustion rate variation. This suggested that the cyclic variation in turbulence and mixture motion were decreased at the higher speeds.

Patterson[8] examined cycle-to-cycle pressure rate variation in a conventional automotive V-8 engine. By using a shroud on the intake valve, mixture swirl was increased past the spark-gap. This resulted in a significant increase in combustion rate, a decrease in the percent cyclic pressure rate variation, but did not change the cyclic pressure rate spread. These results suggested that a major cause of cyclic pressure variations could be cyclic variations in swirl, with the swirl effects in the vicinity of the spark-gap being the most important. Poor mixing of the fuel and air, and cycle-to-cycle variation in spark timing were found to account for less than 1/3 of the total pressure variation. The geometry of the spark electrodes, the spark-gap, the spark energy and exhaust residual were varied with no measurable effect on cyclic variation.

It is the consensus of these authors that turbulence and mixture motion have a significant effect on combustion in the spark-ignition engine, although quantitative results are not available indicating the effect of this motion on cycle-to-cycle pressure and rate of pres-

sure rise variation. The effect of the other operating variables, listed on pages (6 and 7), have been studied sufficiently to determine their effect on cycle-to-cycle pressure variation. Factors which themselves have a significant effect on flame propagation probably have the greatest effect on cycle-to-cycle variation in combustion rate when cycle-to-cycle variation of these factors is considered.

B. CONSTANT PRESSURE COMBUSTION

The author believes there is a degree of similarity between the constant pressure and constant volume combustion processes since the early flame develops in an approximately constant pressure atmosphere in constant volume combustion and therefore data pertaining to the constant pressure process is relevant to the constant volume process. The literature surveyed indicated that turbulence has a significant effect on flame speed and combustion rate in the steady flow, constant pressure combustion reaction.

Swett[13] induced a turbulent field in a flowing air/fuel mixture, with the aid of grates and screening in the flow duct, to determine the influence of the scale and intensity of turbulence on the flame speed. Turbulence was found to increase the flame speed in proportion to the increase in intensity. When the scale of the turbulence was large compared to the thickness of the flame front, the effect of scale was found to be negligible compared to the effect of intensity of turbulence.

Dugger and Gerstein[4] made a comprehensive literature survey. They found that flame velocity increased with an increase in Reynolds number in a turbulent flame, when the Reynolds number was greater than 2000. Below a Reynolds number of 2000 the flame velocity was the laminar flame velocity and was independent of flow velocity.

They concluded that the increased burning rate of turbulent flames may have been caused by any one or a combination of three processes with the first one being the most important in moderately turbulent flow fields:

1. The turbulent flow may distort the flame, increasing the surface area with the normal component of the burning being the laminar flame velocity.
2. Turbulence may increase the rate of transport of heat and active species, thus increasing the actual burning velocity normal to the flame surface.
3. Turbulence may rapidly mix the burned and unburned gas in such a way that the flame becomes essentially a homogeneous reaction.

Among the works surveyed by Dugger and Gerstein were those of Damkohler, Karlovitz, and Scurlock and Grover. Important aspects of these works follow:

1. Damkohler considered separately the effect of large scale turbulence (greater than the flame thickness) and small-scale turbulence on the flame. Large scale, low intensity turbulence was believed to wrinkle the flame with the laminar transport processes remaining virtually unaffected. Thus, the increase in burning rate was caused by process (1) indicated earlier.

2. Karlovitz theoretically studied large-scale turbulence by considering the effect produced when an eddy passed through a laminar flame front. He developed an equation for the turbulent flame velocity. The eddy was believed to distort the flame in such a way that no net movement of the flame was produced. The turbulent flame velocity component was added to the laminar flame velocity to determine the overall turbulent flame velocity.

3. Scurlock and Grover also theorized that an eddy passing through a laminar flame would produce wrinkling. They believed the laminar flame velocity within the wrinkled flame would remain unchanged. Thus, the ratio of the turbulent flame velocity to the laminar flame velocity was believed to be equal to the ratio of the area of the distorted flame to the area of the laminar flame.

Bolz and Burlage[2] studied the propagation of free flames in laminar and turbulent flow fields. The turbulent field was generated by using screens in the flow duct. High speed motion pictures, using the shadowgraph technique, were used to determine the effect of the flow field on flame propagation. The flame propagation velocities were obtained by measuring the slope of the curve showing flame kernel radius, corrected for expansion, plotted against the time following ignition. The flame propagation velocity was found to increase nonlinearly with an increase in the intensity of turbulence and to be almost independent of the scale of turbulence although conclusive results were not achieved in the latter case. The flame surface appeared very smooth and regular in the laminar flow field and rough and irregular in the turbulent flow field. Only relatively weak turbulence with a scale greater than the flame front thickness was studied in this experiment. Results were very repeatable.

It was concluded from the observed literature on constant pressure combustion that large-scale turbulence affects the flame propagation through an area change of the flame and that the component of flame velocity normal to any surface of the flame is the laminar flame velocity. Also, it was concluded that the intensity of turbulence has a more significant effect on the flame propagation velocity than the scale of turbulence.

CHAPTER III

EXPERIMENTAL APPARATUS

The basic experimental apparatus was employed in an earlier doctoral research program.[12] Numerous equipment additions and apparatus modifications were made to facilitate the research.

Combustion was contained in a constant volume cylindrical bomb. The various physical components associated with the bomb and the pertinent instrumentation are described in the following sections. Three areas are considered:

A. System Components;

B. Instrumentation; and

C. Calibration of Instrumentation.

A. SYSTEM COMPONENTS

1. Constant Volume Bomb (Figures 2 and 3)

The combustion chamber was constructed of 316 stainless steel. It was a cylinder of 6-1/2 in. O.D., 4 in. I.D., and 1-1/4 in. thickness. The cylinder was fitted with two quartz windows, each 5 in. in diameter and 1 in. thick. The windows were held in place by two 316 stainless steel heads. A soft 1/8 in. rubber gasket provided sealing between the quartz windows and the cylinder.

The positive and negative spark electrodes were installed horizontally in the bomb. The spark-gap was positioned at the center of the bomb. Each electrode was easily removable for cleaning or replacement. The cathode located at the rightin Figures 2 and 3 was electrically insulated from the bomb by a long Teflon sleeve. The anode on the left was fitted with a micrometer head so that the electrode spacing could be set and varied accurately.

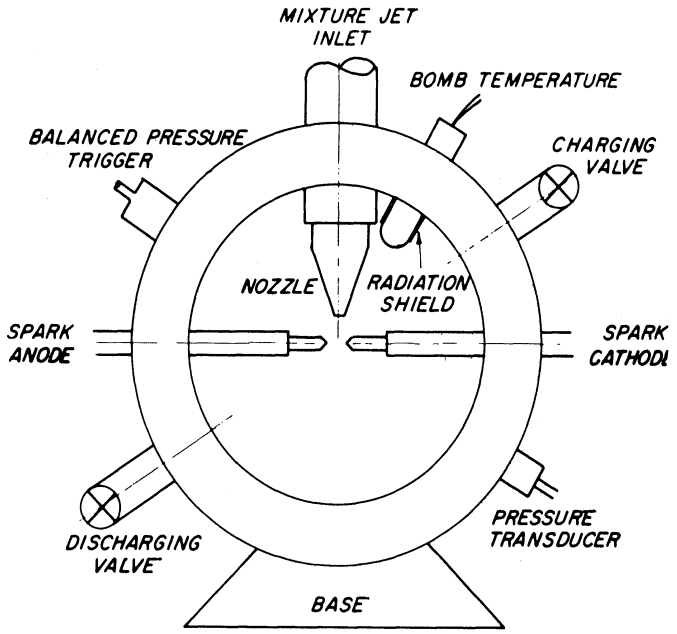

Figure 2. Schematic diagram of the constant volume combustion bomb.

A pressure transducer was attached to the bomb through a 14 mm drilled and tapped hole just below the cathode. The bomb was charged and exhausted through steel piping located respectively at the upper right and lower left of Figure 2. Stainless steel ball valves designed for high pressure and high vacuum were fitted into the inlet and exhaust porting.

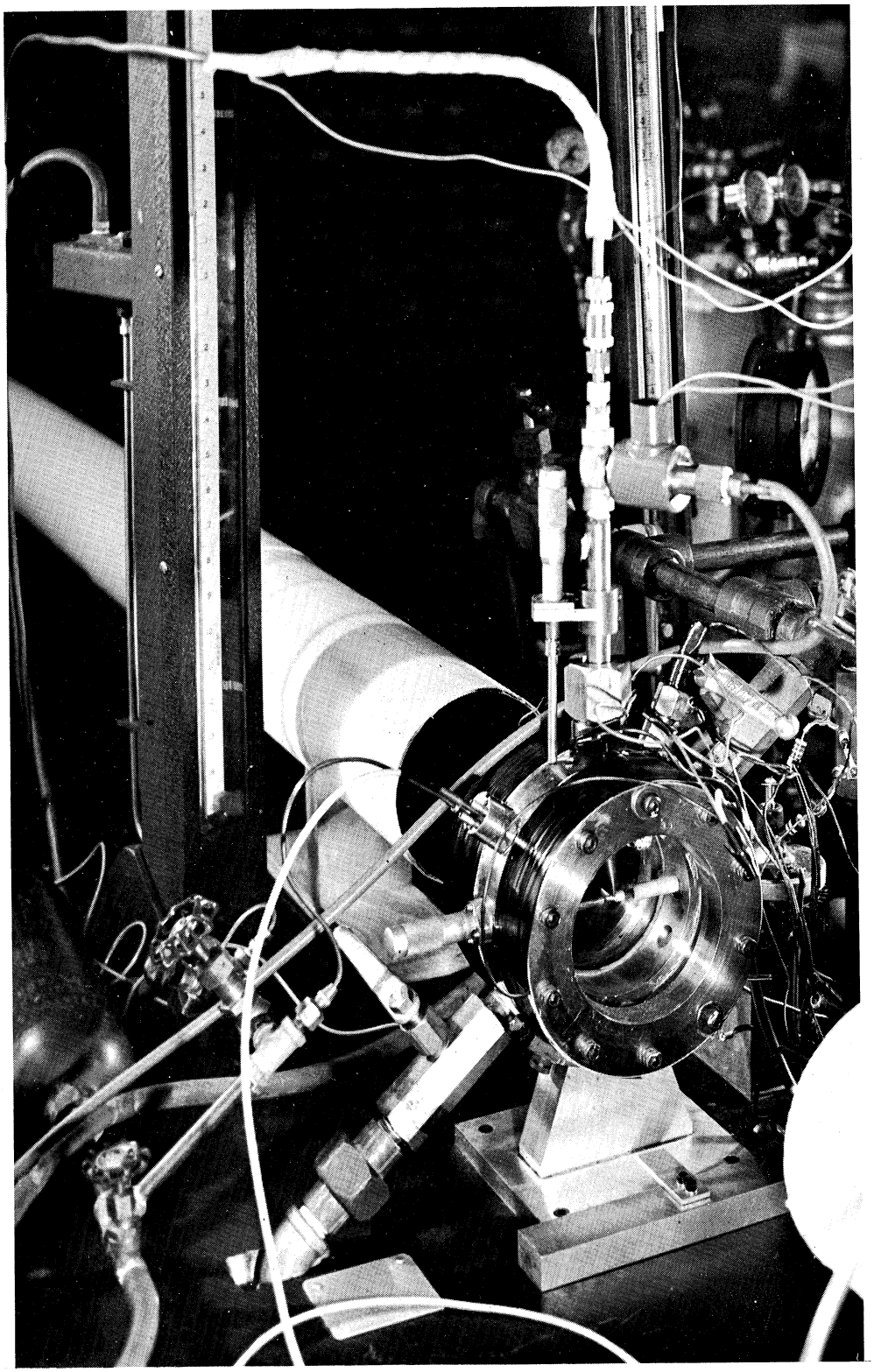

Figure 3. Constant volume bomb and associated equipment.

The mixture temperature was measured by a shielded thermocouple inserted into the bomb directly above the charging inlet. The wires were sealed by means of a Conax high pressure fitting.

The mixture-jet system was positioned vertically in the bomb. Mixture was delivered through a 5/8-in. diameter stainless steel tube. The tube was attached and sealed with a Conax single hole Teflon lined fitting.

Above the anode a balanced pressure diaphragm switch was installed in an 18 mm drilled and tapped hole.

The temperature of the bomb and the initial temperature of the mixture before ignition were controlled manually by heating the outside surface as desired. Two hundred ohms of electrical heating element wire were wrapped around each head. High temperature electrical tape was used as insulation between the heating element wires. A Variac was connected in series with the wire to control the current and thus the temperature.

2. Mixture-Jet Delivery System

The mixture-jet delivery system had an important function in this research. It directed and regulated the mixture-jet impinged on the spark gap. It is shown schematically in Figure 4.

The mixture source was a high-pressure steel tank in which the propane and air were mixed and stored. A Matheson high-pressure gas regulator was connected to the tank outlet. This device limited and regulated the mixture feed pressure.

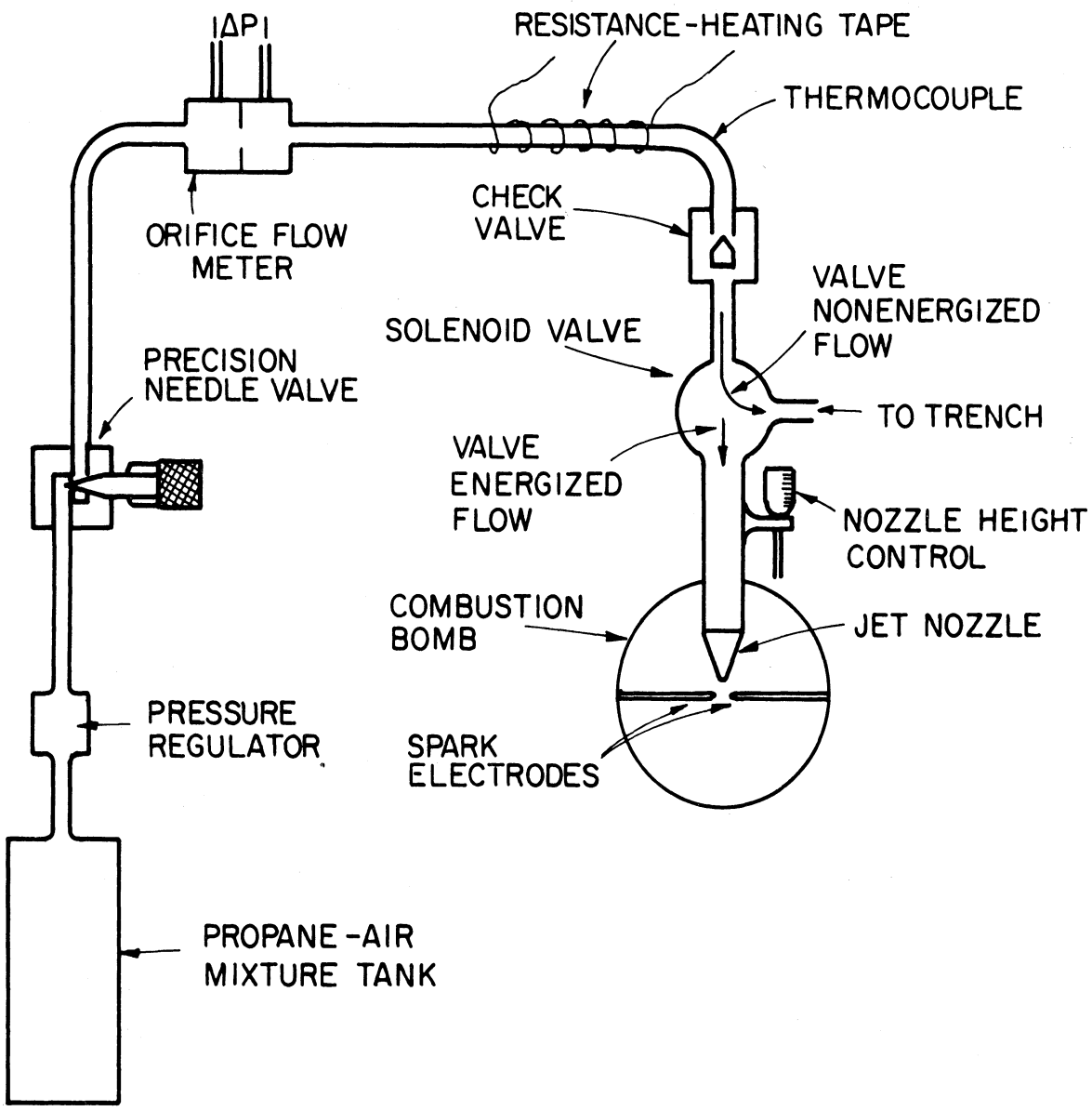

Figure 4. Schematic diagram—mixture jet control and delivery system.

The components in the remaining parts of the mixture-jet system were connected by 1/4-in. soft seamless copper tubing.

From the regulator the flow passed through a Nupro precision stainless steel needle valve. Mixture flow rate was controlled at this point. The flow rate was measured with a sharp-edged orifice flow meter. Mixture then entered the part of the system adjacent to the bomb, note Figure 4. It was heated at this point by resistance tape wrapped around the copper tubing.

A Nupro check valve prevented high-pressure combustion gases from entering the remainder of the system and was a limit on the total volume in the combustion chamber. The check valve return spring was removed to decrease the pressure required to close the valve.

A two-way electric solenoid valve (Hoke 595 A 334 CH) controlled the initial flow into the bomb. In the normally nonenergized position mixture was dumped into an exhaust trench. Flow was established and regulated under this condition. The pressure drop in the dump line was balanced with that of the system downstream from the solenoid by means of a hose clamp. The steady state flow rate therefore did not change when the solenoid valve was switched.

The solenoid valve was connected to a stainless steel tube of 5/8 in O.D., 1/2 in. I.D., and 6 in. long which conducted the mixture into the bomb. This tube was packed with stainless steel mesh which acted as a flame arrestor.

Three different nozzles were used in this research, Figure 5. The openings for the small, medium, and large nozzles were, respectively, .026 in. x .88 in., .066 in. x .85 in., and .156 in. x .79 in. The jet nozzles, made from brass tubing, were fitted to the inlet tube by means of a brass collar.

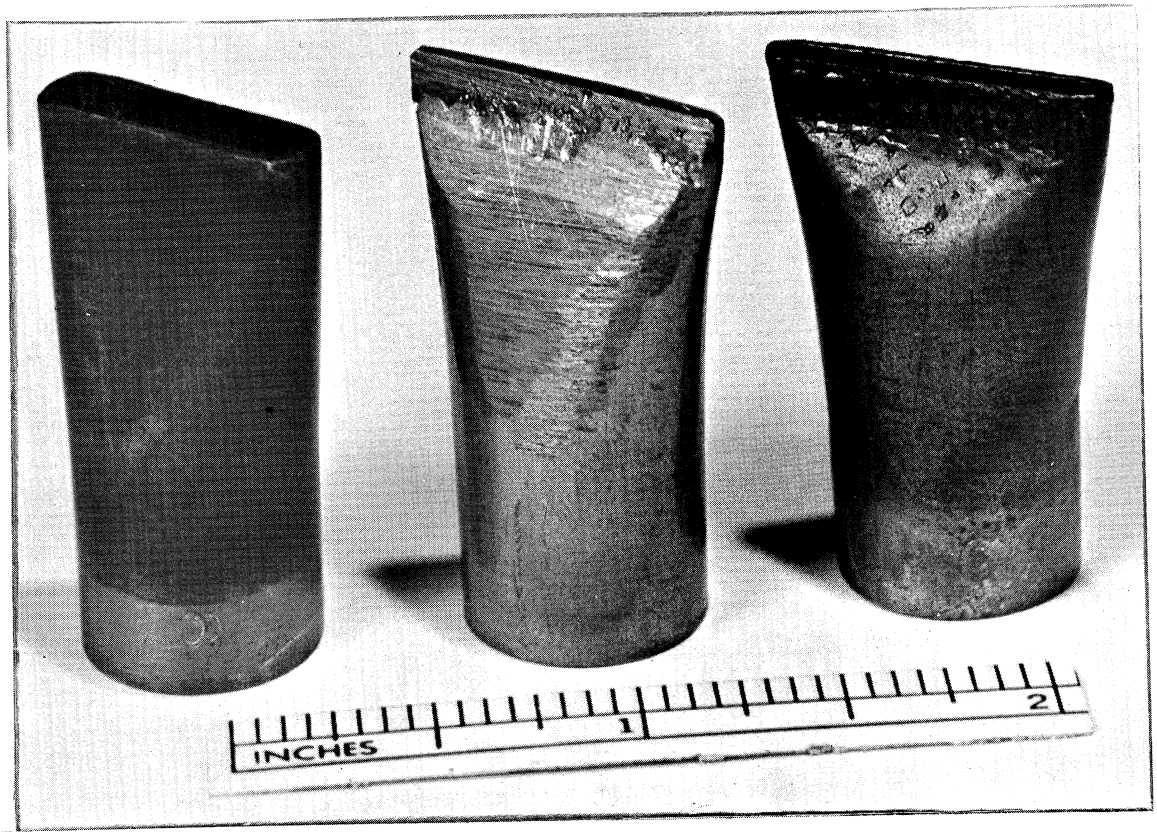

Figure 5. Mixture-jet nozzles. Left to right: Large, small, and medium nozzles.

The vertical position of the nozzle with respect to the spark-gap was established by a micrometer attached to the inlet tube outside the bomb. The top surface of the bomb was used as a reference.

3. Ignition Spark Control Circuit

Spark energy was obtained through the use of a specialized transistor

control circuit which initially opened and then closed the primary circuit in an ignition coil, note Figure 6. The breakage of the primary current resulted in a high voltage discharge at the spark electrode gap. By turning the primary current back on, the secondary breakdown ceased with the flux reversal and extinguished the spark. This controlled the duration of the spark. The spark voltage and current were controlled by regulating the primary current.

A schematic of the circuit is shown in Figure 45 of Appendix A. The spark was initiated by opening switch S-2. The duration was controlled by adjustment of variable resistance R_3. The values of the circuit components are indicated in Table IV of Appendix A.

Energy for the primary of the spark coil was provided by a 12-volt automotive storage battery. The coil used in this research was a special low capacitance coil made by the Delco-Remy Division of General Motors.

The oscilloscope, which was used to record the pressure data, was triggered by a pulse from the control circuit when the switch S-2 was opened. A series of high resistances was placed in series with the spark coil secondary to limit the spark current and minimize burning of the electrodes.

All tests were conducted with a constant electrode spacing of .050 in. which was slightly greater than the quench distance as reported in Reference 12.

4. Spark Trigger Control

When the mixture-jet was flowing at the spark-gap it was necessary

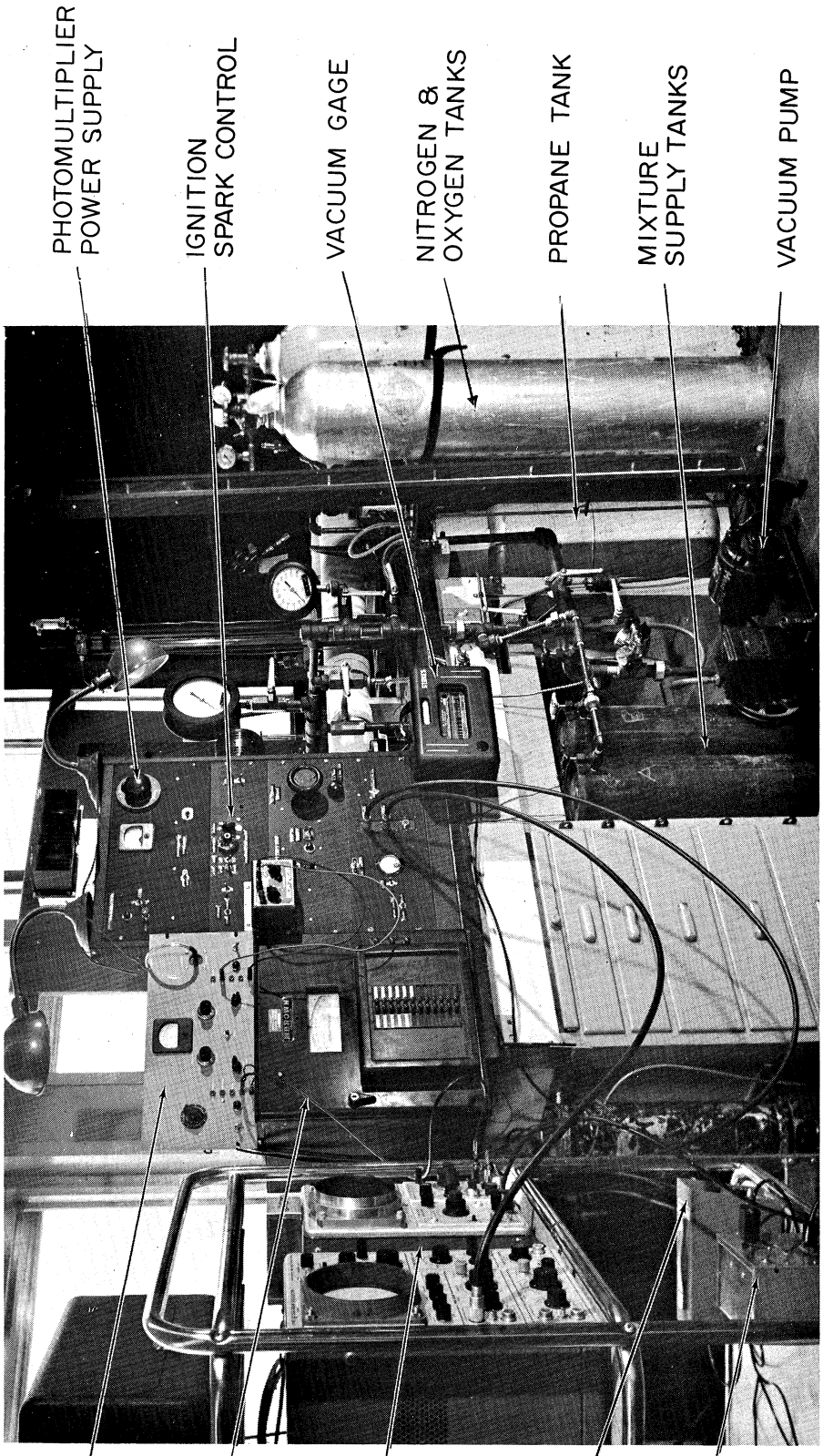

Figure 6. Front view of equipment.

to fire the ignition spark at a precise, repeatable condition. In this research pressure was the controlled variable i.e., ignition was desired at a predetermined pressure in the bomb. At this pressure the switch S-2 of the spark control circuit had to be opened to break the ignition coil primary current.

The basic component of this circuit was a balanced pressure switch built by General Motors Research Laboratories. It is shown in detail in Figure 7. The switch operated basically on an "oil can" effect. At

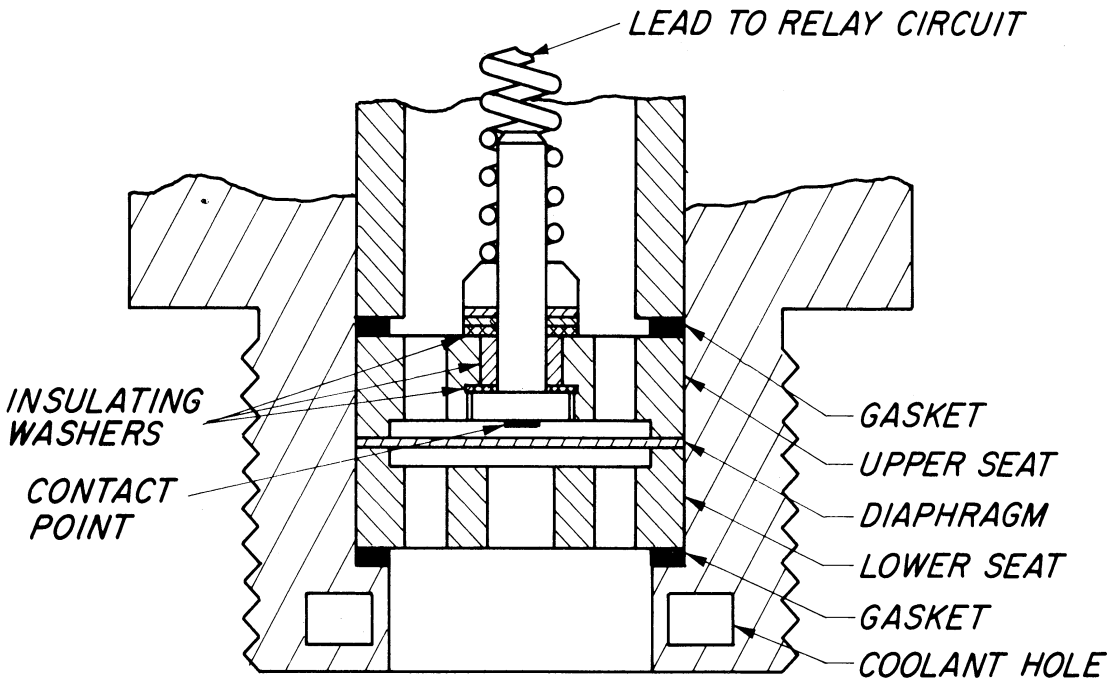

Figure 7. Section view of balanced pressure diaphragm switch.

a predetermined pressure a thin diaphragm flipped or switched, completing an electrical circuit. The switching pressure or balancing pressure was set by the back pressure on the diaphragm. The back pressure system is shown at the left in Figure 3. The triggering pressure was established at 29.5 in. of mercury absolute for every test. The pressure switch was calibrated periodically by evacuating the bomb and then

gradually filling the bomb with nitrogen until the switch closed. The switching pressure was monitored on a mercury manometer. The balance pressure was adjusted until the switching pressure was 29.5 ± .05 in. of mercury. It was found to be reproducible within ± .05 in. of mercury.

The balanced pressure switch was not connected directly with the transistor spark control circuit at switch S-2 but instead through a low voltage relay circuit to prevent arcing at the diaphragm. The relay circuit is shown schematically in Figure 46 of Appendix B. A 12-volt Potter and Brumfield KRP 11D relay was used.

5. Manifold System

The fuel/air mixture was premixed in three steel mixing tanks shown below the bench in Figure 6, and shown schematically in Figure 8. Each tank was equipped with two valves; one valve was used to throttle the mixture into the bomb, and the second was used in conjunction with the first when scavenging the tank before evacuation. Ball valves were used at all points where throttling was not required. Piping was schedule 80, 1/2 in. black iron pipe. This large diameter was chosen to reduce evacuation time to a minimum. One Cenco vacuum pump was used. The system could be evacuated to less than 200 microns of mercury absolute with this pump. Small absolute pressure measurements were made with a Stokes model 276 AS McLeod gage having a scale of 0 to 5000 microns. Pressures from 0 to 67 in. of mercury absolute were measured with a mercury manom-

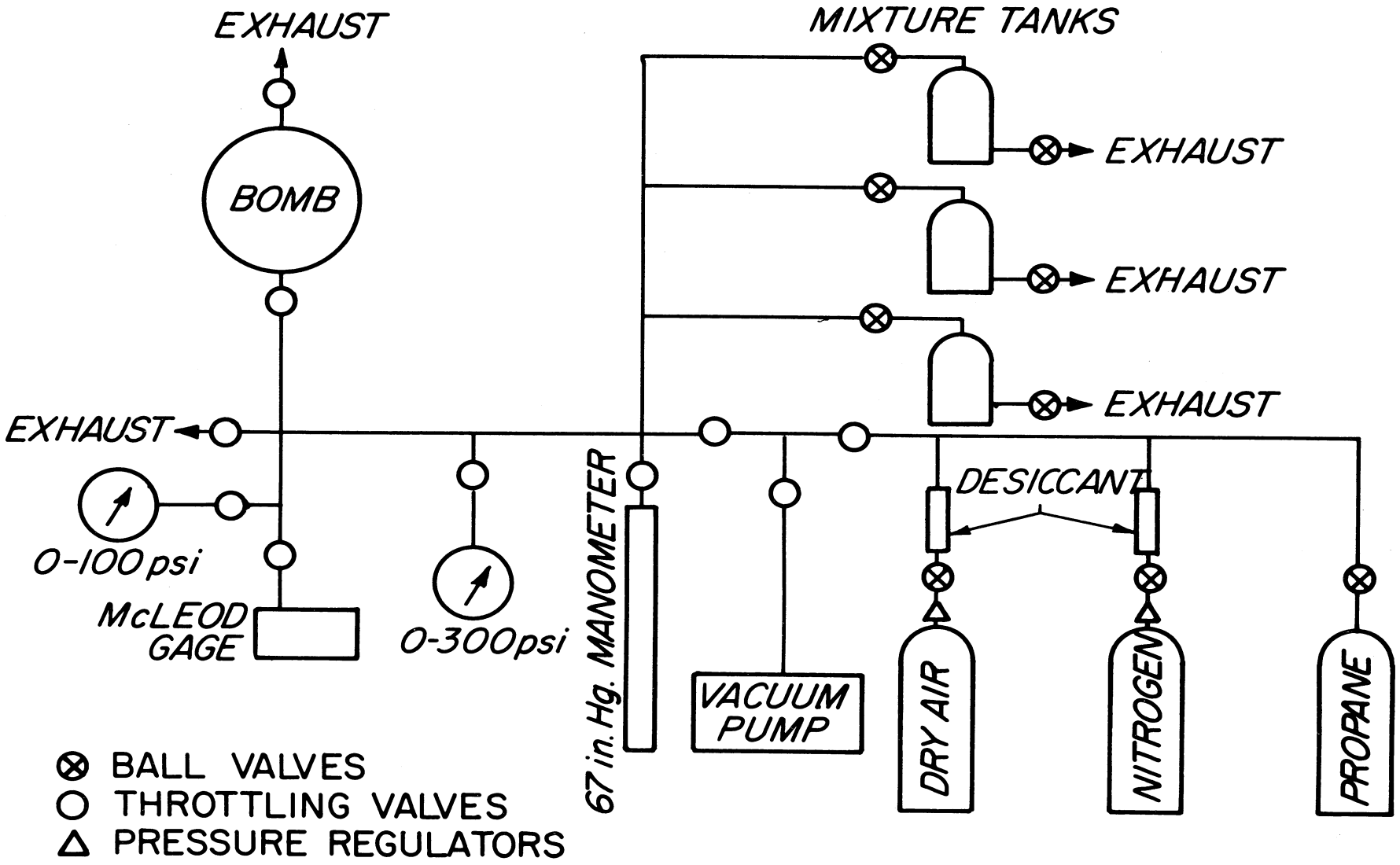

Figure 8. Manifold system.

eter which could be read to the nearest 1/50 of an in. Higher pressures were measured with either of two Bourdon gages, a Lonegran-Maximan (0-300 psi), and a U.S. Gauge Company-Supergauge (0-100 psi).

Both nitrogen and dry-air were passed through Drierite desiccant to assure a negligible moisture content. The desiccant was contained in two 8-in. lengths of pipe of 1-1/2- and 2-in. diameters, respectively. The nitrogen and dry air size 1-A cylinders were equipped with standard pressure regulators. The propane, which was commerical grade (96% propane, 4% propylene), was supplied from a cylinder with a built in regulator.

B. INSTRUMENTATION

1. Temperature Measurement

Iron-constantan thermocouples were used for all temperature measurements in conjunction with a Minneapolis-Honeywell Brown model 156 x 63P24 continuous indicating potentiometer. The temperature inside the bomb was measured by a thermocouple of 24-gauge wire. It was looped once in a stainless steel tube radiation shield. The loop was necessary to minimize conduction along the wire. An additional radiation shield of aluminum was placed over the stainless steel shield. The shield is seen protruding into the bomb next to the mixture-jet inlet in Figure 2.

A thermocouple was taped to each head of the bomb. They were placed below the resistance heating tape. A similar thermocouple was placed under the heating tape in the mixture-jet delivery system.

A well-type thermocouple was fitted to each mixture tank near the inlet.

2. Pressure Measurement

Bomb combustion pressure was measured with a Kistler model 601 piezoelectric transducer in conjunction with a Kistler model 568 electrostatic charge amplifier.

The desired pressure characteristic in this research was the rate of pressure rise, dP/dt. A differentiating circuit built by General Motors Engineering Staff was used to provide a direct measurement of the pressure rate. It is shown in Figure 6 below the oscilloscopes, and schematically in Figure 47 of Appendix C. The output of the charge amplifier was fed into the differentiating circuit. The differentiated signal was recorded on a model 564 Tektronix storage oscilloscope.

3. Velocity Measurement

The profile of the mixture velocity from each of the three jet nozzles was obtained with a Flow Corporation hot-wire anemometer, model HWB3. A single wire probe, model No. HWP-B-W3, with a .00035 in. diameter tungsten wire was used as the sensing device. A special fixture fitted with a lathe cross-slide was used to precisely traverse the flow in two directions.

A special circuit to be used in conjunction with the hot-wire probe was constructed as shown schematically in Figure 48 of Appendix D, to measure the unbalance of the hot-wire bridge. This circuit was used to measure

the time required to establish steady flow at the jet exit after the solenoid was opened shunting the mixture into the bomb.

4. Flow Measurement

It was necessary to know the flow rate of the mixture-jet into the bomb in order to establish the correct velocity profile for combustion runs. A sharp-edged orifice meter was used to measure this flow rate. It was built in the Automotive Laboratory of The University of Michigan. The orifice could be changed to provide a wide range of capacities. A U-tube water manometer was used to record the pressure drop across the orifice.

5. Schlieren System

A schlieren mirror system was used to obtain photographs of the combustion front. The system is shown in the schematic diagram of Figure 9. The two schlieren mirrors were 6-in. diameter, front-surface parabolic mirrors with 48-in. focal length. The point light source was a specially constructed spark unit, and is shown as an assembly drawing in Figure 49 of Appendix E. It consisted of a bank of ten, 500 μf, 20,000 volt capacitors. They discharged across a 1 in. gap when a small "tickler" spark ionized the gap. The light supplied was intense and lasted about one microsecond, thus stopping the flame front photographically. Power for the light source was obtained from a Del Electronics Model 30-1-5, 30 kv d-c power supply. The primary of the power supply was controlled by a Variac connected to 115 volt,

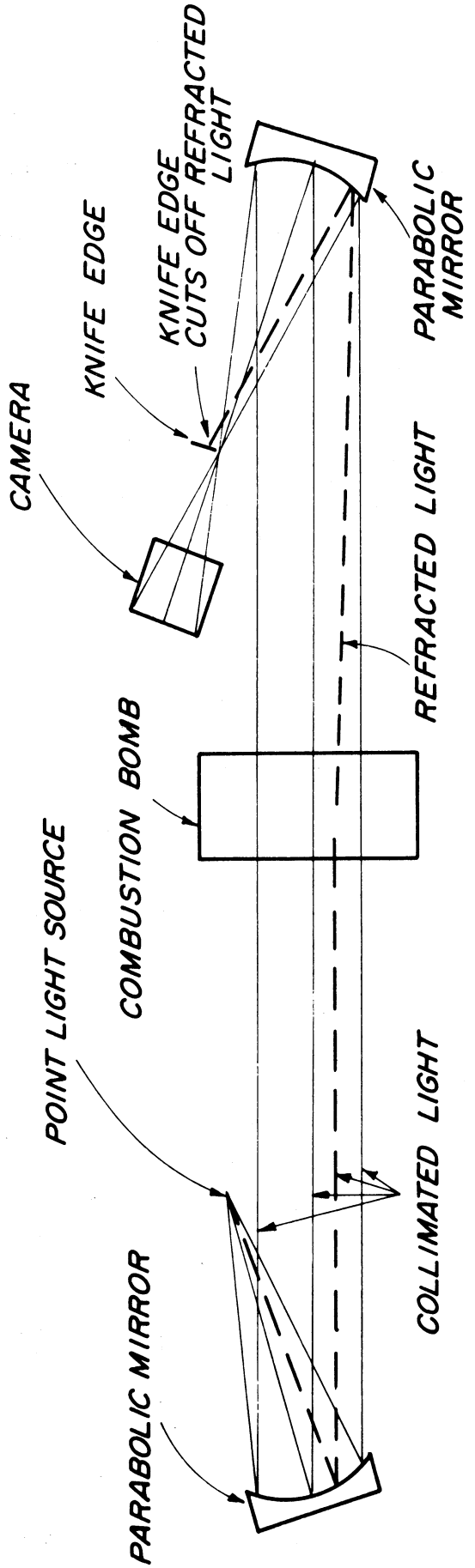

Figure 9. Schematic diagram—schlieren system.

a-c line voltage. The complete light source system is shown schematically in Figure 50 of Appendix E.

A special time delay circuit furnished the "tickler" spark. This unit shown in Figure 6 and schematically in Figure 51 of Appendix E, was designed by engineers at the Aircraft Propulsion Laboratory of The University of Michigan. Firing the bomb spark initiated the delay sequence. The time delay was a function of both the resistance and capacitance of the delay circuit. A Cornell-Dubilier .01-1.1 μf decade capacitor was used to control the delay time in steps, and a linear potentiometer was used as a vernier control on the time delay.

A razor blade was used as the knife edge. It was set in an adjustable mount which was secured to a heavy floor jack.

Flame photographs were taken with a lensless bellows-type camera fitted with a 4 in. x 5 in. Polaroid sheet film pack. Type 57, ASA 3000 Polaroid film was required.

6. Streak Camera

A streak camera was used in conjunction with the schlieren system to study the spatial velocity of the flame front in the bomb. This specialized camera was designed by Mr. David Mellen for use in his doctoral research. A continuous high-intensity point light source provided the required illumination. A vertical slit was taped to the bomb quartz window nearest the knife edge. A rotating flat mirror in the camera focused the slit image on the film. As the flame front passed down the slit

a trace of the front swept the film plane. The vertical position of the trace was a measure of the position of the flame front with respect to the spark-gap and the horizontal position was a measure of time. The flame spatial velocity was obtained by measuring the slope of the trace.

7. Photomultiplier

A photomultiplier was used to measure the repeatability of the spark timing and start of combustion. An R.C.A. 931-A photomultiplier tube was fitted to one bomb window, and the interior of the bomb was completely shielded from outside light. The circuit diagram for the photomultiplier is shown in Figure 10.

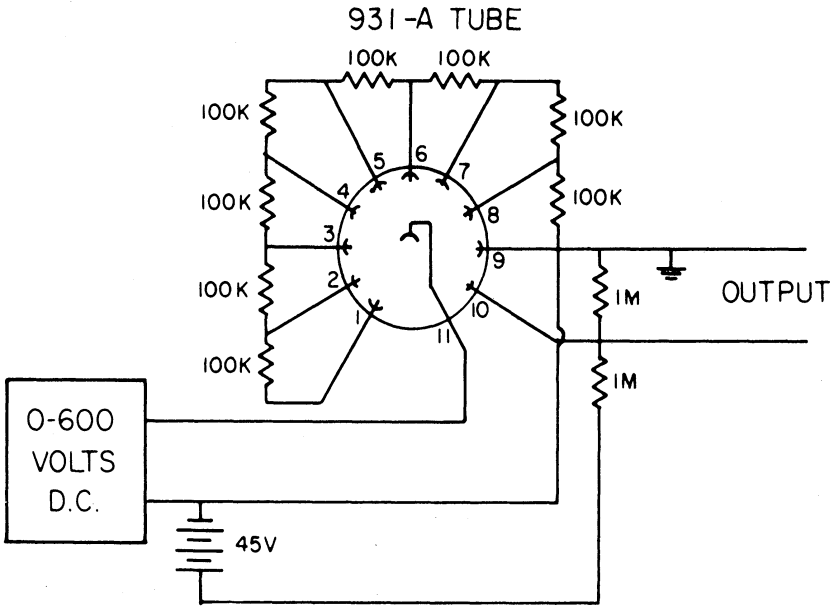

Figure 10. Photomultiplier circuit.

C. CALIBRATION OF INSTRUMENTATION

1. Thermocouple Calibration

All iron-constantan thermocouples were calibrated in conjunction with the Brown potentiometer. The ice point and boiling point of water

were used as references.

2. Pressure Calibration

The 0-100 and 0-300 psi Bourdon pressure gauges were calibrated with a dead weight tester. The calibration data is found in Table V of Appendix F.

The Kistler pressure transducer was calibrated periodically with the aid of the 0-100 psi Bourdon gauge by pressurizing the bomb with dry nitrogen. The charge amplifier was operated in the long time-constant position during calibration and the calibration factor of the charge amplifier was adjusted to give a voltage output of .01 volt per psi.

The pressure differentiating unit was calibrated by measuring the slope of the pressure vs. time curve and making correction for the slight phase difference between the pressure rate and the pressure traces. The vertical displacement of the pressure rate curve is proportional to the rate of pressure rise.

It would have been desirable to calibrate the differentiating circuit from pressure and pressure rate data from the same combustion run. Since it was not possible to do this, traces from a great number of different runs with the same initial conditions were observed to insure accurate calibration.

A pressure rate and pressure versus time curve are shown in Figure 11. Note that the pressure rate curve is inverted and must be measured from the top. This is a result of the sign-inverting property of a dif-

ferentiating circuit. The pressure rate calibration curve is shown in Figure 52 of Appendix F.

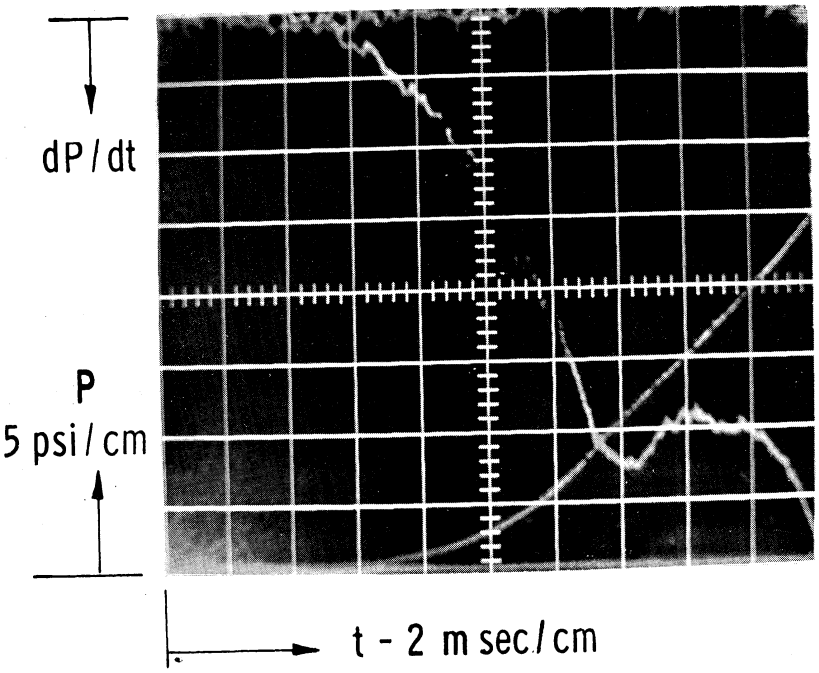

Figure 11. Superimposed pressure and pressure rate traces.

3. Oscilloscope

The sweep rate of the model 564 oscilloscope was calibrated with an Erie model 400 counter-timer, which itself was calibrated with station wwv. It was also checked with the 60 cps square wave voltage available internally within the scope.

The vertical amplifier deflections were checked and calibrated with the aid of the internal square wave generator.

4. Hot-Wire Anemometer

The hot-wire anemometer was calibrated in a nozzle flow stand with air used as the calibrating fluid. There is a negligible difference between the flow characteristics of air and the air-propane mixture.

The nozzle arrangement consisted of a container with a series of fine mesh screens at the inlet. The flow exited through a smooth converging nozzle of 1 in. diameter. The flow stand itself was calibrated with a positive displacement air bell.

The velocity profile at the nozzle exit was flat as noted qualitatively with the hot-wire. Since $V = \dot{m}_{air}/\rho_{air} A_{nozzle}$, and ρ_{air}, and A_{nozzle} are constant, V can be plotted against orifice pressure drop.

The hot-wire probe was placed in the exit plane of the calibrating nozzle, perpendicular to the flow. Hot-wire current ($i_{H.W.}$) plotted against flow velocity (V) is shown in Figure 53 of appendix F.

5. Jet System Orifice Meter

The orifice flow meter of the jet delivery system was calibrated with a bubble flow meter. Three different orifices were calibrated. Flow rate versus pressure drop across the orifices in inches of water is shown in Figure 54 of Appendix F for orifices nos. 2 and 3. All calibration data was obtained with air at ambient temperature and pressure.

CHAPTER IV

EXPERIMENTAL PROCEDURE

A. FUEL-AIR MIXING

Stoichiometric Propane-Air mixtures were used in all of the combustion work. The mixture tanks were first scavenged with dry nitrogen. The tanks and manifold system were then evacuated to less than 200 microns absolute pressure. Propane was introduced until the desired partial pressure was attained. The tank valves were closed and the manifold system again evacuated. Dry air was introduced in the manifolding until its pressure was significantly above the propane pressure in the tanks. The tank valves were then opened and the total pressure brought to the level required for a stoichiometric mixture. This procedure was necessary to minimize propane diffusion from the tanks while filling.

The partial pressure was calculated in the following manner: Propane-Air Mixture

$$C_3H_8 + \eta(5)O_2 + \eta(5)(3.76)N_2 \rightarrow 3CO_2 + 4H_2O$$
$$+ \eta(5)(3.76)N_2 + (\eta-1)(5)O_2 \qquad (4.1)$$

This equation applies for stoichiometric and lean air-fuel ratios where:

$$\eta = \frac{\text{Actual air-fuel ratio}}{\text{Stoichiometric air-fuel ratio}}$$

$$\phi = \frac{1}{\eta} = \text{equivalence ratio} = \frac{\text{Actual fuel-air ratio}}{\text{Stoichiometric fuel-air ratio}}$$

Fuel-air ratio may be expressed in two ways:

$$(F/A)_{volume} = \frac{1}{(5)(4.76)(\eta)} = \frac{1}{23.8\ \eta} \tag{4.2}$$

$$(F/A)_{mass} = \frac{M.W._{fuel}}{23.8\ \eta\ M.W._{air}} = \frac{1}{15.66\ \eta} \tag{4.3}$$

The partial pressure is based on the $(F/A)_{volume}$ and is expressed as follows:

$$\frac{P_f}{P_t} = \frac{1}{23.8\ \eta + 1} \tag{4.4}$$

P_f = partial pressure of fuel

P_t = total pressure of mixture

A sample tabulation of pertinent mixing data is presented in Table VI of Appendix G.

B. FLAME FRONT STUDY

The flame front was studied in quiescent and motion-disturbed combustion processes. Two types of experiments were performed.

1. A detailed photographic study was made of the flame kernel at a prescribed time after ignition.
2. The flame development was studied photographically with time, a sequential analysis.

In all of the studies the bomb and manifold system were evacuated to less than 300 microns. The throttling valve on a mixture storage

tank was opened and the bomb charged to the required initial pressure.

For the quiescent mixture studies the bomb was charged to 29.5 in. of mercury absolute pressure. The bomb charging valve was closed and the mixture allowed to stabilize until it attained a temperature of 80°F. The charging valve was reopened and the pressure checked and adjusted if required. Two minutes of additional stabilization time were alotted to assure quiescence.

Switch S-2 on the spark control panel was opened, firing the bomb. The rate of pressure rise (dP/dt) was recorded versus time on the oscilloscope. The bomb spark triggered the time delay circuit; a period of time (t_p) elapsed; then the "tickler" spark triggered the schlieren light source. The flame front was thus stopped photographically at time (t_p) after bomb ignition. This time was noted as a slight discontinuity on the pressure rate trace.

The sequence of operations in the jet-disturbed combustion was essentially the same as in the quiescent combustion study but with several variations. The bomb initial pressure was set and stabilized as for the quiescent mixture but with the exception that the pressure was set lower—29.1 in. of mercury absolute. The balanced pressure trigger was set to close at 29.5 in. of mercury. Thus, switch S-2 was opened at 29.5 in. of mercury.

The test was initiated by opening the jet system solenoid valve. Flow of mixture developed at the nozzle exit and through the spark-gap. The mixture flow rate was pre-selected to provide the desired velocity

profile. The needle valve in the jet delivery system controlled this flow rate. The mass of mixture added by the jet raised the bomb pressure to the firing pressure.

C. ELECTRODE SPACING

Zero spacing of the spark electrodes was determined by connecting an ohmmeter across the electrodes. The gap was reduced until the gap resistance dropped, indicating the electrodes were just touching. The micrometer controlled adjustable electrode was then backed off to set the desired gap relative to the zero gap, .050 in. in this research. This distance was slightly greater than the quench distance for the given electrodes. The quench distance, as measured in Reference (12), was approximately .045 in.

D. MIXTURE-JET VELOCITY MEASUREMENTS

Two aspects of mixture velocity at the nozzle exit were important:

1. The velocity profile of the mixture-jet at the spark-gap.
2. The transient flow characteristics of the mixture-jet when the solenoid valve was actuated, releasing mixture into the bomb.

The velocity profile was measured by traversing a plane parallel to the exit plane of the nozzle with the hot-wire anemometer probe. The traverse pattern is indicated in Figure 12. A modified lathe cross-slide was used to precisely locate the hot-wire in the desired traverse pattern.

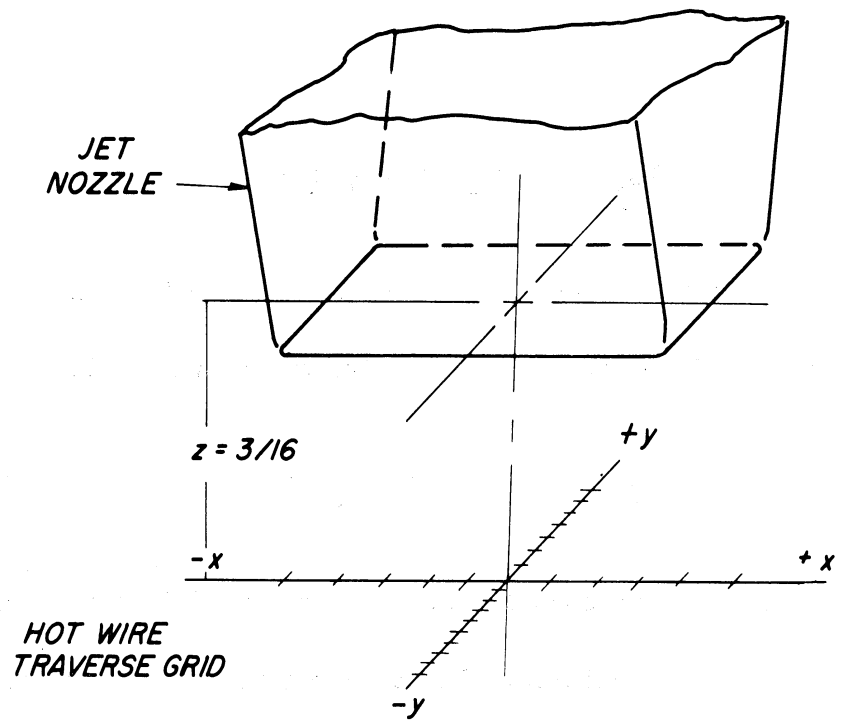

Figure 12. Hot-wire traverse grid for velocity profile measurements.

Air was used as the working fluid in the profile analysis. The hot-wire current $i_{H.W.}$ was determined at each position of the traverse. Jet velocity was indicated by the calibration curve, Figure 53 of Appendix F.

Flow rate was controlled at the precision needle valve. The flow rate was noted as a pressure drop across the mixture delivery system metering orifice and was used to establish the proper flow pattern for combustion experiments.

The transient behavior of the jet upon opening the solenoid valve was measured by observing the unbalance of the hot-wire bridge circuit. The voltage drop across the bridge was displayed on the oscilloscope. The circuit used for this measurement is shown in Figure 48 of Appendix D.

The voltage drop across the bridge with no mixture flow across the hot-wire was:

$$V_{B_3B_4} = i_{HW} \times (R_{27}+R_{HW}) \qquad (4.5)$$

When the mixture began to flow, the resistance of the hot-wire changed and the new voltage drop across the hot-wire bridge was given by:

$$V_{B_3B_4} = i_{HW} \times (R_{27}+R_{HW}+\Delta R_{HW}) \qquad (4.6)$$

When the voltage drop stabilized, this indicated that the flow had reached a steady state condition. The time required to establish steady flow was observed from the oscilloscope trace.

E. SPARK AND COMBUSTION INITIATION—REPRODUCIBILITY MEASUREMENTS

The light intensity of the ignition spark and initial combustion was measured with the aid of the photomultiplier circuit. The important time sequence of the spark and the flame formation was recorded on the oscilloscope.

The procedure with respect to combustion in the bomb was outlined in Section B of Chapter IV.

The photomultiplier power supply voltage was set at approximately 350 volts. This voltage setting was high enough to provide adequate sensitivity but low enough to prevent saturation of the photomultiplier tube.

CHAPTER V

RESULTS

The experiments performed were divided into two general classes:

A. Observation of the system before ignition

B. Analysis of the combustion process

A commentary on the results appears in the following chapter.

A. PHENOMENA STUDIED PRIOR TO IGNITION

Before it was possible to obtain pertinent data for the mixture-jet affected combustion process, two questions were posed pertaining to the characteristics of the different mixture-jets before ignition.

1. What were the velocity profiles of the mixture-jets as a function of nozzle size and flow rate?
2. How long did the mixture-jet take to stabilize at the spark-gap after the electric solenoid valve was opened, and did stabilization occur before bomb ignition?

1. Mixture-Jet Velocity Profile

The velocity of the mixture-jet was measured in a plane parallel to the exit plane of the nozzle. The hot-wire was traversed in this plane according to the grid pattern shown in Figure 12 of Chapter IV. Increments on the long axis (X) were .1 in. and on the short axis (Y) were .01 in.

Two vertical positions of the jet nozzle with respect to the spark-gap were investigated Z = 3/16 and 3/8 in.

Results of this part of the experiment are shown in Figures 13 through 18 for a jet nozzle to hot-wire distance of Z = 3/16 in. Velocity profile curves are shown for the small, medium, and large nozzles.

The peak mixture-jet velocity on the Y-axis profile (V_j) was selected to characterize the velocity profile of a given jet and served as a measure of jet intensity.

As shown by Figures 13, 15, and 17, the mixture jet velocity profiles were not obtained for the same peak flow velocities. Therefore it was necessary to control the flow rates from each nozzle to provide a comparable set of velocity profiles for the combustion experiments. To facilitate this control the mixture flow rate (indicated as metering orifice pressure drop) was plotted against the Y-axis peak profile velocity for each nozzle (Figure 19). By interpolating these curves it was possible to select a series of flow rates for each nozzle which provided an identical set of peak profile velocities (V_j = 1, 3, 5, and 7 ft/sec).

2. Mixture-Jet Starting Transient

As described earlier, the time required to establish steady flow at the spark-gap after energizing the solenoid was measured by the hot-wire bridge unbalance. Two sample photographs from this study are shown in Figure 20. The results for all three nozzles and a wide range of flow rates are given in Table I.

The time required for the bomb pressure to attain the firing pressure was calculated using the perfect gas relationship, $\rho = P/RT$, and the cali-

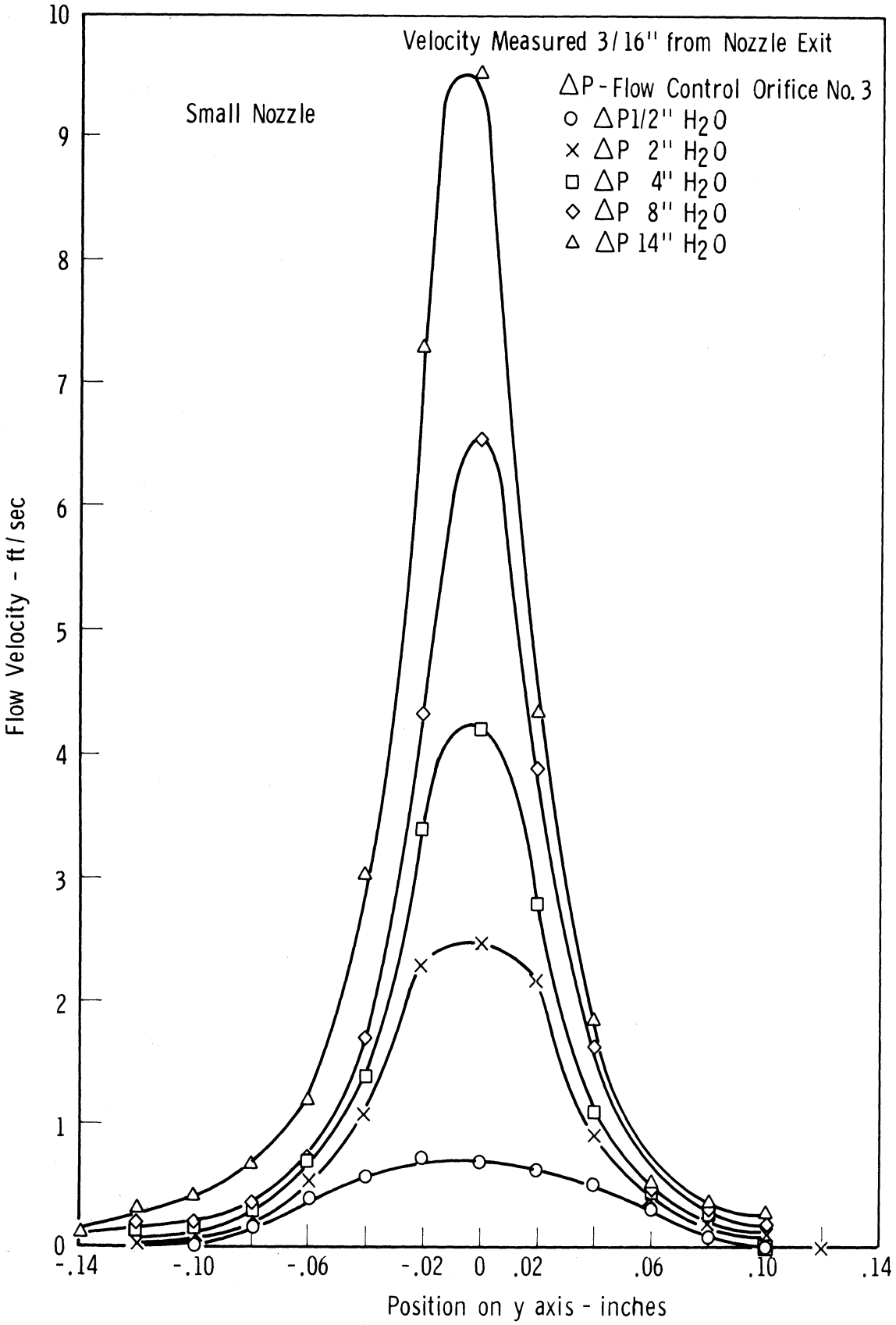

Figure 13. Mixture jet-velocity profile on Y axis.
Small nozzle: .026 in. width.

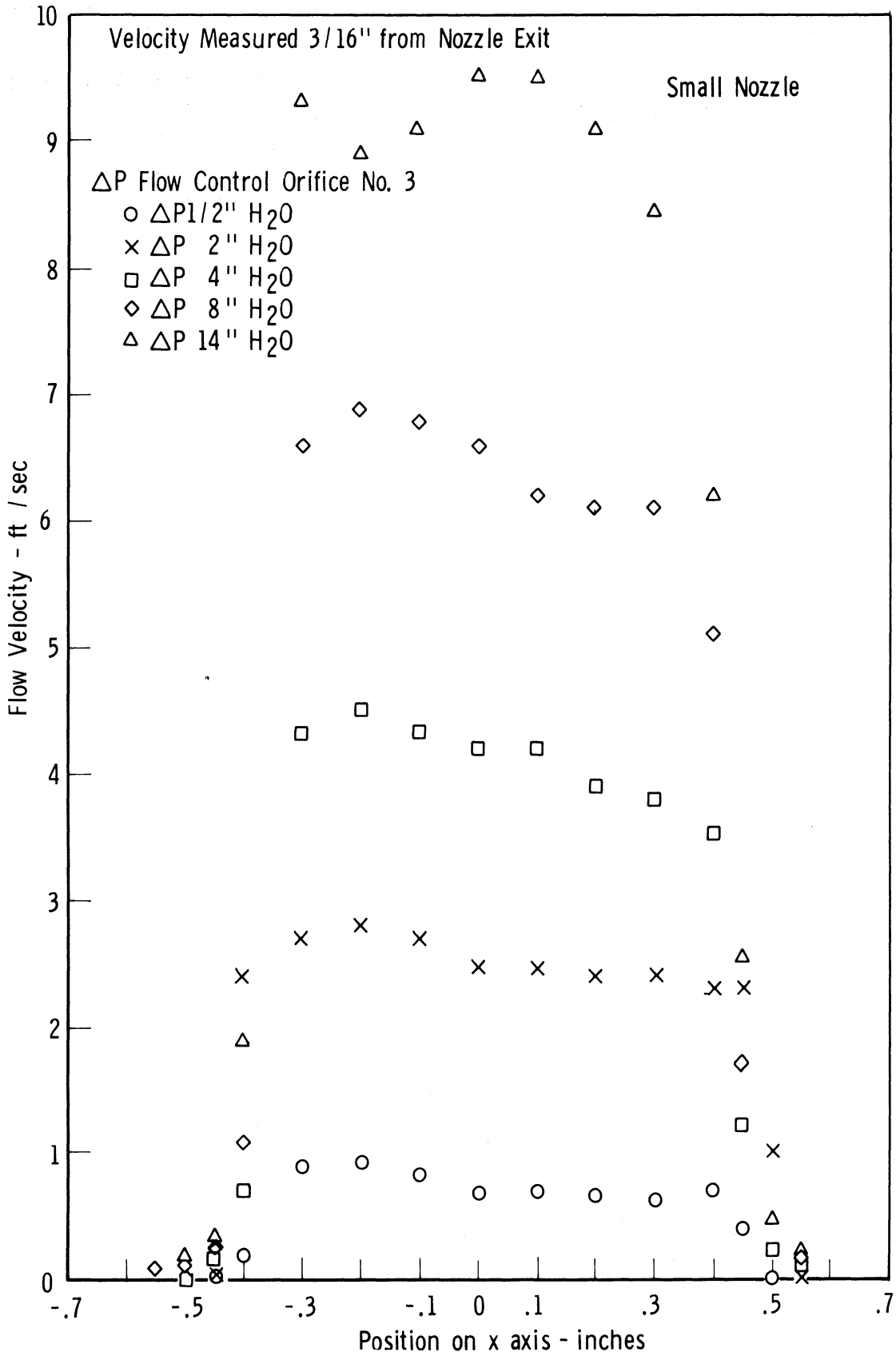

Figure 14. Mixture jet-velocity profile on X axis.
Small nozzle: .026 in. width.

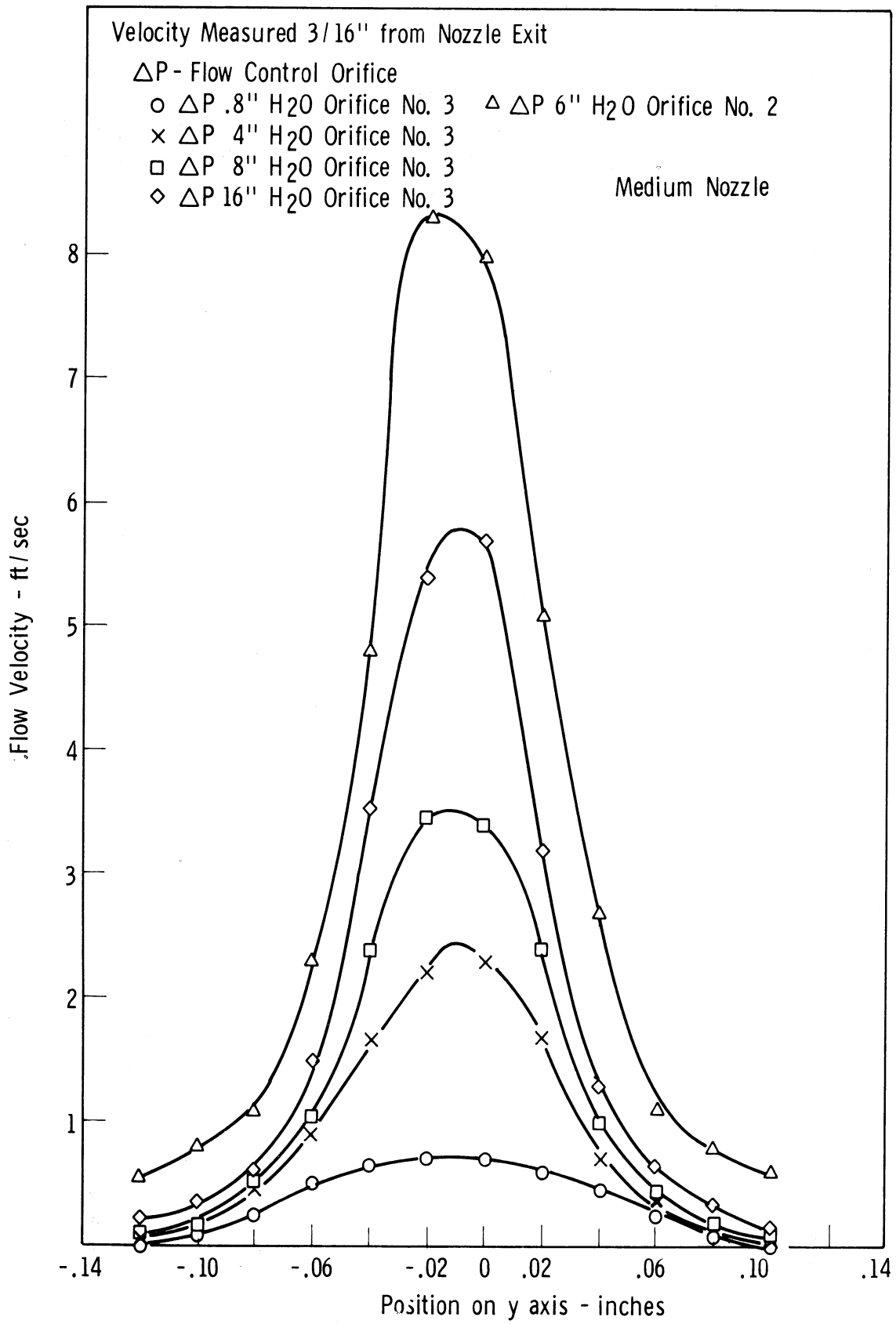

Figure 15. Mixture jet-velocity profile on Y axis.
Medium nozzle: .066 in. width.

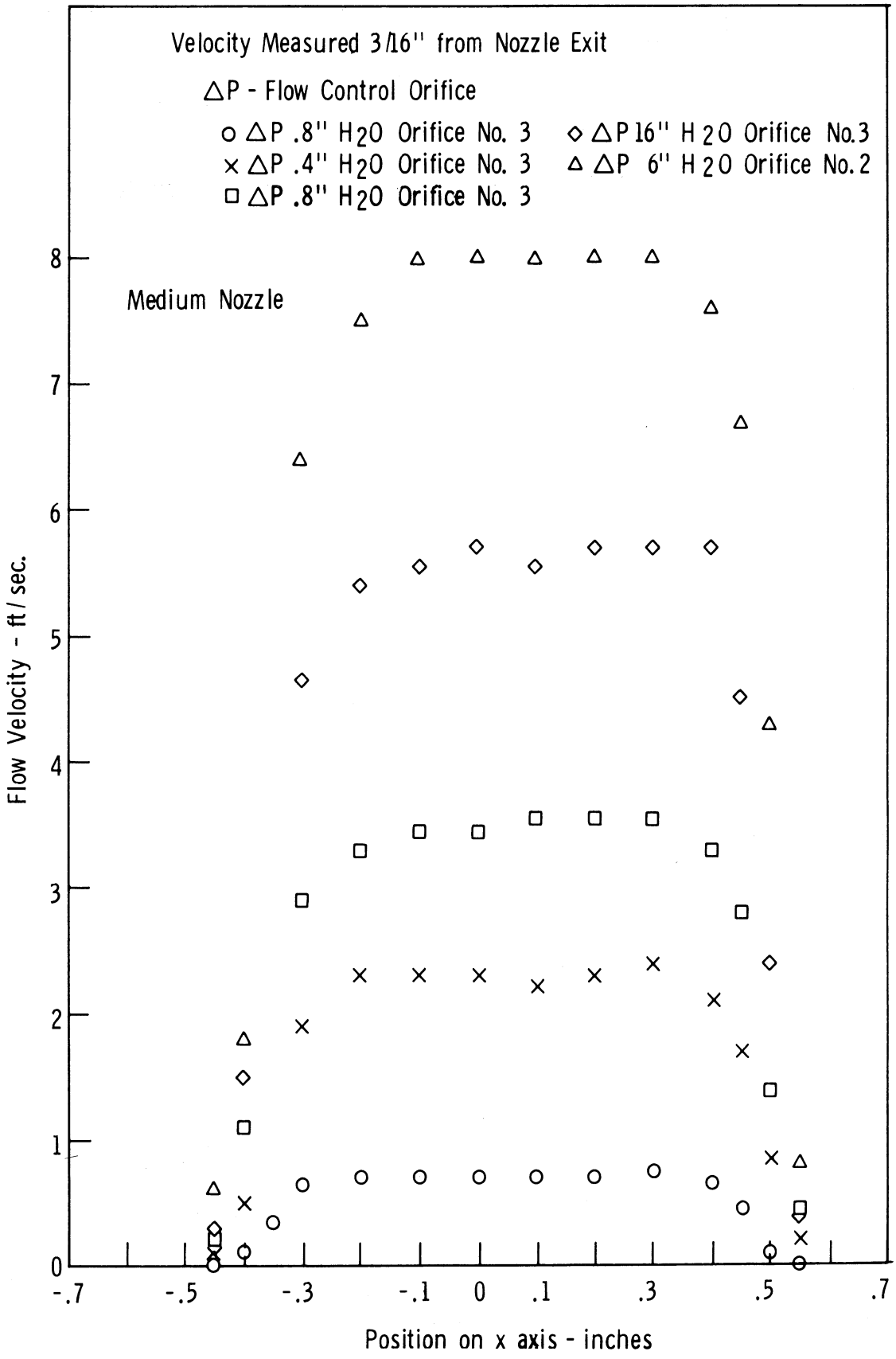

Figure 16. Mixture jet-velocity profile on X axis.
Medium nozzle: .066 in. width.

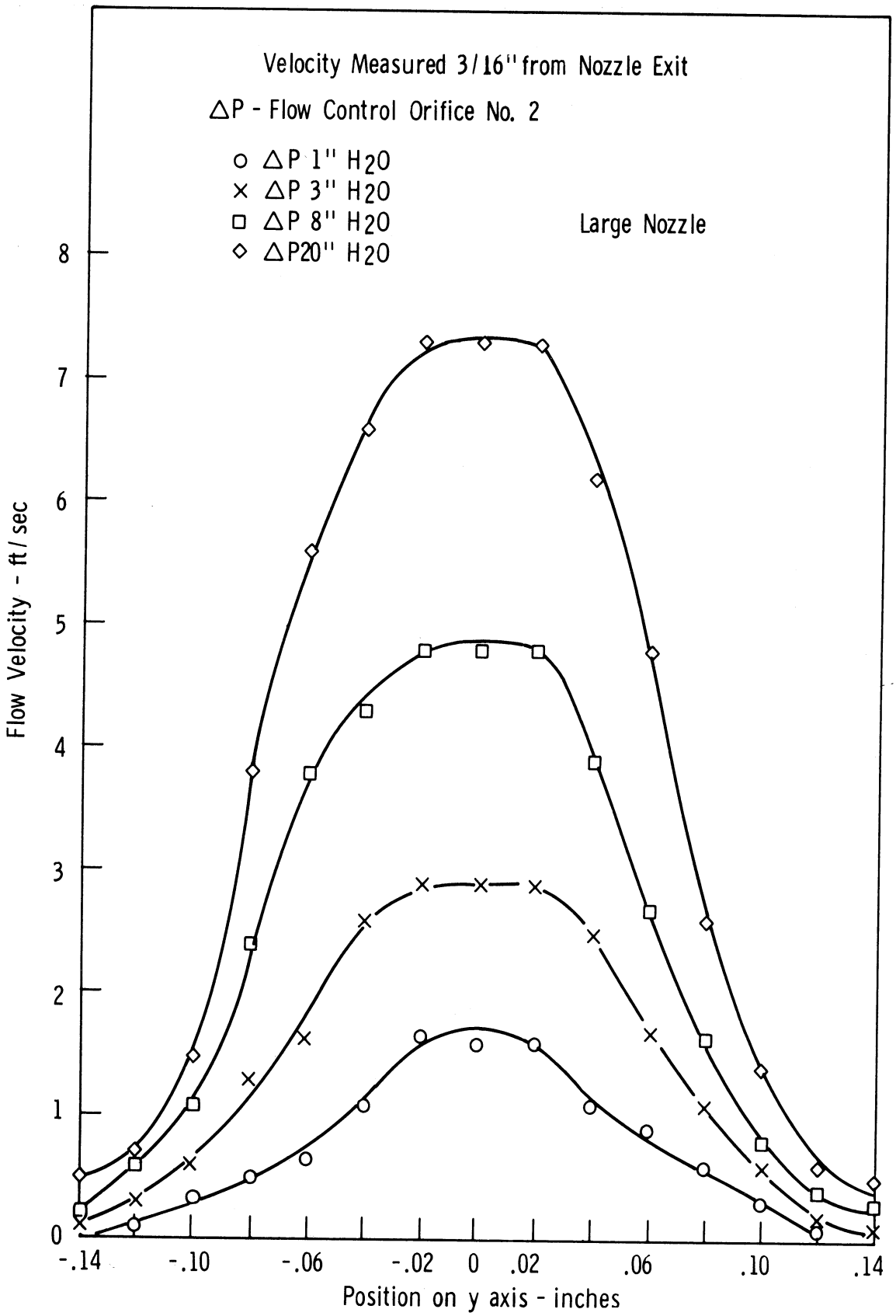

Figure 17. Mixture jet-velocity profile on Y axis.
Large nozzle: .156 in. width.

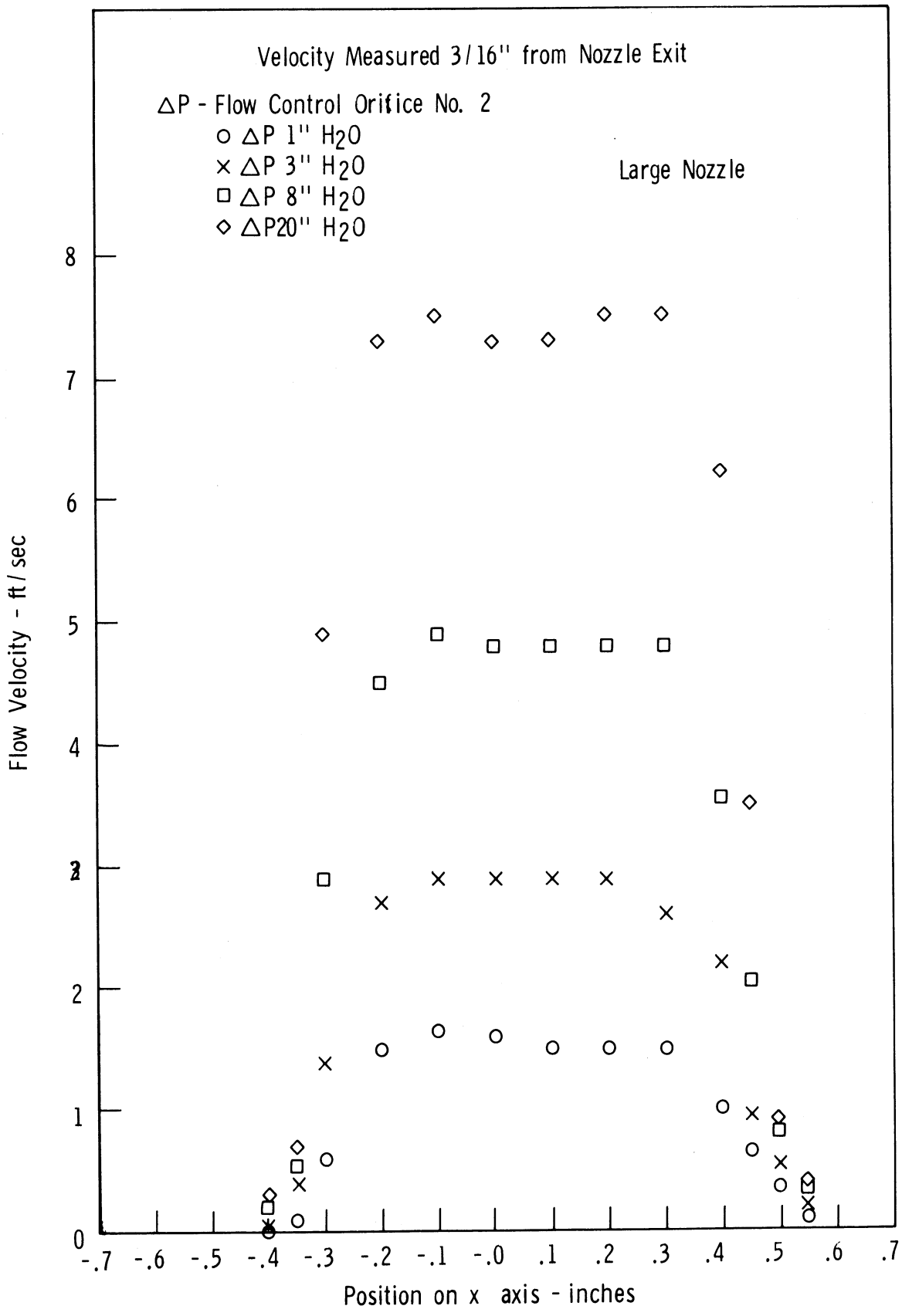

Figure 18. Mixture jet-velocity profile on X axis.
Large nozzle: .156 in. width.

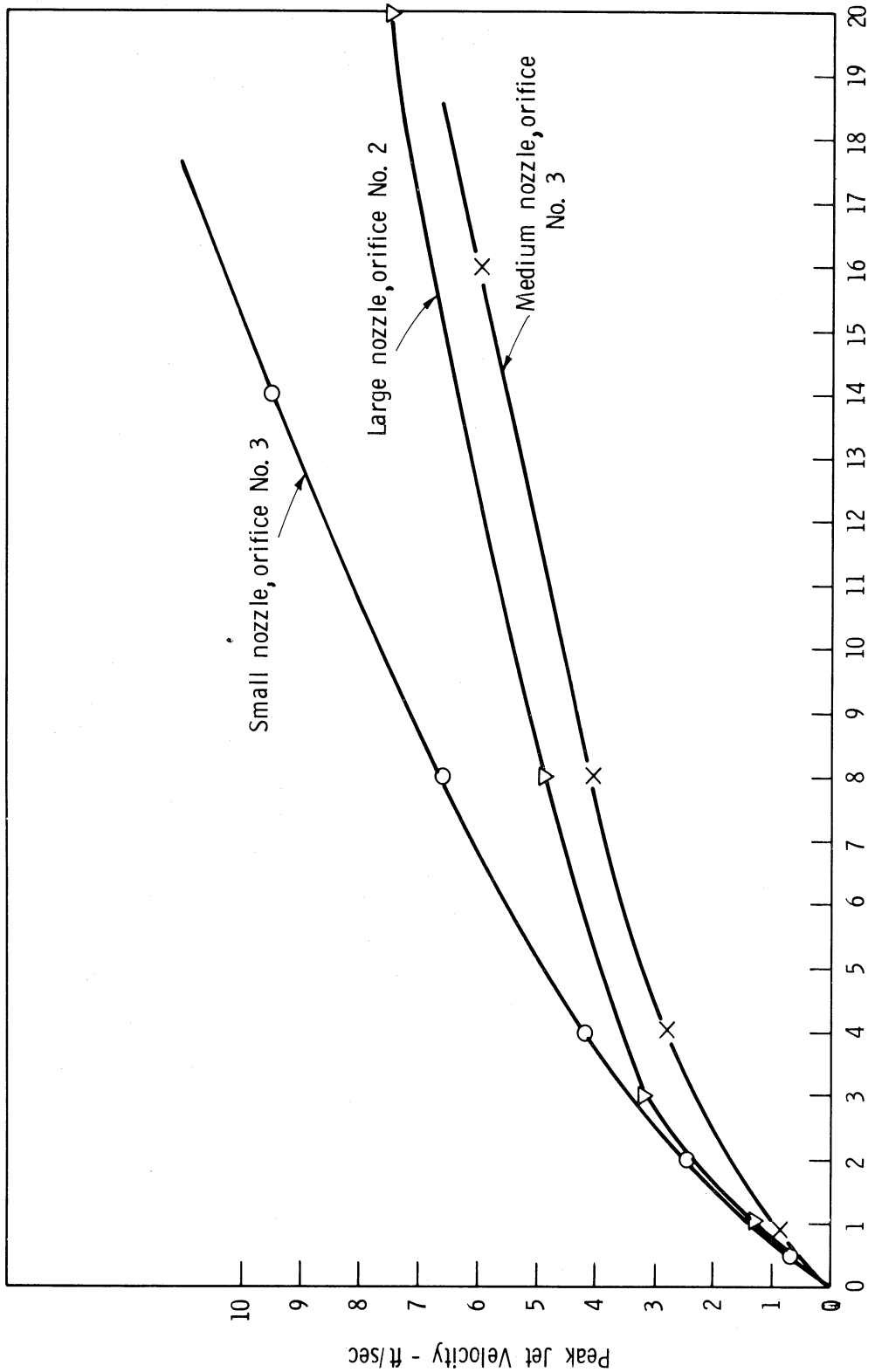

Figure 19. Peak mixture-jet profile-velocity vs. metering orifice pressure drop.

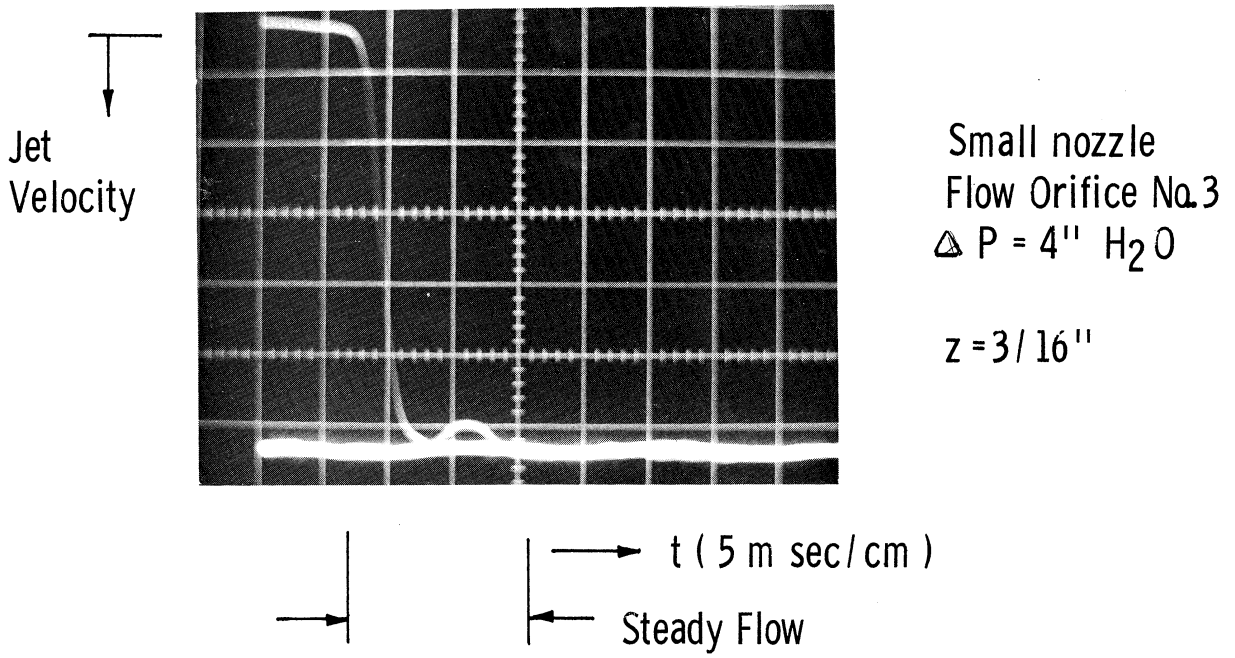

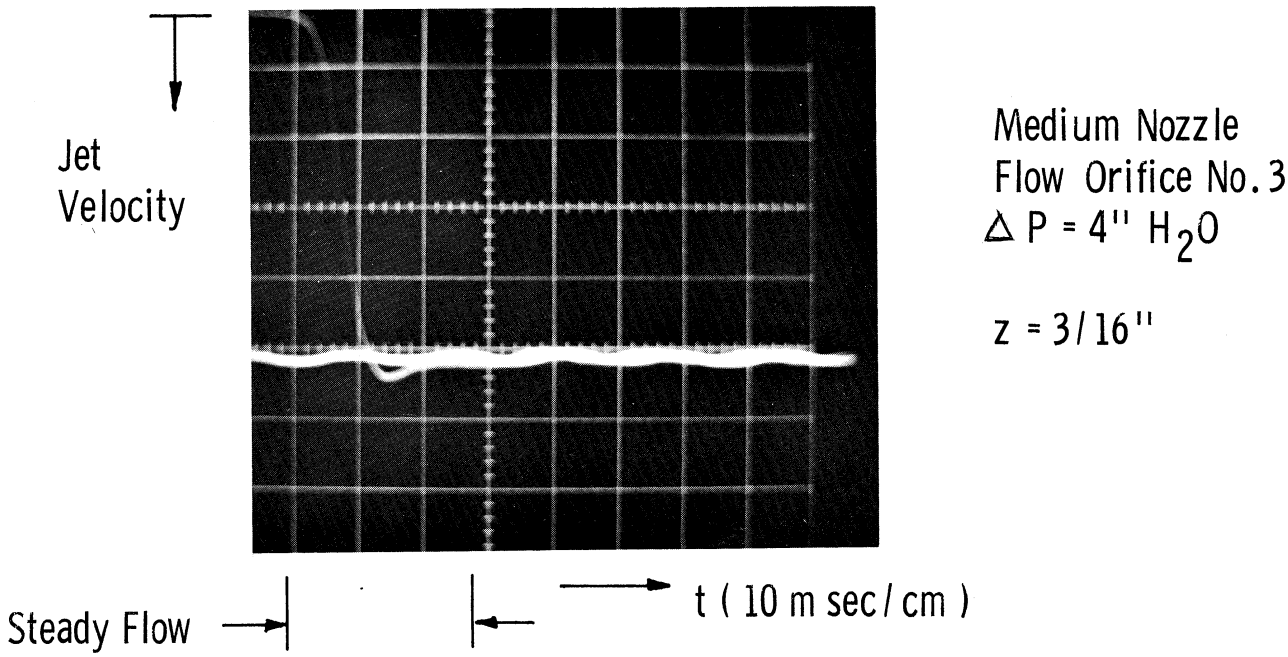

Figure 20. Sample data—time required for mixture jet to attain steady flow.

brated flow rate of the mixture-jet system. The initial pressure in all motion-disturbed combustion studies was 29.1 in. of mercury. The balanced pressure which triggered the ignition spark was set at 29.5 in. of mercury. Thus, when the mixture-jet increased the bomb pressure by .4 in. of mercury, ignition occurred. The jet was assumed added at an average pressure of 29.3 in. of mercury. The temperature was assumed constant at 80°F. The mixture mass addition providing the required pressure rise was then calculated. By observing the flow rate for a given orifice pressure drop in the mixture-jet system the time delay to ignition was calculated. The results of these calculations are also shown in Table I.

TABLE I

TIME REQUIRED FOR MIXTURE JET TO ATTAIN STEADY FLOW AND TIME REQUIRED FOR MIXTURE JET TO TRIGGER COMBUSTION

	Measured from Solenoid Switching			
	Flow Rate, ΔP "H_2O	Flow Orifice No.	Time to Steady Flow, msec.	Time to Bomb Ignition, msec
I. Small Nozzle	1/2	3	180	524
	2	3	31	240
	4	3	13	168
	8	3	11	116
	14	3	9	88
II. Medium Nozzle	8	3	120	364
	4	3	25	168
	8	3	16	116
	16	3	8	82
	6	2	6	62
III. Large Nozzle	1	2	44	151
	3	2	31	85
	8	2	20	53
	20	2	18	

B. COMBUSTION

The second experimental phase involved analysis of the actual combustion process. Before investigating the effect of mixture flow on the flame kernel several studies were made to answer other important questions.

1. How reproducible was the bomb spark and the formation of the initial flame?
2. How reproducible was the combustion process in the desired region of study?

1. Reproducibility of Spark and Early Combustion

The first of these studies was performed with the light-sensitive photomultiplier. An example of the data obtained is shown in the photographs of Figures 21 and 22.

Figure 21 shows the light intensity trace of eight consecutive ignition sparks. The following observations were made:

a. The ignition spark occurred .09 ± .01 millisecond after the oscilloscope triggered.

b. The sparks lasted .60 millisecond ± .02 millisecond.

c. The light intensity of the sparks varied slightly.

Figure 22 shows the light intensity from the ignition spark and early combustion for a single reaction. By extrapolating the combustion light trace to the no light reference line the approximate time of the initial flame appearance may be noted. The delay time measured from

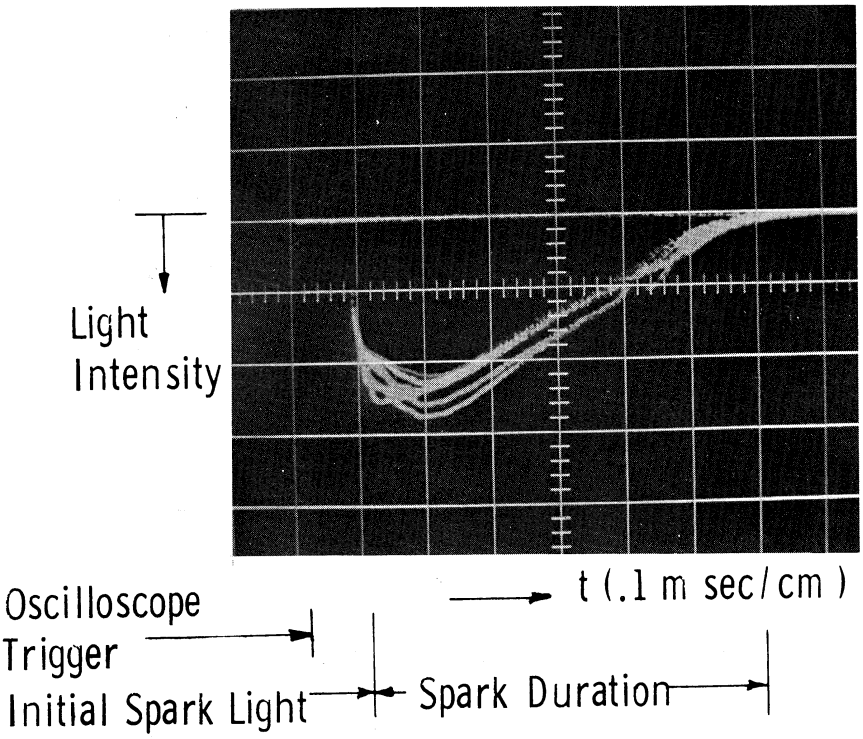

Figure 21. Light intensity of the ignition spark—8 sparks.

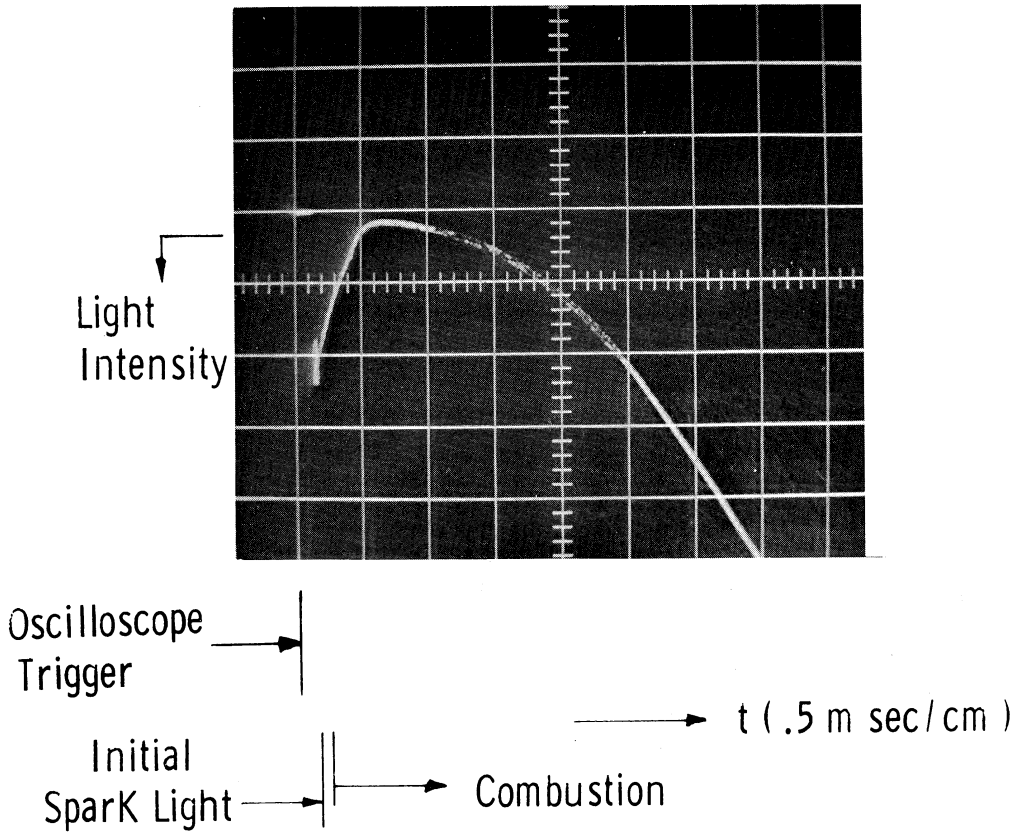

Figure 22. Light intensity of the ignition spark and initial flame formation.

oscilloscope triggering for a number of traces varied from .20 to .30 millisecond. Since the initial spark delay was approximately .09 msec, the combustion delay as measured by light emission was .10 to .20 millisecond. It must be emphasized that these results involved a certain degree of "eyeballing", and thus may be in error by as much as .05 millisecond.

The light study of the flame kernel formation was corroborated by another technique. Schlieren pictures were taken of the early flame development. Successive runs were made with decreasing time delays between ignition and the flame photograph until no visible flame kernel was observed.

One result of this study is shown in Figure 23. This photograph taken .24 millisecond after the trigger pulse or about .16 millisecond after the appearance of the spark shows the earliest observed flame kernel.

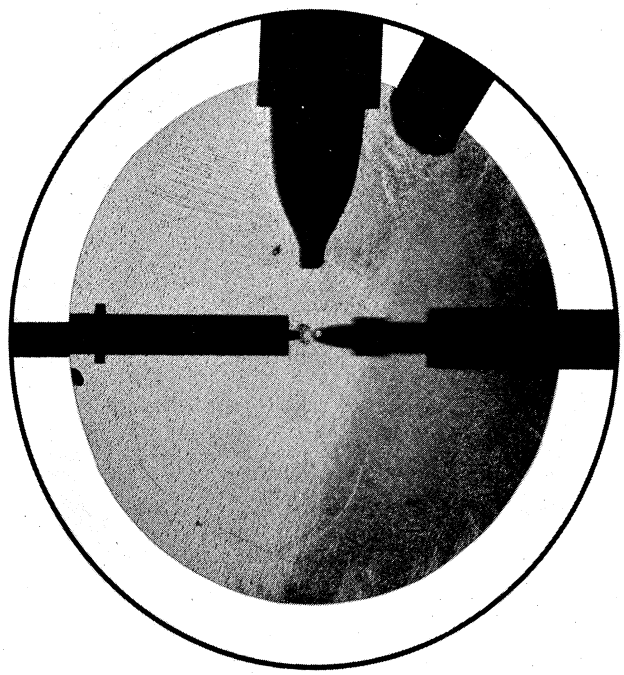

Figure 23. Schlieren photograph of initial flame kernel (.16 millisecond after ignition).

The kernel has been artifically darkened in the photograph to facilitate observation. An earlier picture taken .15 msec after oscilloscope triggering showed no indication of a flame kernel. This was about .07 millisecond after the appearance of the spark. Thus, the combustion delay with respect to the ignition spark was between .07 and .16 millisecond.

2. Reproducibility of the Combustion Process

Repeatability studies were made in order to establish a baseline which uses the flame development in a quiescent mixture. It was also necessary to determine how representative one or several combustion runs were of a great number of runs. The flame front was studied in detail 9.5 millisecond after ignition. This time reference was selected because it was early in the pressure development (about 10% of maximum pressure), it was in a region of measurable pressure rate and the flame kernel was of convenient size.

A series of 51 combustion runs was observed. The results are plotted in the frequency distribution shown in Figure 24. The rate of pressure rise (dP/dt) is indicated in centimeters deflection of the oscilloscope trace. The computation of the mean and standard deviation are included in Appendix H. The distribution is assumed to be normal. The mean pressure rate was 5.05 centimeters, or .89 psi/millisecond. The standard deviation was .213 centimeter, or .037 psi/millisecond—only 4% of the mean value.

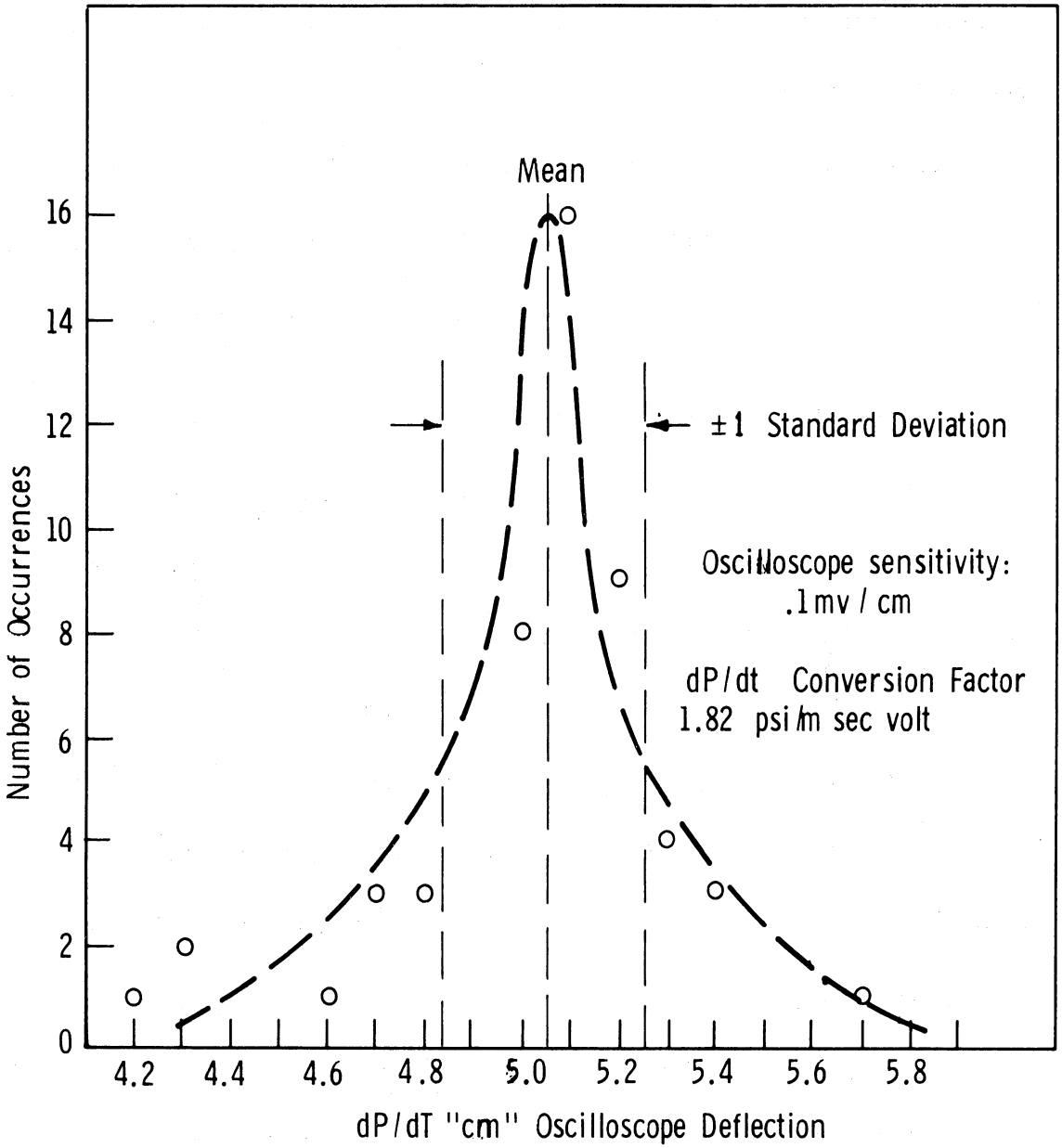

Figure 24. Frequency distribution—rate of pressure rise for combustion in a quiescent mixture—9.5 msec after ignition.

Another indication of the excellent reproducibility is shown in Figures 25 and 26. Figure 25 shows pressure rate versus time for two combustion runs in a quiescent mixture. Only in the latter combustion stages, which were of little interest in this study, was there any noticeable difference. The "hash" at the origin of the trace is caused by ignition spark noise.

In Figure 26 traces of pressure versus time are shown. There is no discernible variation for the four combustion runs observed; they appear as a single trace.

3. Mixture Motion Influence on Combustion

Once the background was firmly established, the experiments of primary interest were performed to answer the fundamental question. What is the effect of directed mixture motion on the flame kernel development in a constant volume bomb?

As described in detail earlier, this study was performed by impinging a jet of fuel/air mixture on the spark-gap. The jet was varied in both scale and intensity. The effect of the jet on the combustion front was observed.

A summary of the important experimental conditions for the study is shown in Table II. Sample photographs of combustion 9.5 millisecond after ignition are shown in Figures 27, 28, and 29 for the

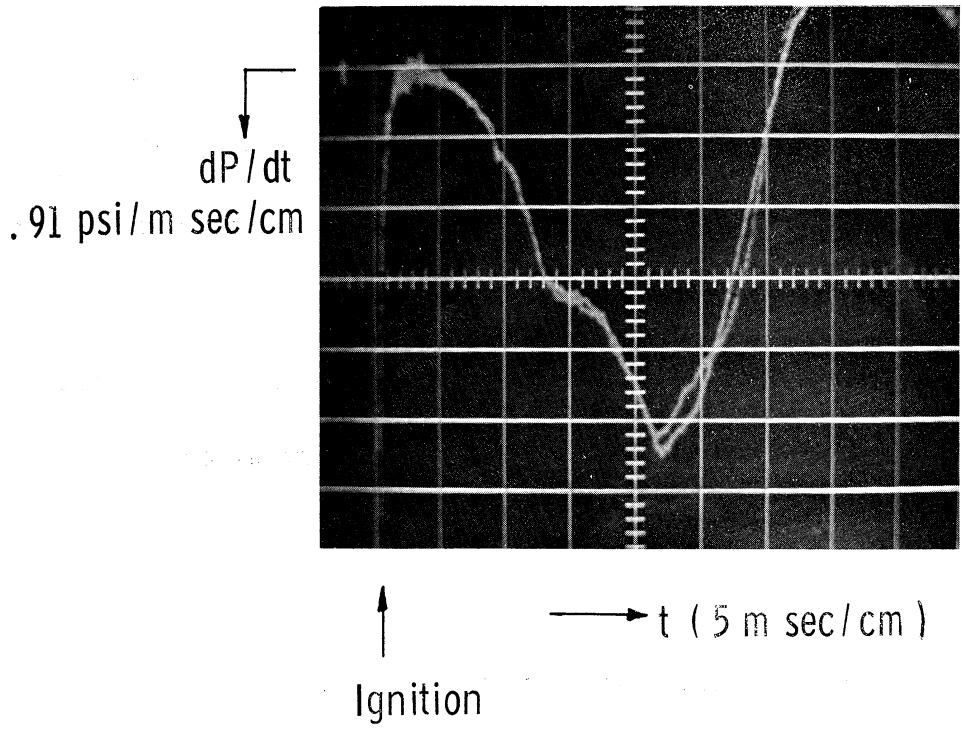

Figure 25. Reproducibility of pressure rate—2 runs quiescent mixture.

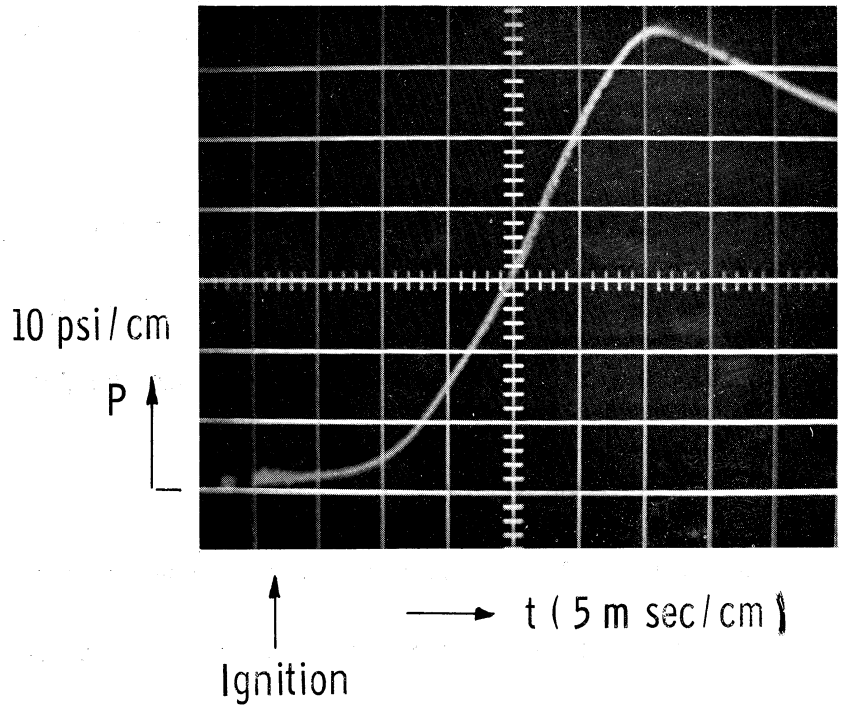

Figure 26. Reproducibility of pressure rate—4 runs quiescent mixture.

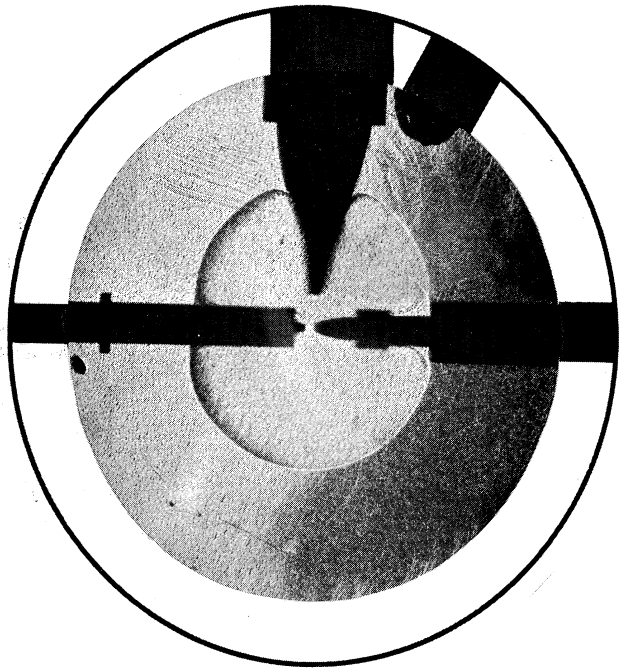

dP/dt = 4.8 cm = .86 psi/m sec
V_{Jet} = 0

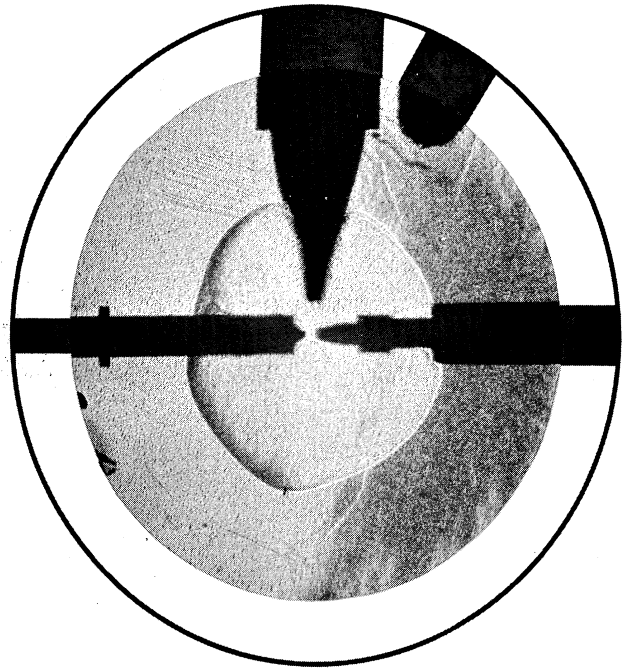

dP/dt = 5.4cm = 1.00 psi/m sec
V_{Jet} = 3 fps

Figure 27. Schlieren photographs—small jet nozzle, 9.5 msec after ignition.

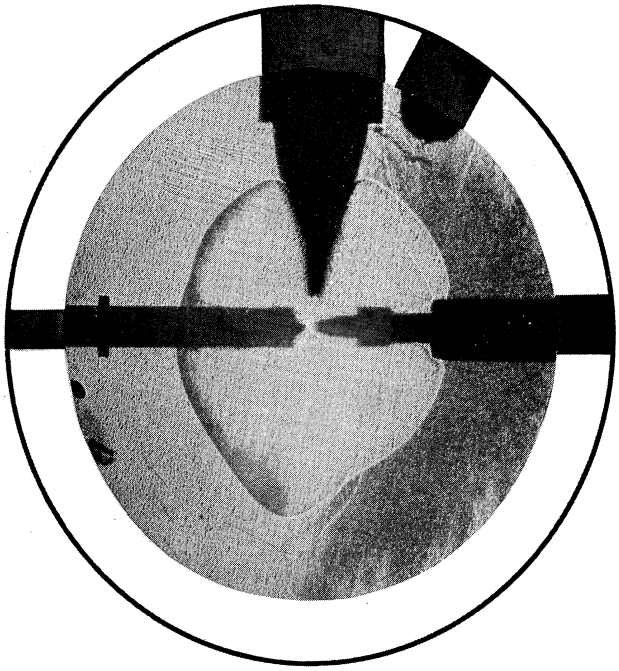

dP/dt = 5.9 cm = 1.07 psi/m sec
V_{Jet} = 5 fps

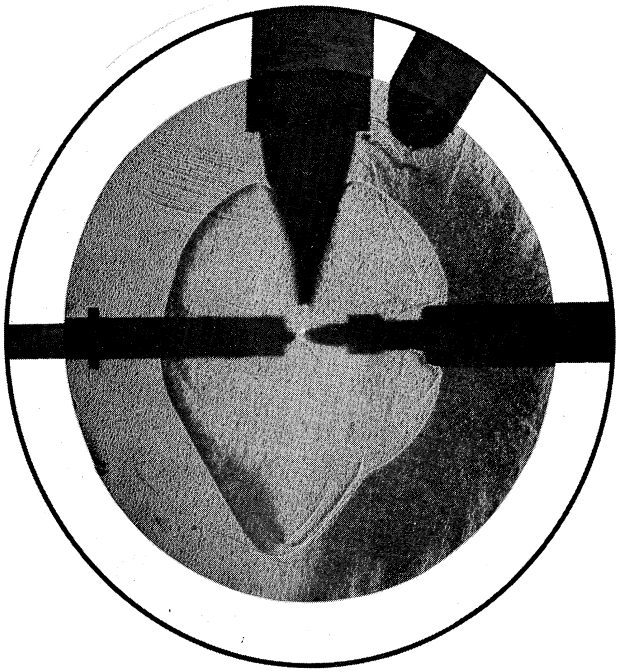

dP/dt = 6.7 cm = 1.20 psi/m sec
V_{Jet} = 7 fps

Figure 27. Concluded.

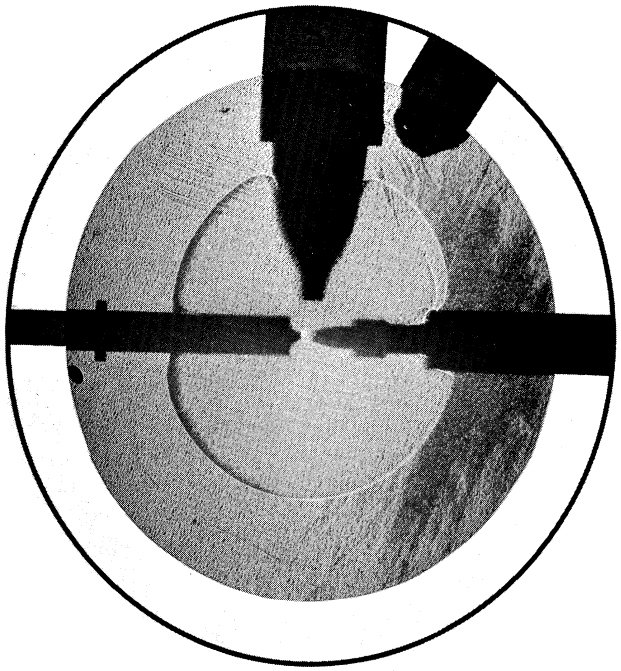

dP/dt = 5.1 cm = ≒90 psi/m sec
V_{Jet} = 0

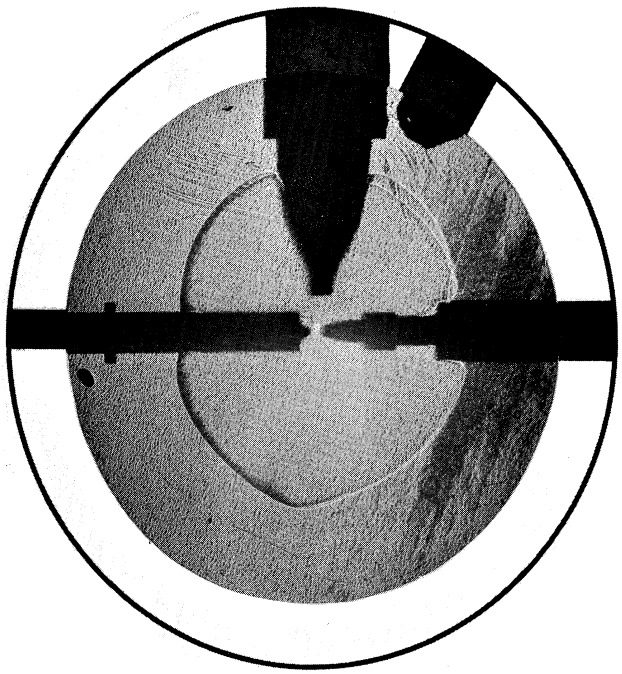

dP/dt = 5.9 cm = 1.07 psi/m sec
V_{Jet} = 3 fps

Figure 28. Schlieren photographs—medium jet nozzle, 9.5 msec after ignition.

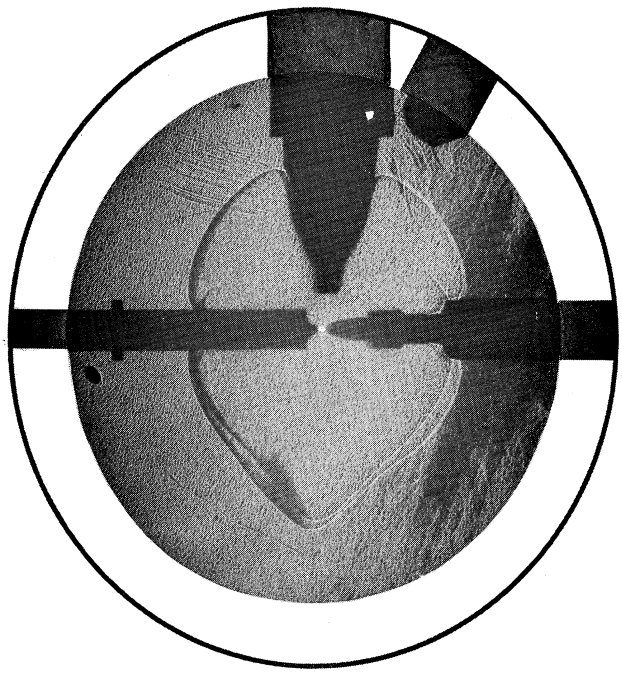

dP/dt = 6.7 cm = 1.21 psi/m sec
V_{Jet} = 5 fps

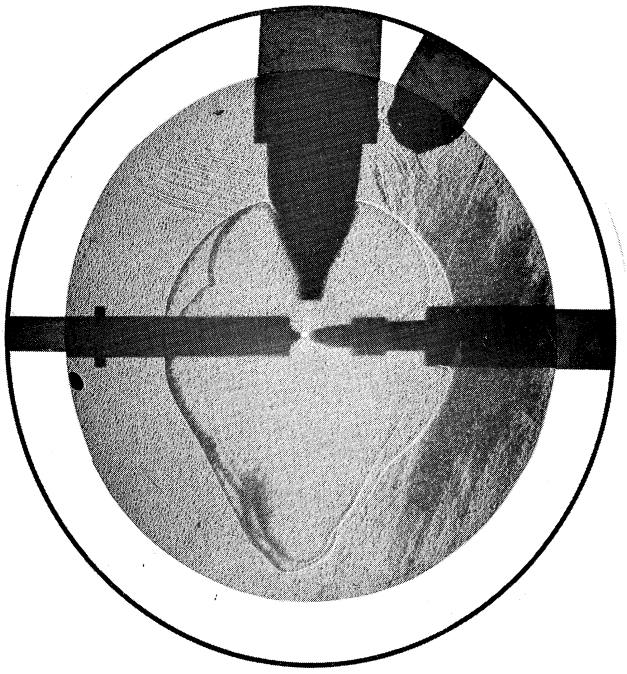

dP/dt = 7.2 cm = 1.30 psi/m sec
V_{Jet} = 7 fps

Figure 28. Concluded.

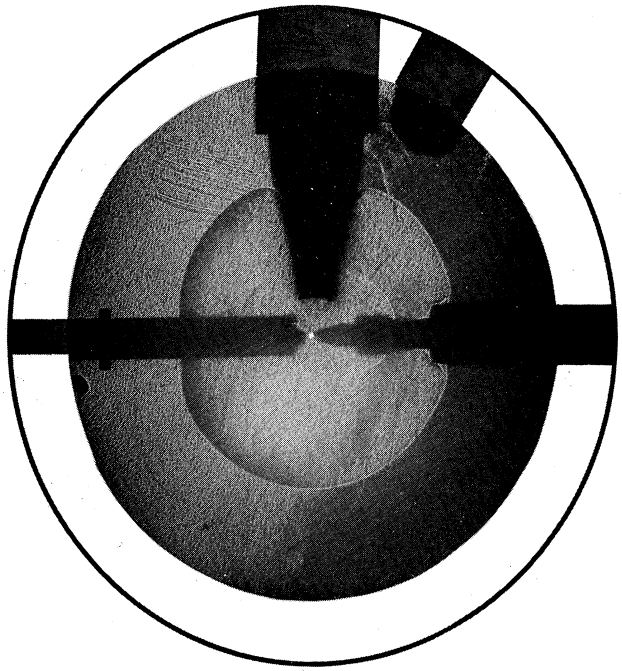

dP/dt = 5.1 cm = .90 psi/m sec.
$V_{Jet} = 0$

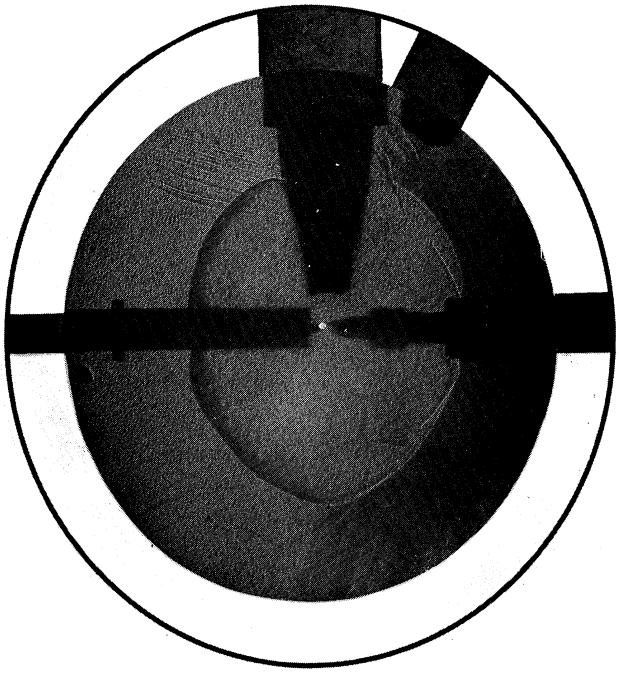

dP/dt = 5.5 cm = 1.02 psi/m sec
$V_{Jet} = 3$ fps

Figure 29. Schlieren photographs—large jet nozzle, 9.5 msec after ignition.

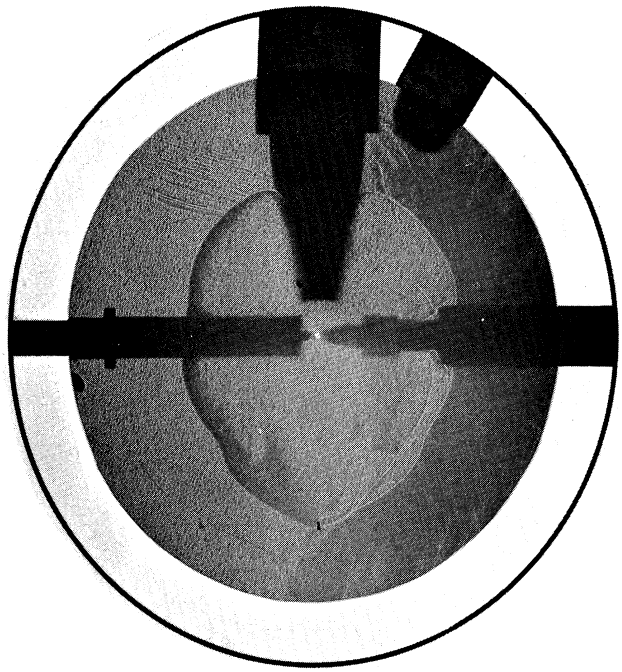

dP/dt = 5.8 cm = 1.05 psi/m sec
V_{Jet} = 5 fps

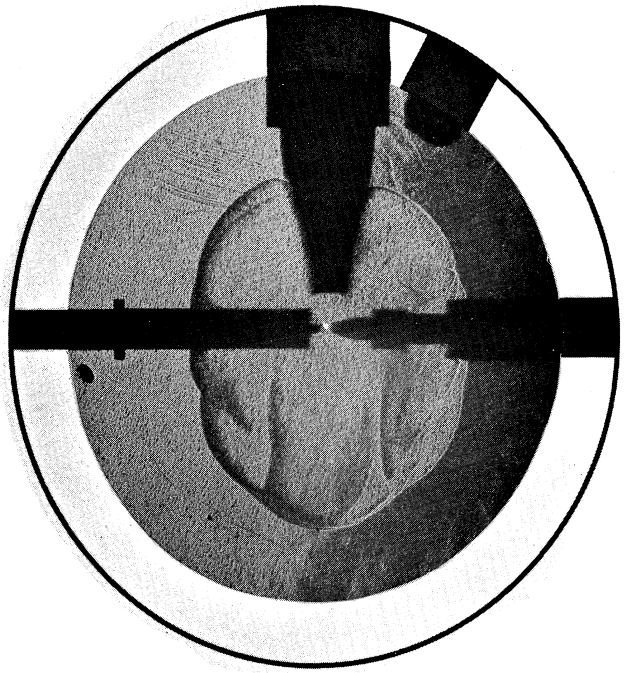

dP/dt = 6.2 cm = 1.12 psi/m sec
V_{Jet} = 7 fps

Figure 29. Concluded.

three different jet nozzles. Combustion with peak-profile jet velocities of 3, 5, and 7 ft/sec, as well as combustion in a quiescent mixture are shown. The flame front with a jet velocity of 1 ft/sec was almost identical to the flame front in the quiescent mixture and hence is not shown. The rate of pressure rise (dP/dt), indicated in centimeters scope deflection and psi per millisecond, is indicated below the appropriate picture.

TABLE II

SUMMARY OF EXPERIMENTAL CONDITIONS

Jet Flow-Spark Gap Velocity at (0,0) Position, ft/sec	Nozzle Size, in. (d)		
	Small	Medium	Large
0	.026	.066	.156
1	.026	.066	.156
3	.026	.066	.156
5	.026	.066	.156
7	.026	.066	.156

Mixture Nozzle Exit to Spark Gap: Z = 3/16 in.
Mixture Initial Temperature: 80°F
Mixture Ignition Pressure: 29.5 in. of mercury
Spark Coil Primary Current: 5 amperes
Spark Gap: .050 in.
Relative Fuel/Air Ratio: 1.0
Fuel: Propane (C_3H_8)

A sample data sheet is presented in Appendix I. Sample pictures of the pressure rate data (dP/dt vs. t) are shown in Figure 30 for several flow conditions with the medium nozzle. The discontinuity at the right side of each picture indicates the time of flame photographing. The high frequency oscillation is caused by electrical noise.

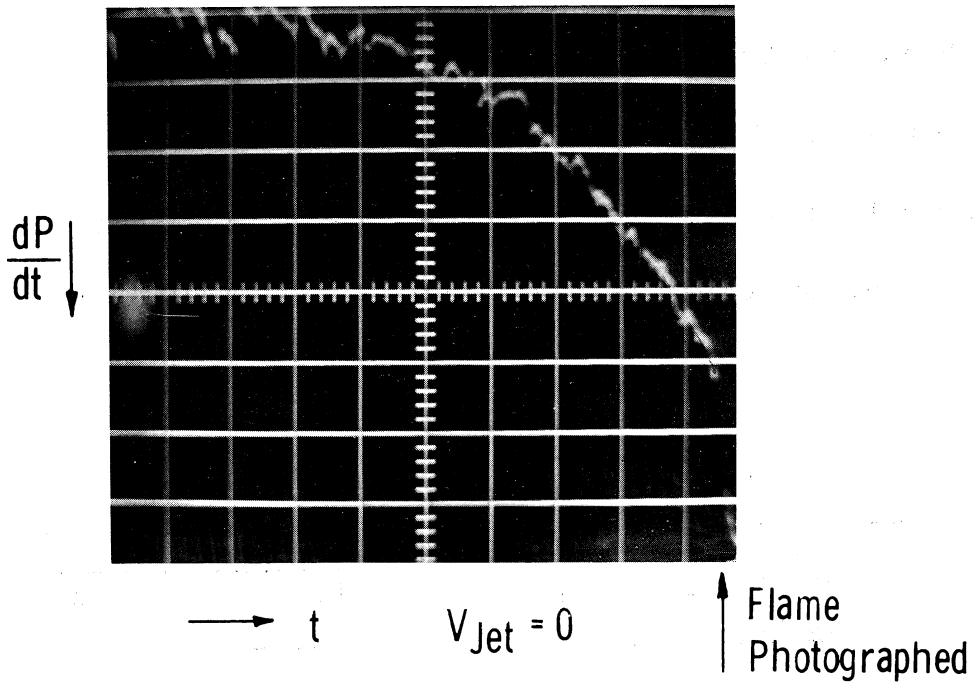

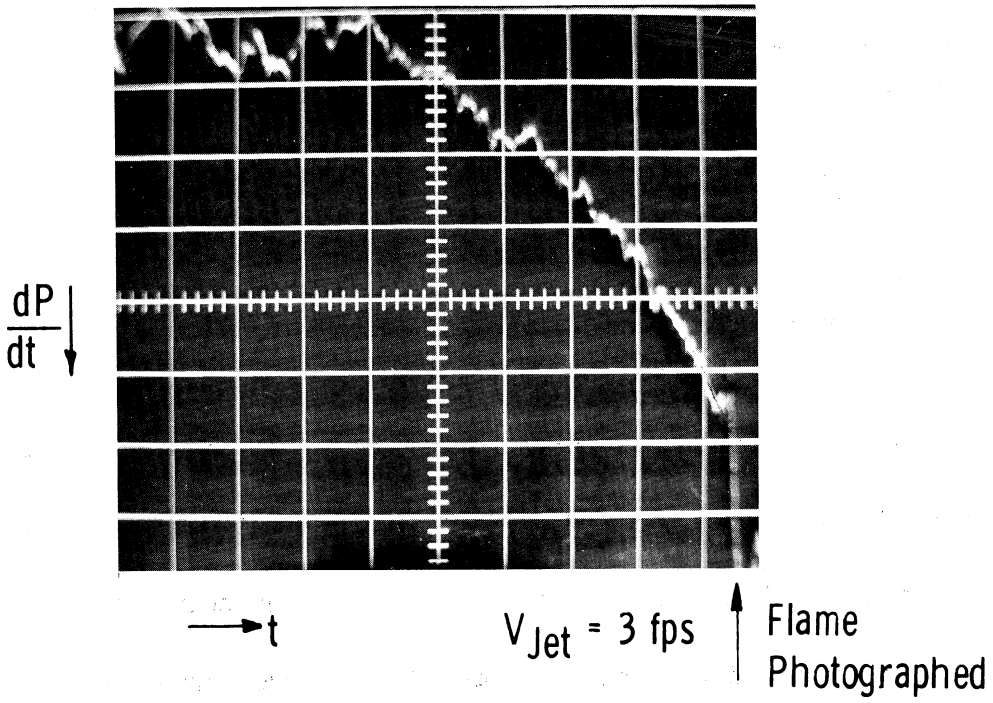

Figure 30. Rate of pressure rise vs. time—medium nozzle.

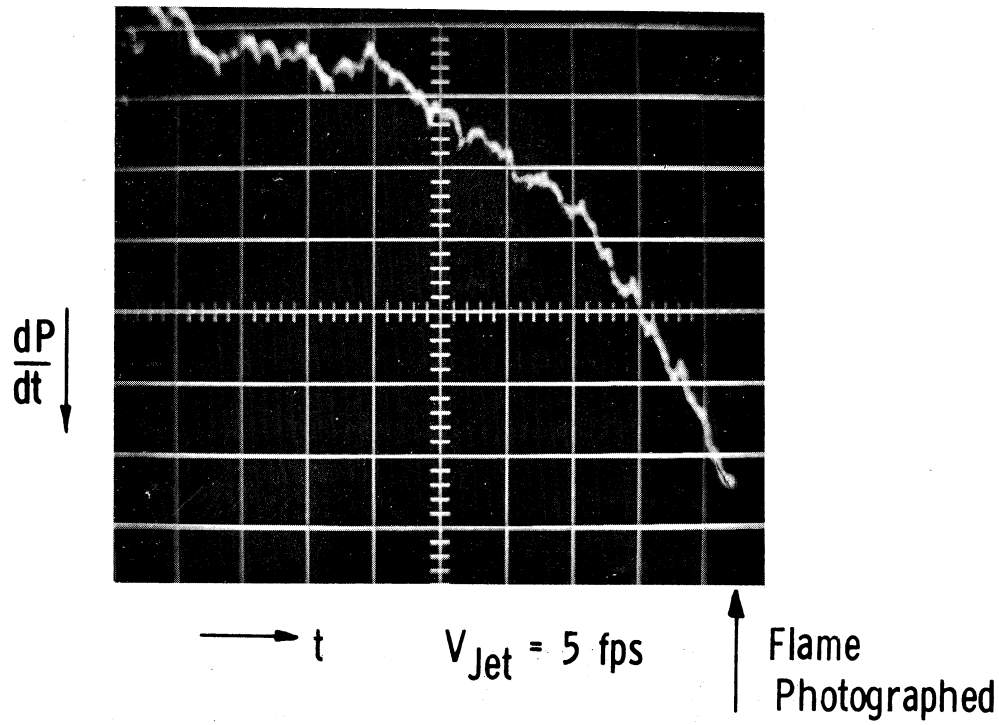

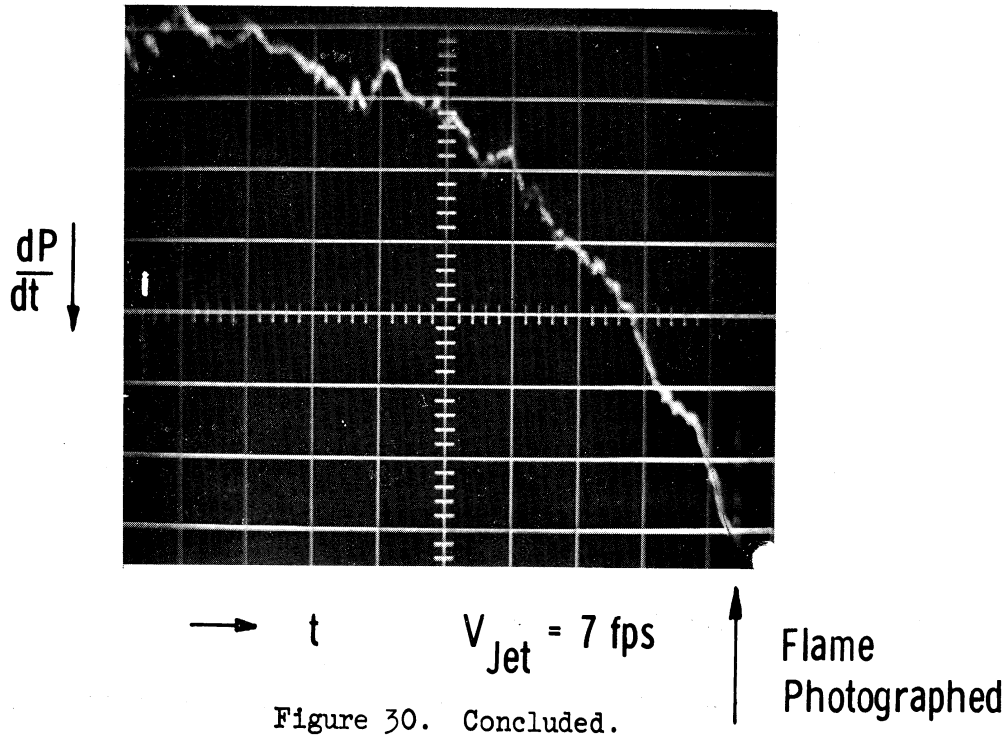

Figure 30. Concluded.

The effect of mixture flow on the developing flame kernel is shown qualitatively by the pressure traces in Figure 31. The right curve is for combustion in a quiescent mixture. Increasing the jet velocity moves the pressure trace to the left. The curve on the far left resulted from a 10 ft/sec mixture jet velocity.

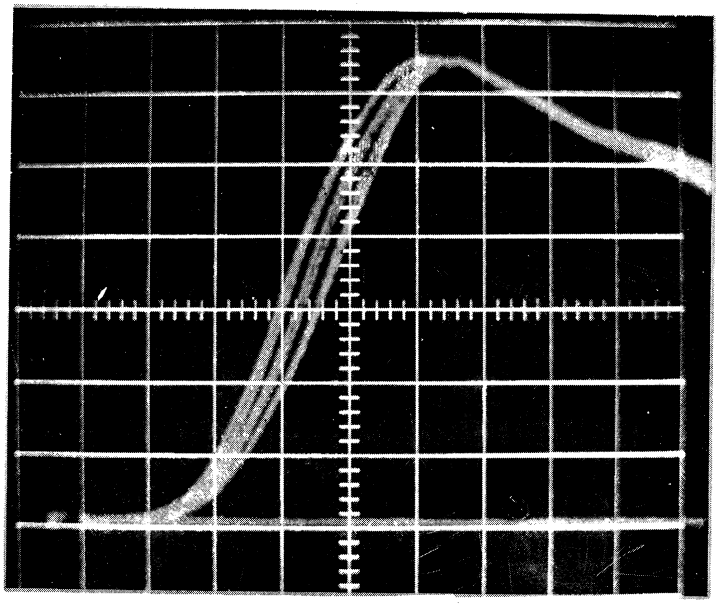

Figure 31. Pressure traces for runs with different mixture-jet velocities.

4. Sequential Combustion Studies

Schlieren photographs of the flame front were taken at varying time intervals after ignition to evaluate the nature of the flame front throughout the combustion process and to determine the flame spatial velocity, which could then be compared to the mixture-jet velocities used.

Pictures where taken which showed:

1. The effect of the directed mixture motion on flame development in its early stages.
2. The flame development in a quiescent mixture from the initial flame kernel through complete combustion.

The flame front was studied under the influence of mixture-jets from the medium and large nozzles. A peak profile jet velocity of 5 ft/sec was used. These two nozzles were selected because they exhibited different rates of pressure rise 9.5 millisecond after ignition. An explanation for the observed difference in rate of pressure rise was sought qualitatively from analysis of the early flame shape. The results are shown in Figures 32 and 33. Pictures were taken at different time intervals during the first 6 milliseconds of four successive combustion runs.

Combustion in the quiescent mixture was photographed beginning 1.6 millisecond after ignition. This study examined the spatial velocity of the flame throughout combustion. The sequential series of photographs are shown in Figure 34. Each picture is keyed to the pressure-time trace shown.

Continuous schlieren streak photographs provided an additional technique for the measurement of flame spatial velocity. An example for one run is shown in Figure 35. A point on the lower flame front surface was observed in its travel from the spark-gap down to the lower cylinder wall. The slope of the trace is equal to the flame

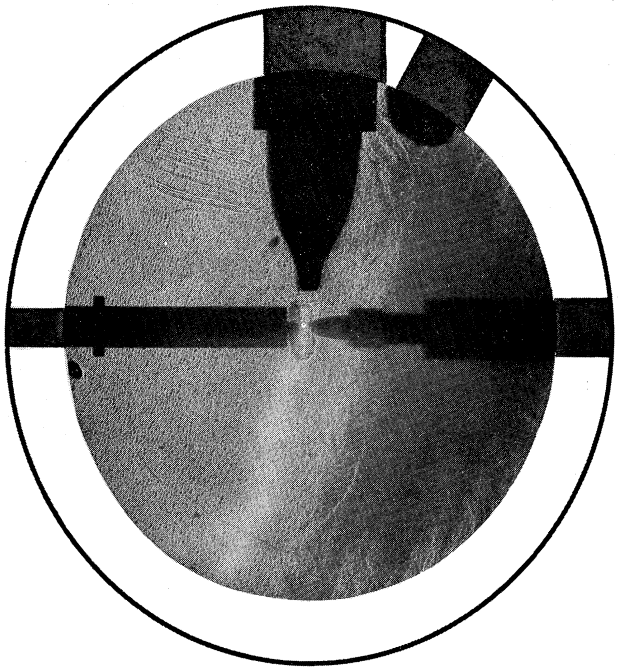

1.6 msec

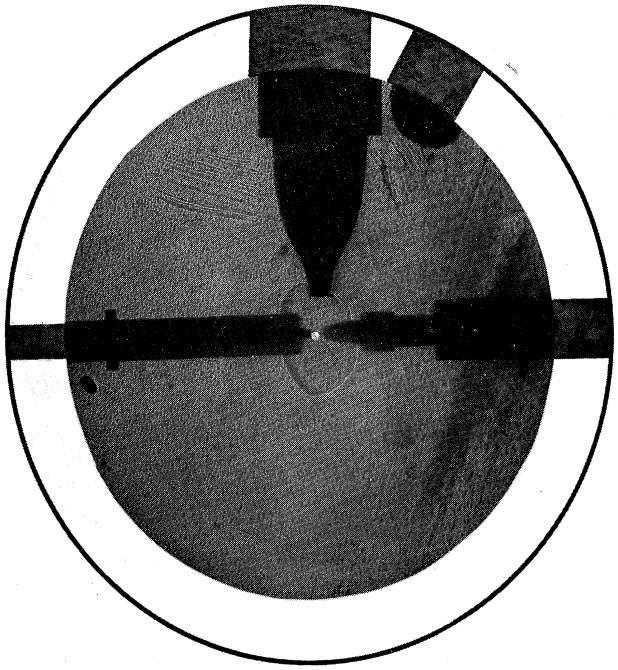

3.2 msec.

Figure 32. Flame photographs at varying times after ignition—medium jet, 5 fps jet velocity—time measured from ignition.

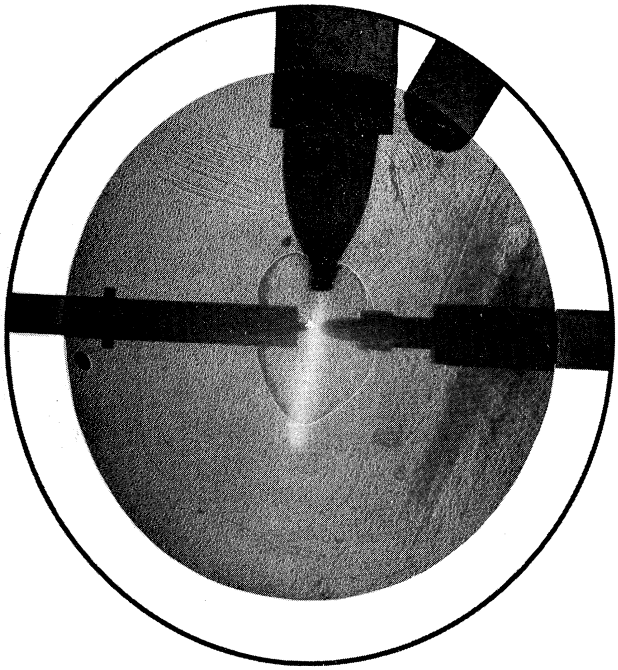

4.7 msec.

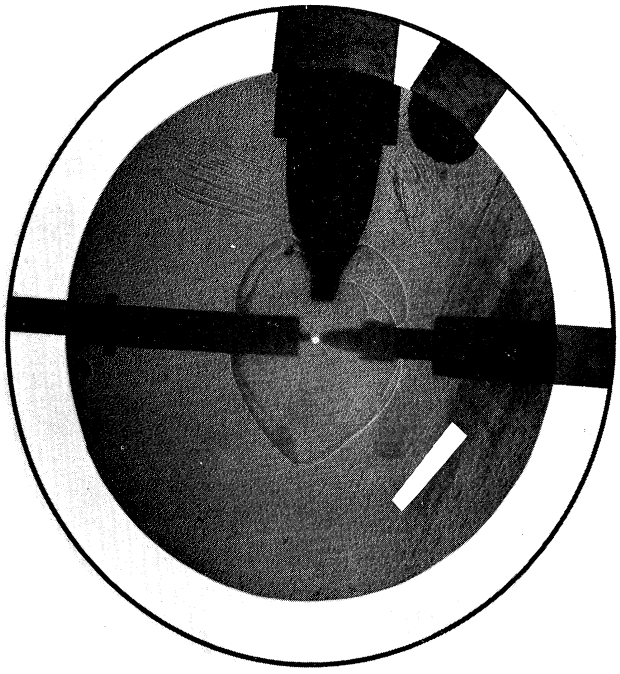

6.2 msec.

Figure 32. Concluded.

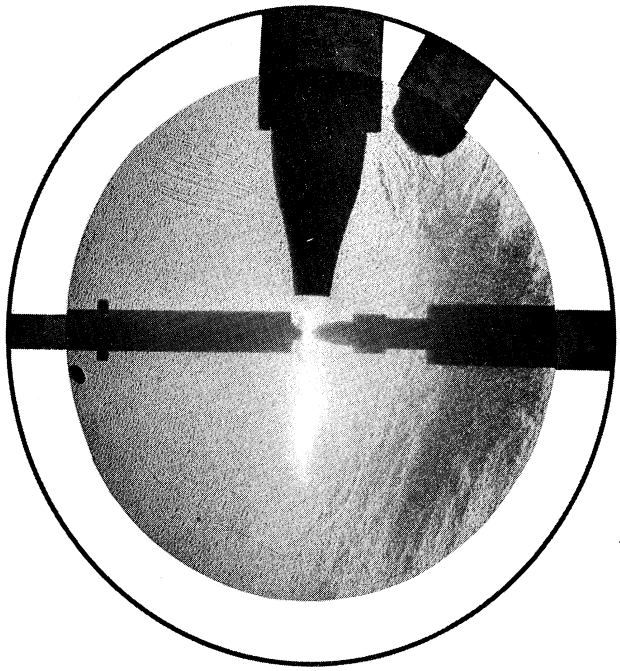

1.5 m sec

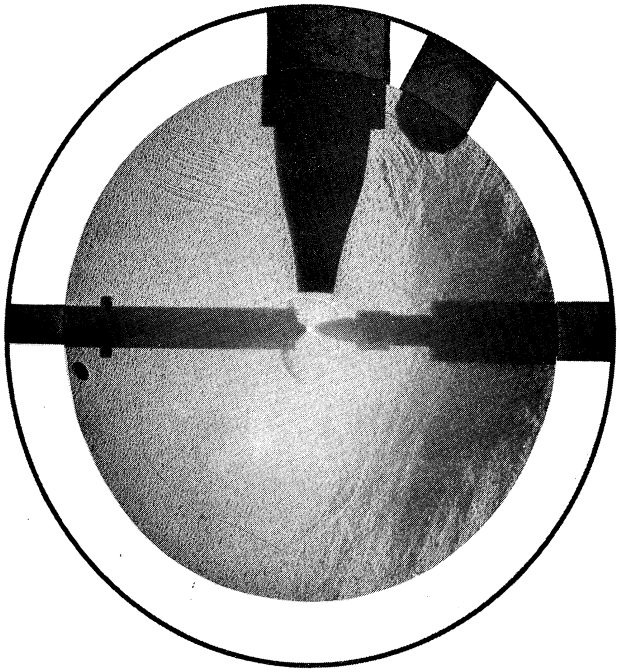

3.0 m sec

Figure 33. Flame photographs at varying times after ignition—large nozzle, 5 fps jet velocity—time measured from ignition.

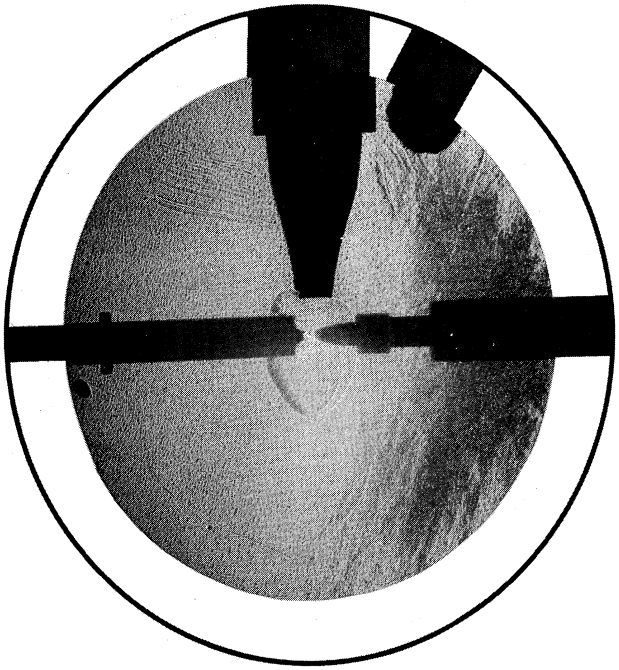

4.5 m sec

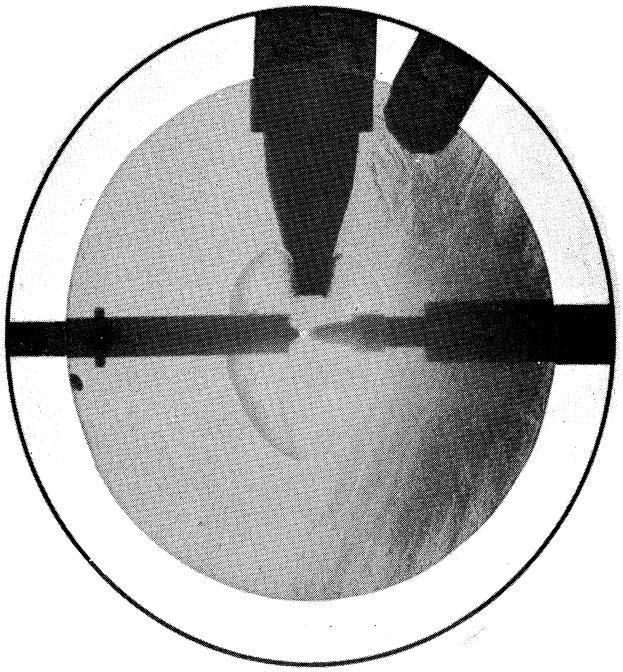

6.0 m sec

Figure 33. Concluded.

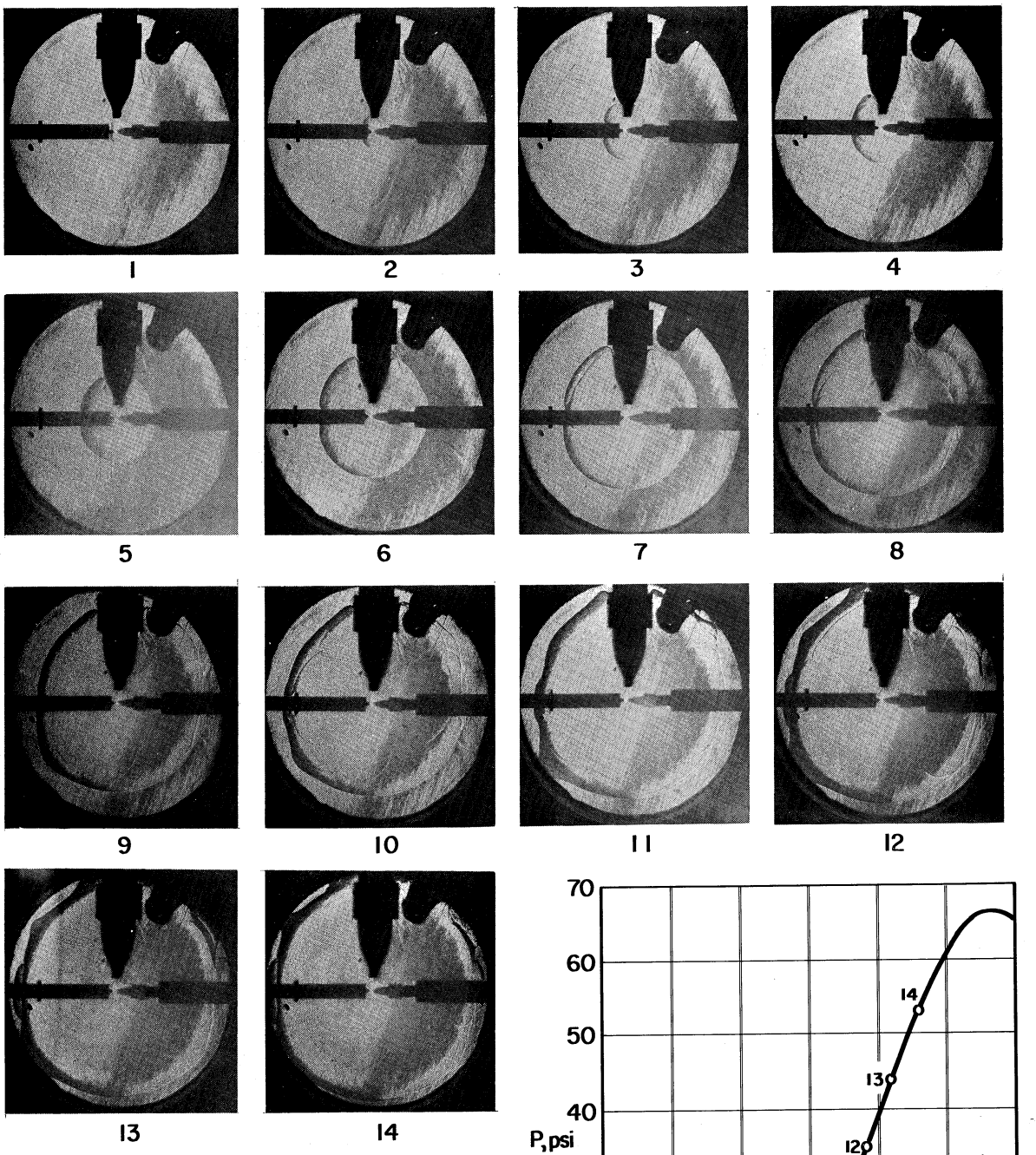

Figure 34. Sequential photographic study of combustion in a quiescent mixture—14 consecutive runs.

spatial velocity (apparent flame velocity).

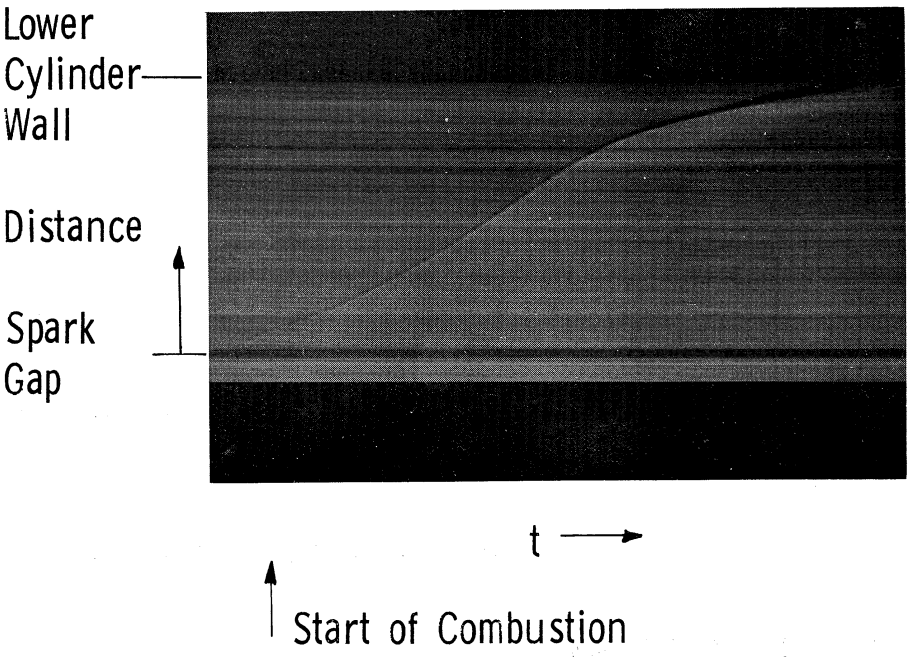

Figure 35. Schlieren streak photograph (lower section of flame kernel).

CHAPTER VI

DISCUSSION

The results are discussed under the following headings:

A. Characteristics of the mixture-jet.

B. Reproducibility of important aspects of combustion.

C. Effect of mixture motion on combustion.

D. Observations relating to the complete combustion process in a quiescent mixture.

E. Extrapolation of results to spark-ignition engine combustion.

A. CHARACTERISTICS OF THE MIXTURE-JET

If the mixture-jet impinging on the spark-gap had been in a transient state at the start of combustion there would have been immense difficulty in quantitatively measuring its effect on combustion. Steady flow existed at the gap with all nozzles at every mixture flow condition. This is shown in Table I of Chapter V, where the time required to establish steady flow was, in every case, significantly less than the time required for the mixture-jet to trigger ignition.

The profile of the mixture-jet before ignition was measured in the hot-wire anemometer experiments reported previously. As shown in Figures 14, 16, and 18 of Chapter V, the X axis widths of the mixture-jet velocity profiles were approximately equal to the inside width of the bomb and the peak profile velocities were almost constant for a given flow condition. The only important variable mixture-jet dimension for the range of flow velocities and nozzles used was the Y axis profile width, hence it was possible to assume that the mixture-jet was two dimensional.

The data from Figures 13, 15 and 17 in Chapter V was interpolated to indicate the shape of the Y axis profile for the three nozzles and the experimental flow conditions (peak profile velocities of 1, 3, 5, and 7 ft/sec). The Y axis velocity profiles are plotted in Figures 36, 37, and 38. The width (W_m) of the velocity profile (Y axis) at 1/2 of the maximum velocity of each profile is used to characterize the scale of the jet. These scale measurements are summarized in Table III. It can be seen that the difference in jet widths from the small and medium nozzle is not as great as the difference in nozzle widths. The mixture flow at the spark-gap diverged significantly from the small nozzle (.026 in. Wd) and only slightly from the medium nozzle (.066 in. Wd). The mixture flow converged slightly from the large nozzle

TABLE III

MIXTURE-JET PROFILE WIDTHS AT THE SPARK-GAP FOR ALL TEST CONDITIONS

Peak Profile Velocity-V_j-ft/sec	Mixture-Jet Width-W_m-inches		
	Small Nozzle, d = .026 in.	Medium Nozzle, d = .066 in.	Large Nozzle, d = .156 in.
0	-	-	-
1	-	-	-
3	.052	.074	.148
5	.045	.069	.147
7	.044	.069	.145

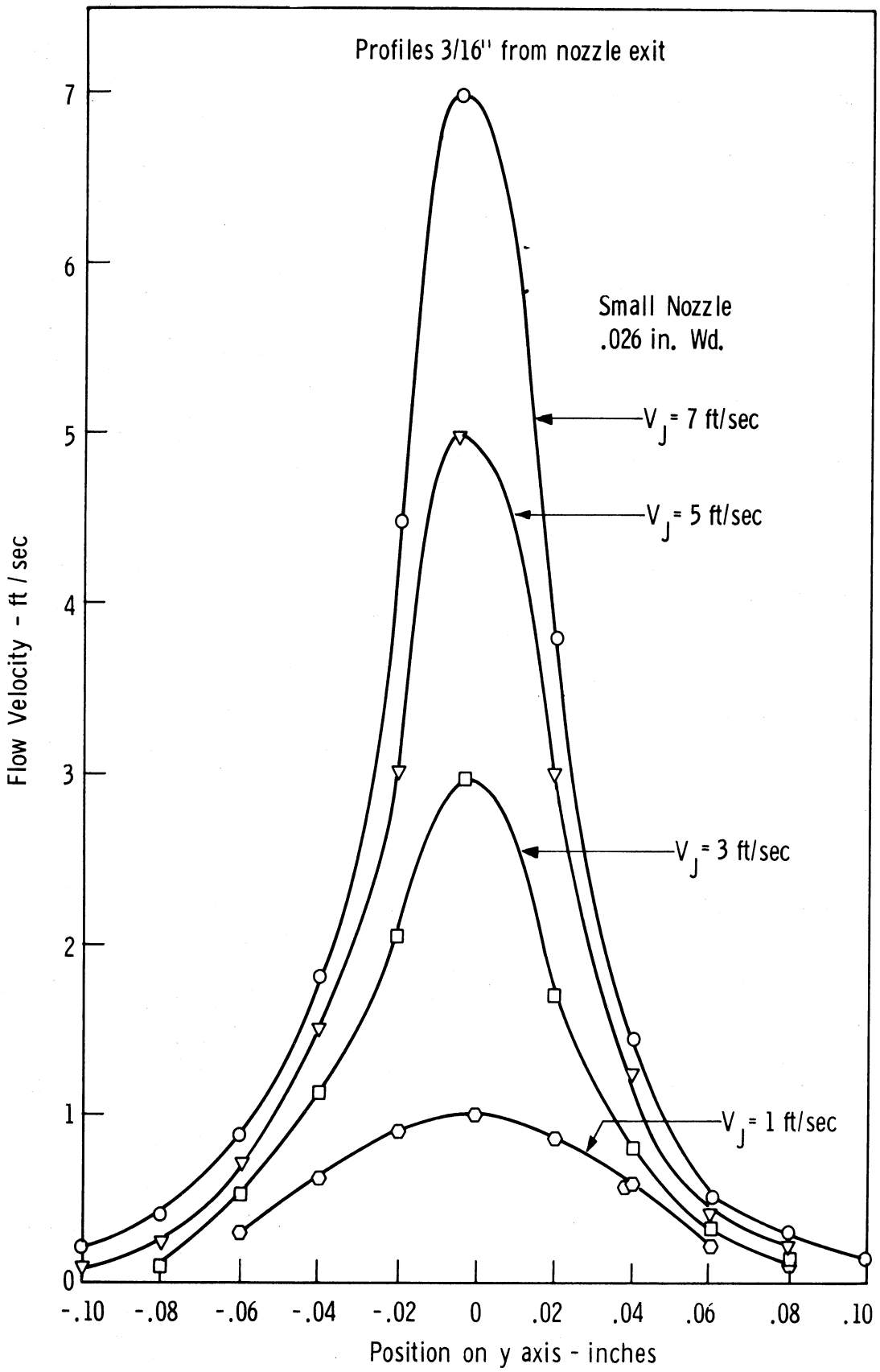

Figure 36. Velocity profiles used in combustion studies—Y axis—small nozzle: .026 in. width.

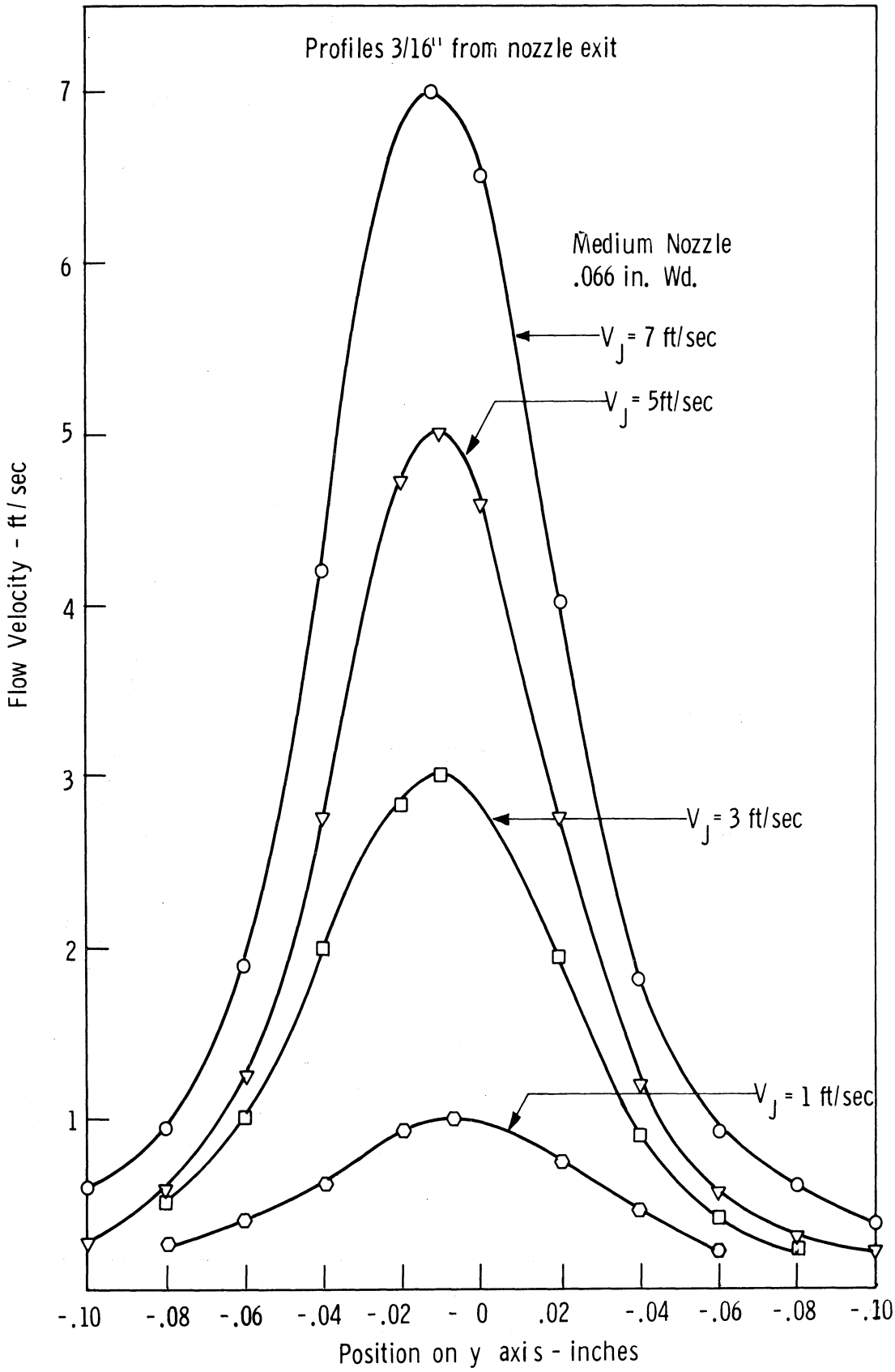

Figure 37. Velocity profiles used in combustion studies—Y axis—medium nozzle: .066 in. width.

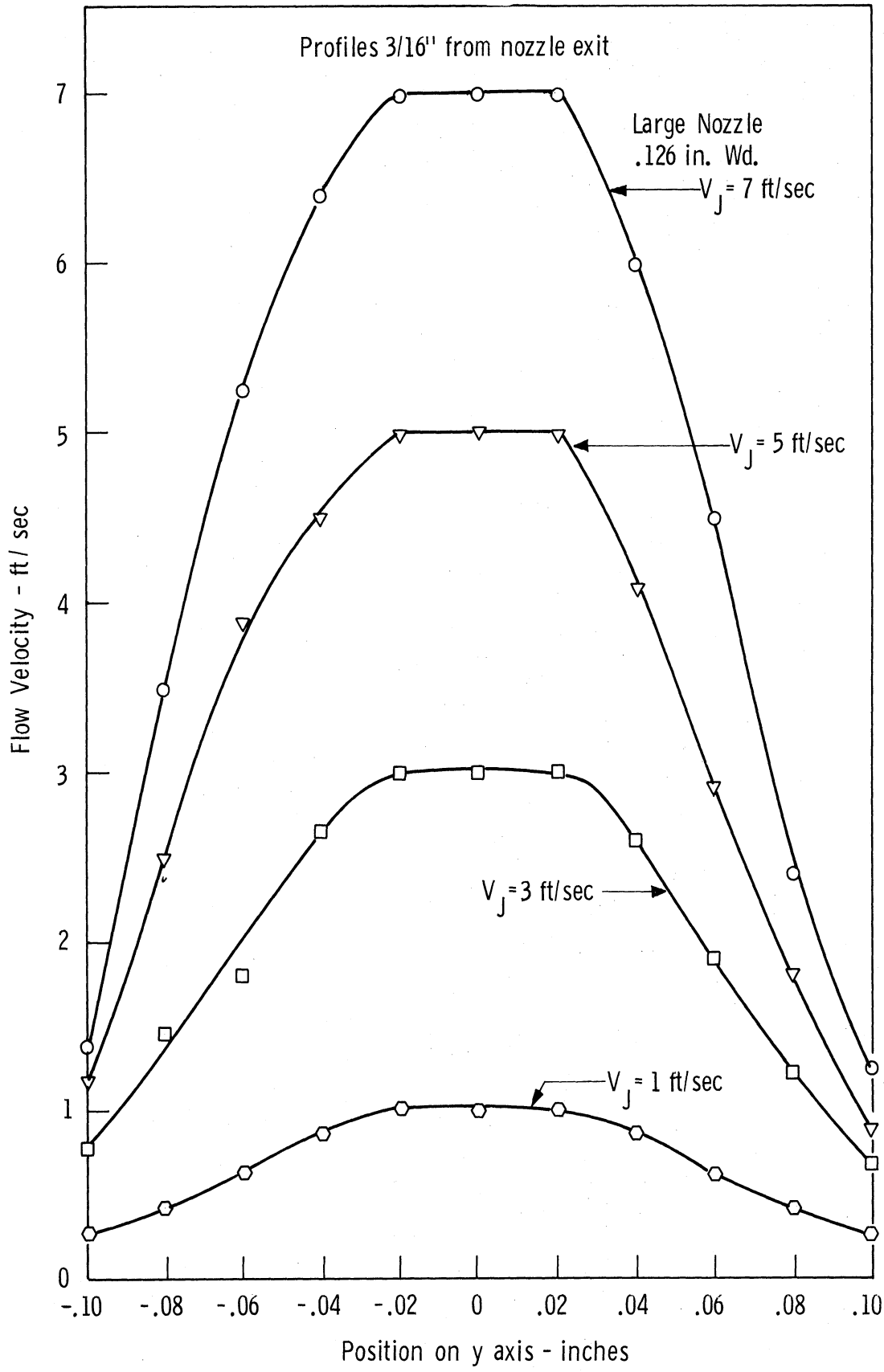

Figure 38. Velocity profiles used in combustion studies—Y axis—large nozzle: .156 in. width.

(.156 in. Wd). It was observed that the median flow width for a given nozzle remained almost constant over the range of flow velocities used.

The Reynolds number $(\frac{V_J \rho_m d}{\mu_m})$ for the mixture-jet was less than 700 for all nozzles and every flow condition. The highest Reynolds number existed in the large nozzle (d = .156 in.) with the highest velocity, (V_J = 7 ft/sec). With a density of ρ_m = .08 lbm/ft^3 and viscosity of μ_m = .038 x 10^{-5} slug/ft sec, the Reynolds number is slightly less than 700. This fact proved that the jet flow profiles were laminar and contained a minimum of fine-grained turbulence This was also observed qualitatively with the hot-wire anemometer, which showed that the only fine-grained turbulence was in the boundary between the jet and the quiescent mixture.

B. COMBUSTION REPRODUCIBILITY

The ignition spark was very reproducible. It occurred at the same instant for every test. The duration of the spark was also constant. The only difference noted between sparks was a slight variation in emitted light which may indicate that the spark followed different paths or that the spark energy varied slightly. It must be noted that the spark energy was set significantly greater than the minimum ignition energy. The minimum ignition energy was approximately .3 millijoules as given in Reference (12). The spark energy used in this research was greater than 4.0 millijoules, thus problems associated with marginal values of spark energy were eliminated.

The measured ignition delay variation of .10 to .20 millisecond may be a partial explanation for slight variations in the rate of pressure rise 9.5 millisecond after ignition.

As shown in the frequency distribution of Figure 24 in Chapter V the physical combustion process was quite reproducible. The mean rate of pressure rise determined from this distribution for quiescent mixture combustion was .90 psi/msec. This value was used as a reference to which the pressure rates of the mixture-jet disturbed combustion were compared. Several pressure rates were observed which differed significantly from the mean value for the quiescent mixture combustion. The most likely explanation for this variation is delayed ignition of the mixture. Rates of pressure rise of this random nature, which departed by more than .075 psi/msec from average values, were neglected in analysis of the data.

A certain amount of electrical noise appeared on all of the pressure rate traces. An attempt was made to eliminate it but with little success. Rates of pressure rise were thus measured from an average curve. The error associated with this technique was minimal in comparison with differences in the pressure rates observed for the different test conditions.

In the combustion studies with directed mixture motion the spread of pressure rates for all runs, measured 9.5 msec. after ignition, at each test condition was small, less than 1 standard deviation based on the frequency distribution of Figure 24. This indicated that the frequency distribution for all cases was narrow and that the probability of several observations being representative of the population was high.

C. EFFECT OF MIXTURE MOTION ON COMBUSTION

Motion-disturbed combustion was compared with combustion in a quiescent mixture. The flame kernel was photographed 9.5 millisecond after ignition. Pressure rate (dP/dt) was the measured variable indicating the overt effect of mixture motion on combustion. Schlieren photographs of the flame front showed how the flame was affected.

The percent increase in rate of pressure rise,

$$\frac{\left(\frac{dP}{dt}\right)_{v_J} - \left(\frac{dP}{dt}\right)_{v_J = 0}}{\left(\frac{dP}{dt}\right)_{v_J = 0}} \times 100 = \pi_P ,$$

is plotted against mixture jet intensity (peak Y axis profile velocity) in Figures 39, 40, and 41 for each of the jet nozzles. At least five experimental measurements were made and the results averaged at each condition. A pressure rate $\left(\frac{dP}{dt}\right)_{v_J = 0}$ of 5.1 centimeters oscilloscope deflection, .90 psi/millisecond, was used as a reference for comparison for the medium and large jet nozzles.

A pressure rate of 4.8 centimeters oscilloscope deflection, .85 psi/millisecond, was used as the reference pressure rate for the small jet nozzle combustion runs. There was some question as to what caused this difference in the quiescent mixture combustion pressure rate. It was also noted on the schlieren photographs that the flame front area was slightly smaller for the small nozzle than for either the medium or large nozzles. Apparently the flame was quenched at the

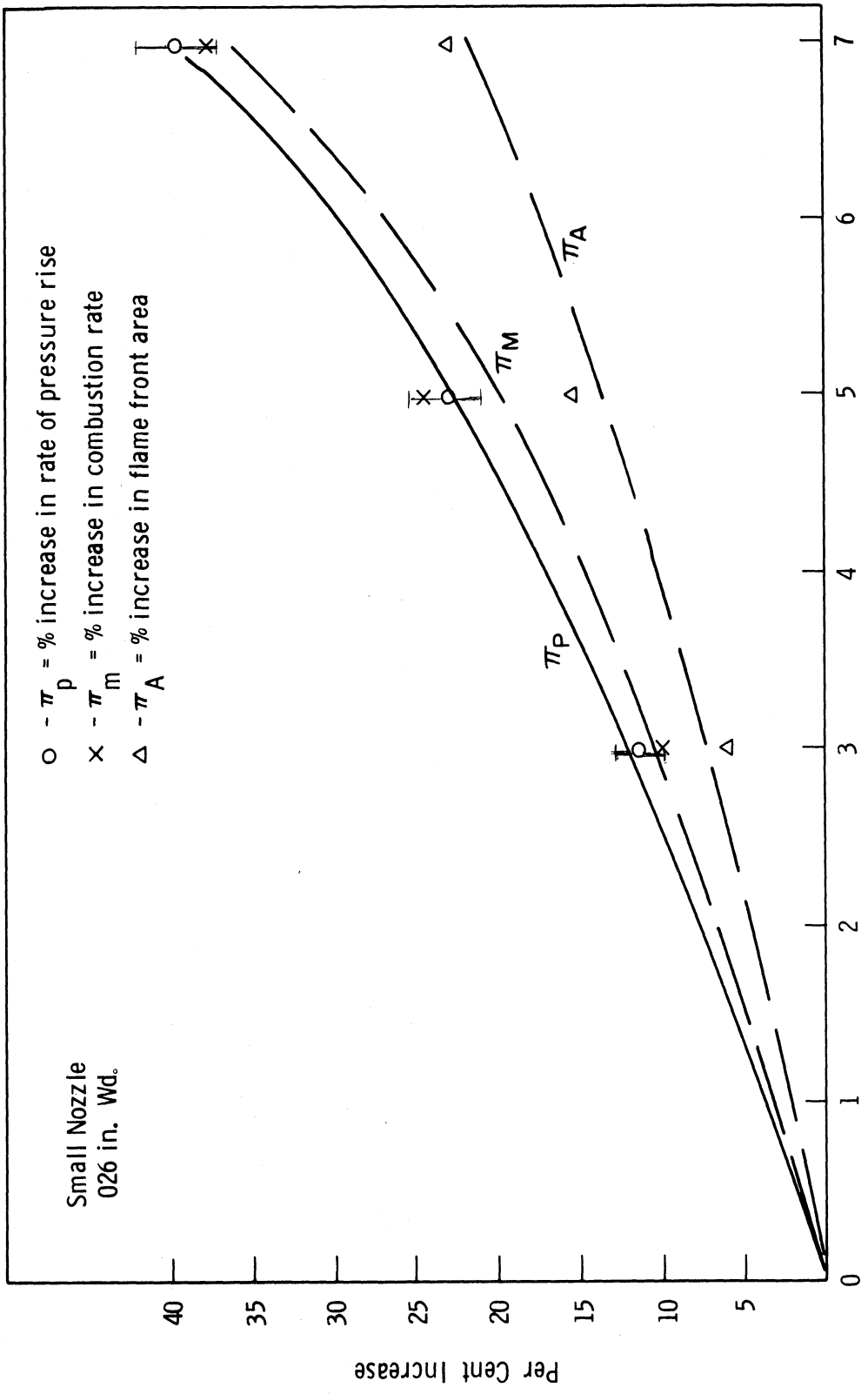

Figure 39. Effect of mixture-jet velocity on combustion, 9.5 msec after ignition, small nozzle.

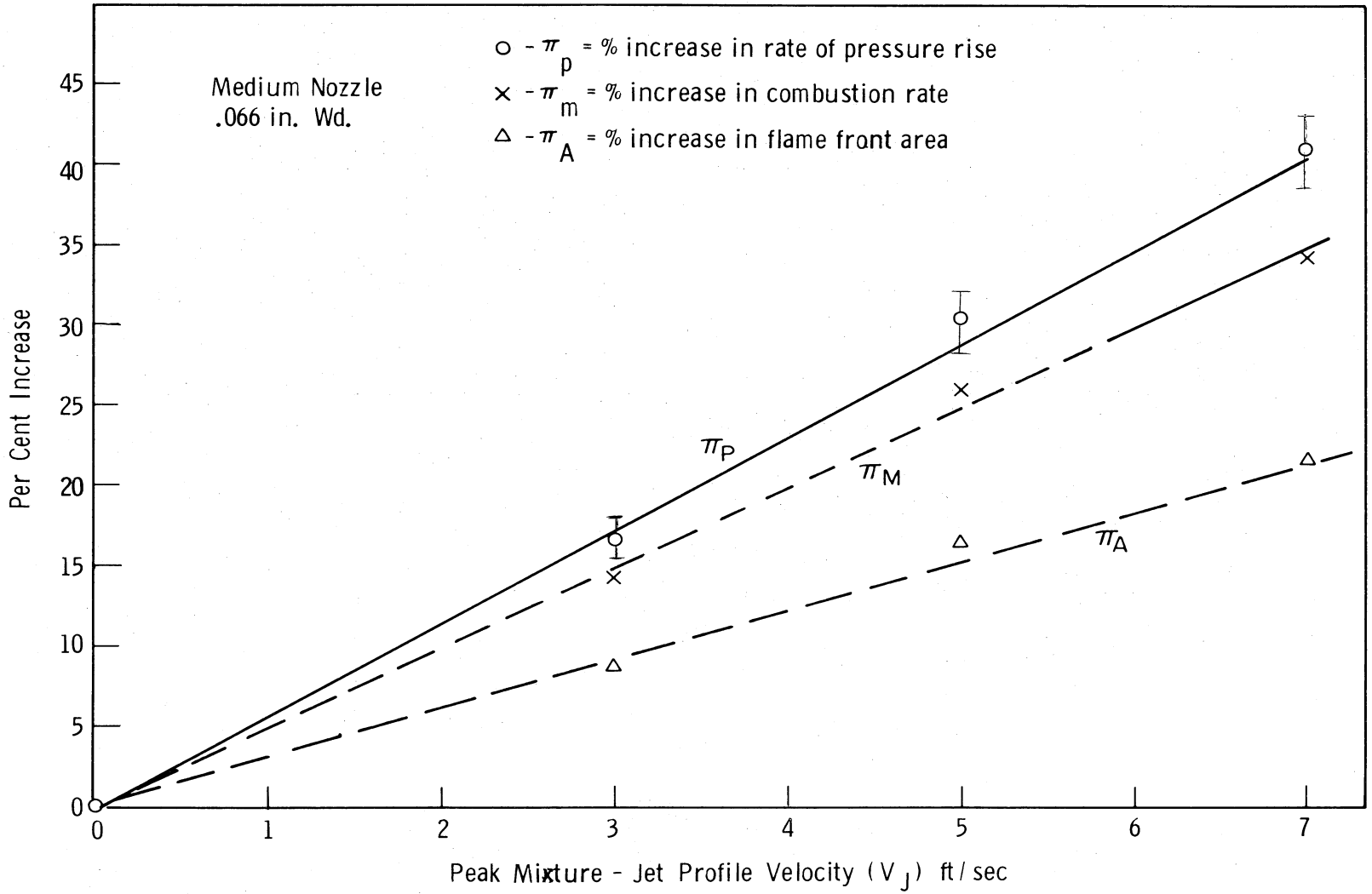

Figure 40. Effect of mixture-jet velocity on combustion, 9.5 msec after ignition, medium nozzle.

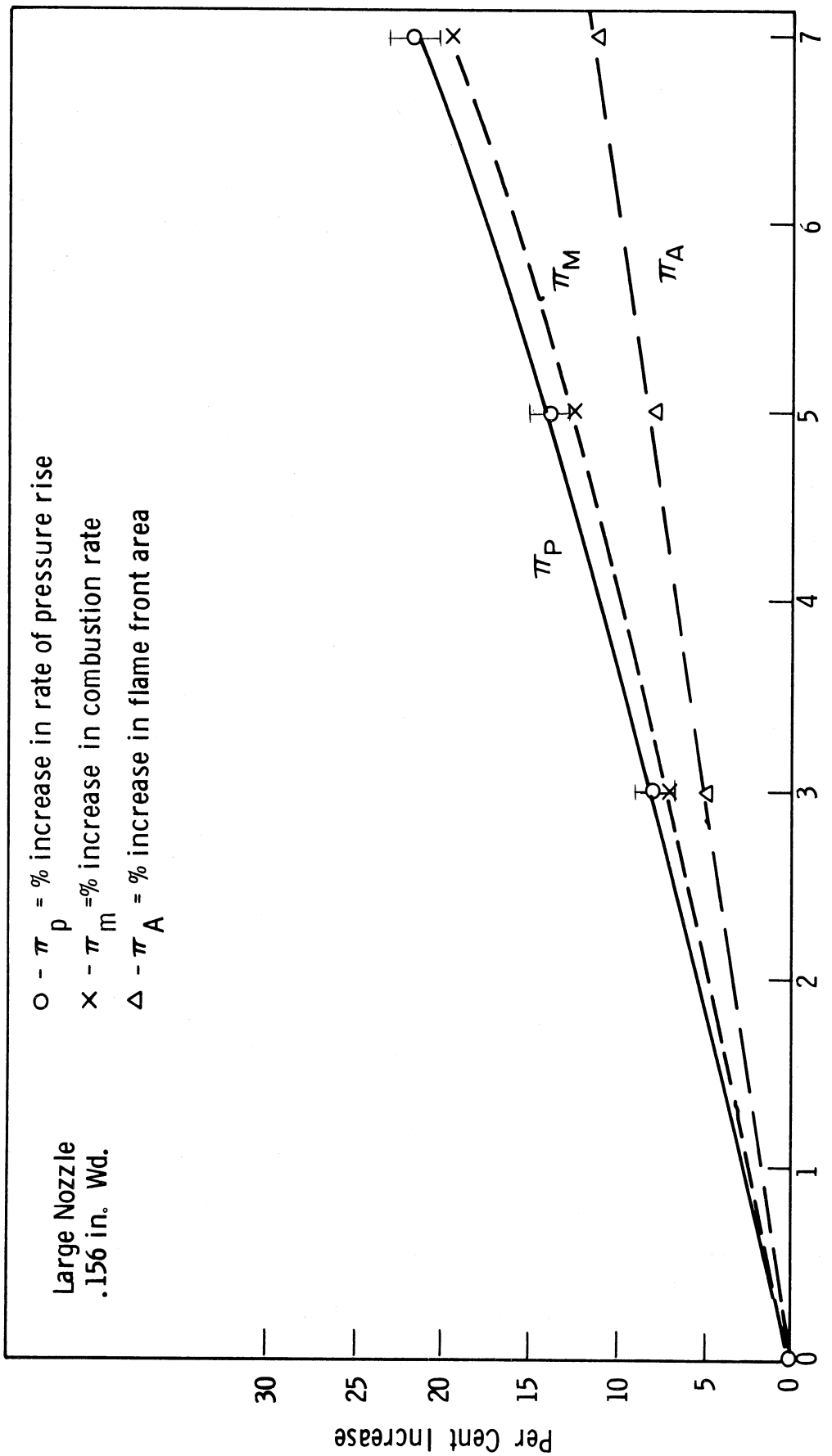

Figure 41. Effect of mixture-jet velocity on combustion, 9.5 msec after ignition, large nozzle.

small nozzle exit preventing combustion of the mixture in the nozzle and thus decreasing the flame size and the pressure rate 9.5 millisecond after ignition.

The curves are plotted through the average measured value of increase in pressure rate for each test condition.

Figure 39, which shows the effect of jet velocity on pressure rate for combustion runs with the small nozzle, shows that the pressure rate increased at an increasing rate with jet velocity. The maximum increase was 39% with V_J = 7 ft/sec.

Combustion runs with the medium nozzle, shown in Figure 40, demonstrated that pressure rate increased almost linearly with jet velocity. The mixture-jet from this nozzle had the greatest effect on pressure rate. A 41% increase in pressure rate was observed with V_J = 7 ft/sec.

The large nozzle mixture-jet had the least effect on pressure rate. The results, shown in Figure 41, showed that the pressure rate increased at a slightly increasing rate with jet velocity. An increase of 22% was observed with V_J = 7 ft/sec.

The three data points used to plot each curve of percent increase in pressure rate are insufficient to define the precise shape of the curves; hence the curves shown are only approximations of the true behavior. The only conclusion that can be safely drawn is that pressure rate increased with mixture-jet velocity approximately linearly.

The effect of mixture-jet width, or scale of motion, on the rate of pressure rise is shown in Figure 42. Percent increase in pressure rate is plotted against the mixture-jet profile width measured at the

median velocity of the profile (W_m). The jet width associated with the medium nozzle had the greatest effect on pressure rate. At all three of the jet velocities, the peak pressure rate occurred with a jet width slightly greater than the spark-gap of .050 in. When the jet width was increased from about .07 in. to .15 in., the pressure rate decreased considerably. The most significant relative decrease occurred at V_J = 7 ft/sec.

The pressure rate decreased when the jet width was decreased from .07 in. to .045 in. This decrease was significant but much less than the pressure rate decrease found with the .15 in. jet.

Several qualitative observations can be made regarding the relative effect of the small and medium mixture-jets on the flame kernel. As shown in the photographs of Figures 27 and 28, neither jet appeared to displace the flame kernel, they only distorted it. It is also apparent that the medium mixture-jet caused a greater distortion of the flame front than the smaller jet; hence a higher combustion rate and rate of pressure rise would be expected for the medium jet influenced combustion.

Since the flame kernel was only distorted by the two mixture-jets, the reason the medium jet had a greater effect on the flame front can be observed from the velocity profiles for the jets in Figures 36 and 37. These indicate that for a given peak profile velocity the area of the envelope curve enclosing the velocity profile and the mass flow rate of mixture into the reaction zone are greater for the medium mixture-jet than for the small mixture-jet.

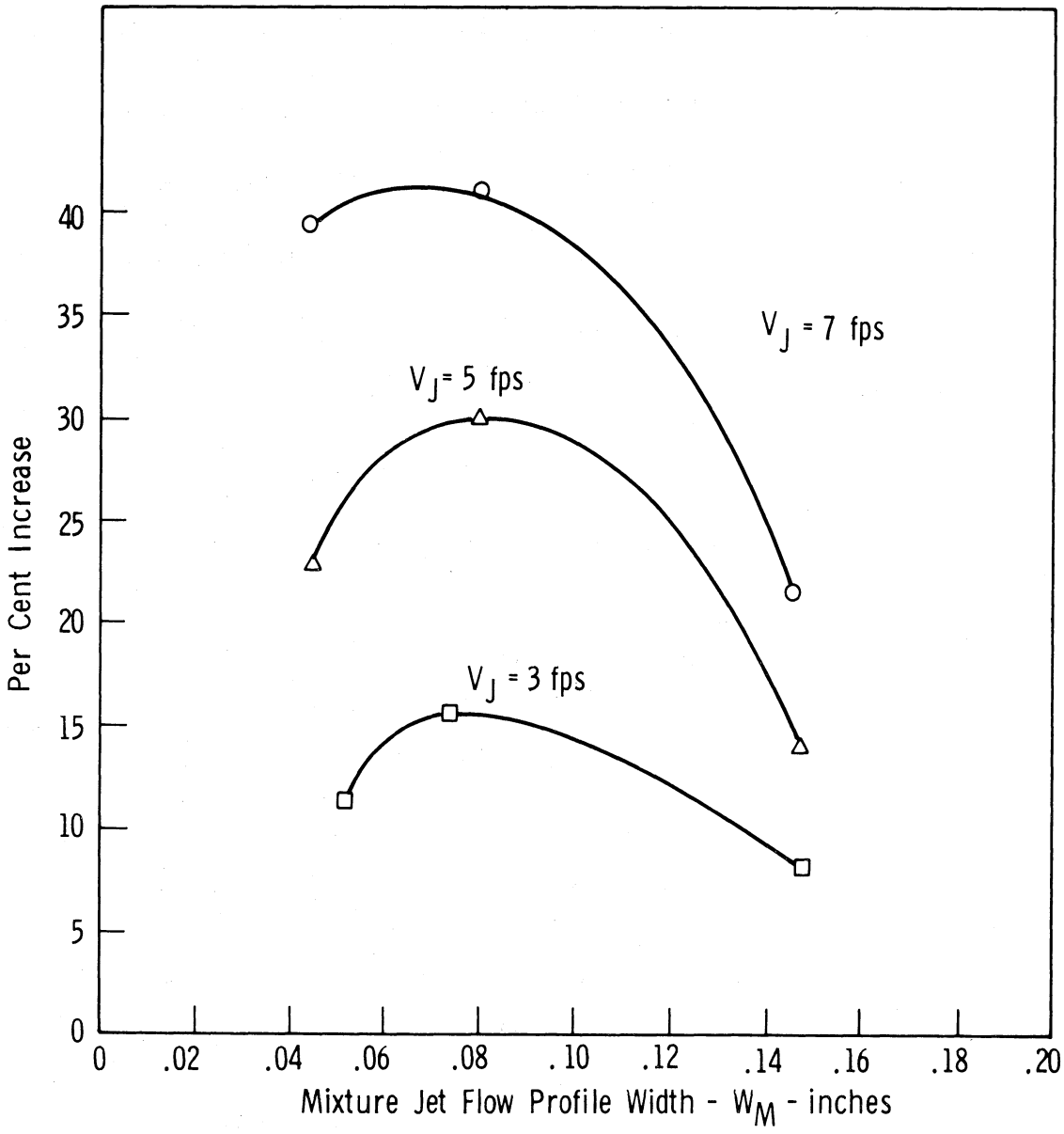

Figure 42. Effect of mixture-jet width on rate of pressure rise.

The reason that the widest mixture-jet had relatively little effect can be seen in the sequential photographs in Figures 32 and 33 of Chapter V. The medium jet tended to distort the flame, increasing its surface to volume ratio, while the large jet tended to displace the total flame kernel and distorted it to a lesser extent. It can be speculated that if the mixture-jet width were increased beyond that used in this research, a point might be reached where the flame would be merely displaced with no flame front distortion and the combustion rate would be that of a quiescent mixture.

As with mixture-jet velocity, no precise functional relationship relating rate of pressure rise to mixture-jet profile width is defined, only a general trend is indicated.

The primary conclusions are:

1. The rate of pressure rise increased with an increase in mixture-jet velocity.
2. The width of the mixture-jet had an effect on the pressure rate. A width slightly greater than the spark-gap produced the highest pressure rate.

The major cause of the pressure rate increase was found to result directly from distortion of the flame front area. The percent increase in flame front area,

$$\frac{(A_f)_{v_J} - (A_f)_{v_J = 0}}{(A_f)_{v_J = 0}} \times 100 = \pi_A \quad)$$

was approximated from the schlieren photographs as indicated in Appendix J and is also plotted in Figures 39, 40, and 41 against peak jet profile velocity. The surface area of several flames at each condition was measured from the schlieren photographs. The average area increase is shown at each test point. Approximately 60% of the increase in pressure rate is directly attributable to an increase in flame front area.

The percent increase in the mass rate of combustion,

$$\frac{(\rho_m A_f V_f)_{V_J} - (\rho_m A_f V_f)_{V_J = 0}}{(\rho_m A_f V_f)_{V_J = 0}} \times 100 = \pi_m ,$$

was also approximated as indicated in Appendix J and is also plotted against peak profile velocity in Figures 39, 40, and 41. The increase in mass rate of combustion accounts for approximately 85% of the increase in pressure rate.

Theoretically the per cent increase in the mass rate of combustion should be equal to the per cent increase in the rate of pressure rise since they are proportional,

$$\frac{dP}{dT} = K\rho_m A_f V_f .$$

A slight error was expected, though, because the proportionality factor (K) is not constant due to a change in heat transfer characteristics from the flame kernel and because the method of flame area measurement did not take into account any three dimensional wrinkling of the flame kernel. The error associated with the highest jet velocity was the greatest and was most probably due to an underestimate of the flame front area caused by minor wrinkling which can be observed in the photographs of Figures 28, 29, and 30.

Results of these calculations for the small nozzle studies were somewhat inconsistent. The percent increase in combustion rate was calculated to be slightly greater than the percent pressure rate increase for a mixture-jet velocity of 5 ft/sec. No explanation is apparent other than that this is a normal error associated with the measuring technique used. It must be noted that the discrepancy is small and probably insignificant.

As indicated earlier, the major cause of the pressure rate increase was the flame front area increase. A certain portion of the increase can be directly attributed to area as shown by π_A. It must be noted that the increase in the density (ρ_m) and relative flame velocity (V_f) are also dependent on the increase in area of the flame. The early flame kernel area increased at a greater rate for the mixture motion disturbed combustion than for the quiescent mixture combustion, therefore the density (ρ_m) and the relative flame velocity (V_f), measured at a fixed time following ignition, were caused to increase.

The complete mechanism by which the mixture-jet affected combustion cannot be evaluated with the data obtained in this research.

In the undisturbed combustion and in regions of the motion-disturbed combustion not affected by the mixture-jet, a smooth, laminar flame was observed. This demonstrated that there was little turbulence in regions not influenced by the jet. Even in the jet-distorted portion of the flame, only a minimum of fine-grained turbulence effect was observed. Thus, the major cause of combustion rate variation was the total mixture

motion of the mixture-jet rather than some type of fine-grained motion created by the mixture-jet.

D. DEVELOPMENT OF THE FLAME THROUGH THE COMPLETE COMBUSTION PROCESS

The total development of the flame in a quiescent mixture was observed with the sequential schlieren photographic study shown in Figure 34 of Chapter V. The flame was laminar through all stages of development. At the periphery of the bomb the flame extended itself toward the various openings in the walls of the bomb. The flame dwelled momentarily at the wall as the spatial velocity approached zero.

Figure 43 shows a plot of the spatial velocity versus position relative to the spark-gap based on the sequential photographic study. The spatial velocity peaked near the midpoint of flame travel. The theoretical flame velocity, relative to the unburned mixture, calculated according to the procedure in Appendix J, is also plotted in Figure 43. It increased gradually with distance from the spark-gap. In the early stages of combustion the relative flame velocity was about 15% of the spatial velocity.

The streak camera photographic study served as a check on the sequential photographic technique of flame spatial velocity measurement. The curve shown in Figure 44 is the same shape but of slightly lower magnitude then Figure 43. The slight difference in magnitude is probably caused by experimental error or by error in the measurement of the photographic data from both techniques.

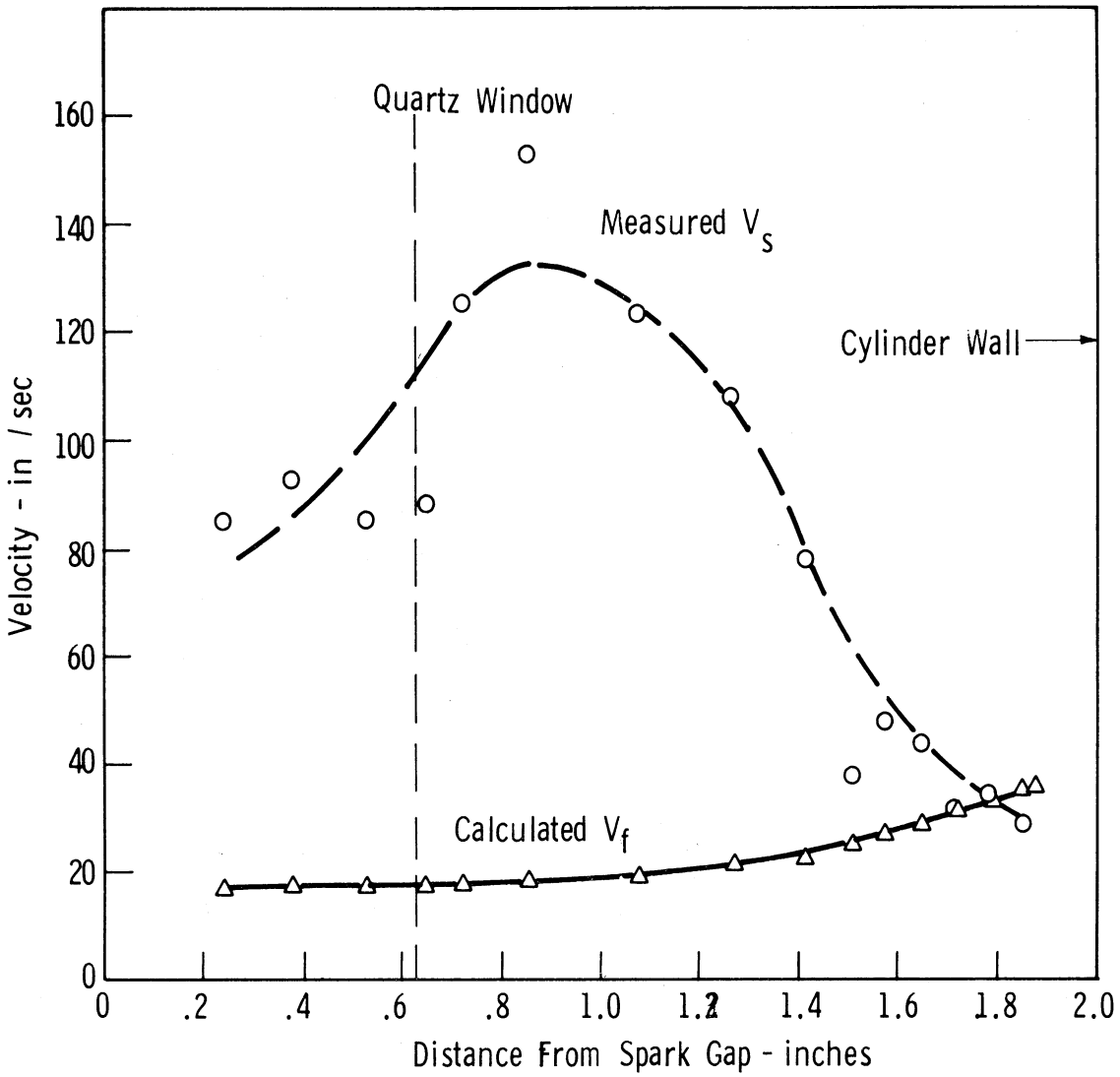

Figure 43. Relative flame velocity and flame spatial velocity in the constant volume bomb—sequential flame photographic study.

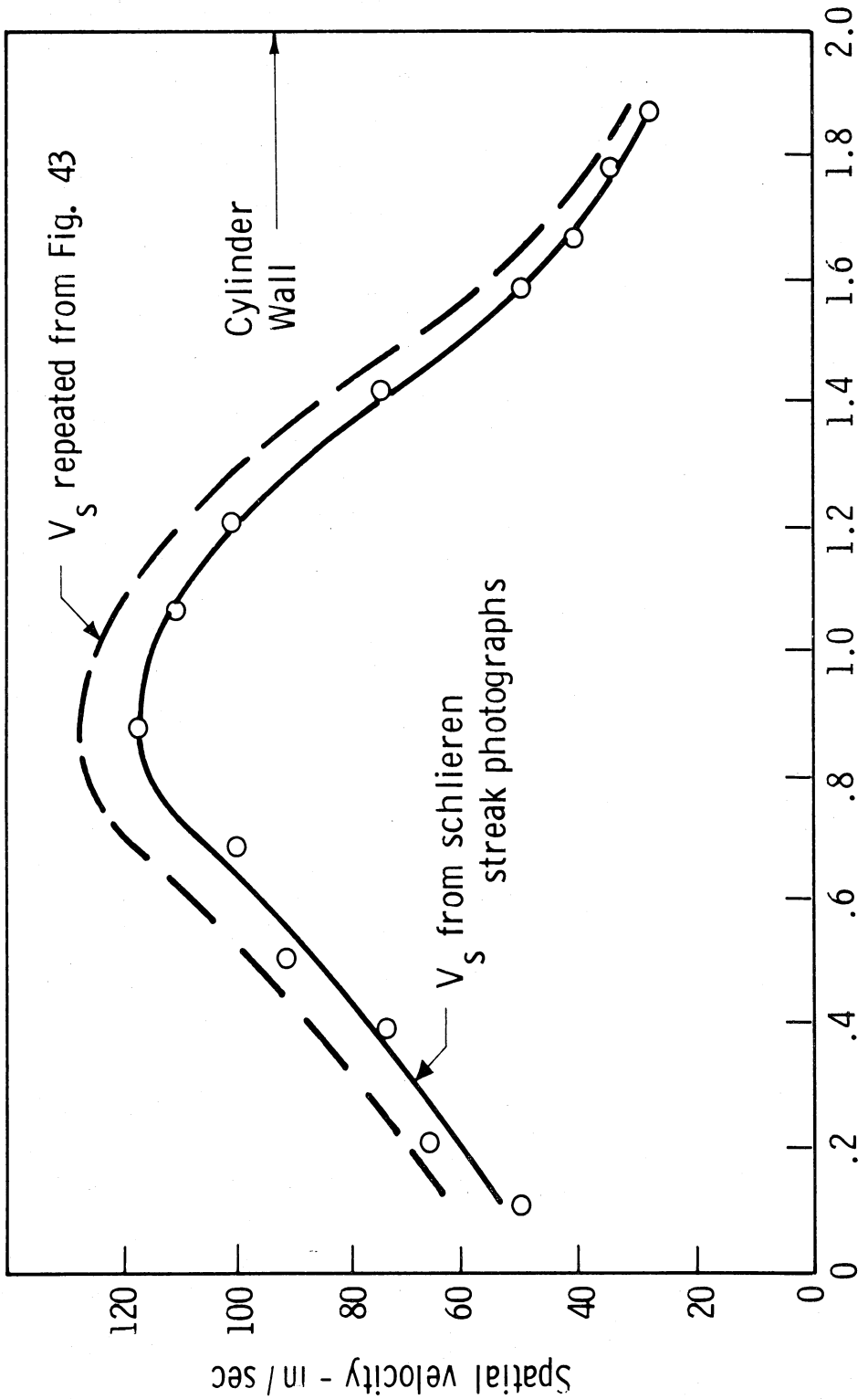

Figure 44. Flame spatial velocity measured on the lower portion on flame kernel—from schlieren streak photograph (Figure 35).

The flame spatial velocity in the motion affected combustion would be the same order of magnitude as that measured in the quiescent mixture combustion. In the region of flame development studied in detail for the effect of mixture motion, the peak mixture-jet velocity (V_J) is the same order of magnitude as the flame spatial velocity. The relationship between the mixture-jet velocity and the spatial velocity is important if the results are to be projected to conditions other than considered in this research.

E. EXTRAPOLATION OF RESULTS TO CONSTANT VOLUME ENGINE COMBUSTION

Despite the fact that there are significant differences between the combustion processes in the constant volume bomb and the engine there exists one important resemblance, the effect of mixture motion on the combustion rate

1. The results of this research clearly demonstrated the effect of mixture motion on the flame kernel development in a constant volume bomb.
2. Turbulence and swirl have a significant effect on engine combustion rate. This effect is well documented in the literature. Also, it has been shown that mixture velocity variations exist in the engine combustion chamber.[8,10]

Projecting the results of this work to spark-ignition combustion, it can be hypothesized that the variation in mixture velocity in the vicinity of the developing flame kernel from one cycle to the next causes

cycle-to-cycle variation in the pressure rate. A high rate of combustion and thus a high rate of pressure rise would occur with a level of mixture motion which disturbed the flame significantly, and a lower rate with a level of mixture motion having a lesser effect on the flame kernel. A distribution of combustion rates and pressure rates would exist and would be a function of the spectrum of mixture motion variation.

If this is the case it should be possible to diminish cycle-to-cycle combustion rate variations by reducing the mixture motion variation in the vicinity of the spark-gap.

CHAPTER VII

OBSERVATIONS AND CONCLUSIONS

A. OBSERVATIONS

Several observations were made concerning this research:

1. The mixture-jet profiles were laminar for all flow conditions.
2. The mixture-jet profile width was almost constant for a given jet nozzle over the range of jet velocities considered.
3. The flame front in the quiescent mixture combustion and in the motion influenced combustion appeared laminar. The only wrinkled flames observed were in the mixture-jet-disturbed sections of the flame for V_J = 7 ft/sec.
4. The spatial velocity (V_S) of the flame 9.5 milliseconds after ignition was approximately 8 ft/sec.
5. The spatial velocity increased with distance from the spark gap over approximately the first half of the total flame path. It then diminished until the cylinder wall was reached, where it appeared to stagnate momentarily.
6. The ignition spark occurred .09 $\pm$ .01 milliseconds after the pressure rate trace was triggered on the oscilloscope.
7. The duration of the ignition spark was essentially constant at .60 $\pm$ .02 millisecond.

8. The ignition delay of the mixture, as determined by the photo-multiplier technique, was between .10 and .20 millisecond.

B. CONCLUSIONS

The main conclusions of this research were:

1. Over the test range, the rate of pressure rise increased approximately linearly with an increase in mixture-jet velocity.
2. The width of the mixture-jet had an effect on pressure rate. A jet profile width slightly greater than the spark-gap produced the highest pressure rate.
3. The increase in the rate of pressure rise observed for the mixture-jet affected combustion process relative to the quiescent mixture combustion process was a result of the increase in flame front area caused by the mixture motion. Approximately 60% of the increase was directly attributable to the increase in flame area. The remainder of the increase was caused by the increase in mixture density and burning velocity which was an indirect effect of the flame front area increase.
4. The increase in pressure rate corresponded closely to the calculated increase in mass rate of combustion.
5. It was possible to obtain reproducible combustion. Successive combustion runs in a quiescent mixture photographed 9.5 milliseconds after ignition revealed a mean pressure rate of .89 psi/msec with a standard deviation of .037 psi/msec.

CHAPTER VIII

RECOMMENDATIONS

Several modifications of the test conditions and test equipment would be advisable for future investigation in this area.

1. The effect of higher mixture-jet velocities and larger mixture-jets should be studied to extend the range of information.

2. A background of swirl or turbulence could be provided in addition to the mixture-jet. This would be a better simulation of the environment in an engine combustion chamber.

3. The equipment could be modified to provide ignition at a point near a surface rather than in the central position used in this research. This would correspond more closely to the spark plug location in an engine combustion chamber.

4. The flame development could be studied by other techniques, such as high speed photography, to indicate the effect of the mixture motion throughout the total flame path of one combustion run.

APPENDIX A

SPARK CONTROL CIRCUIT

TABLE IV

SPARK CONTROL CIRCUIT DATA

R_{1A} = 50Ω, 5w	R_{16} = Variable resistance
R_{1B} = 130Ω, 10w	R_{17} = 150Ω, ± 1%, 1w
R_2 = 820Ω, 0.5w	C_1 = 0.005 μf
R_3 = 0-5K, 10 turn precision pot.	C_2 = 0.01 μf
R_4 = 5K, 0.5w	C_{3A} = 1.0 μf
R_5 = 60Ω, 1w	C_{3B} = 2.0 μf
R_6 = 50Ω, 0.5w	C_5 = Variable capacitance
R_7 = 1M, 0.5w	D_{1A} = D_{1B} = Type 1N100
R_8 = 3.3K, 0.5w	Q_1 = Q_2 = Type 2N1481
R_{9A} = 60Ω, 10w	Q_{3A} = Q_{3B} = Type 2N1099
R_{9B} = 60Ω, 10w	Q_4 = Type 2N1183B
T_{10A} = R_{10B} = 30Ω, 10w	Z_1 = Type 1N3008B
R_{11} = 680Ω, 0.5w	T_1 = Type TA-7 (Stancor)
R_{12} = 2.7Ω, 2w	V_1 = 12v
R_{13} = 0-6Ω, 10w	V_2 = 6v
R_{14} = 0-4Ω, 125w	V_{3a} = V_{3b} = 3.0v
R_{15} = 0-4Ω, 125w	V_4 = 6v

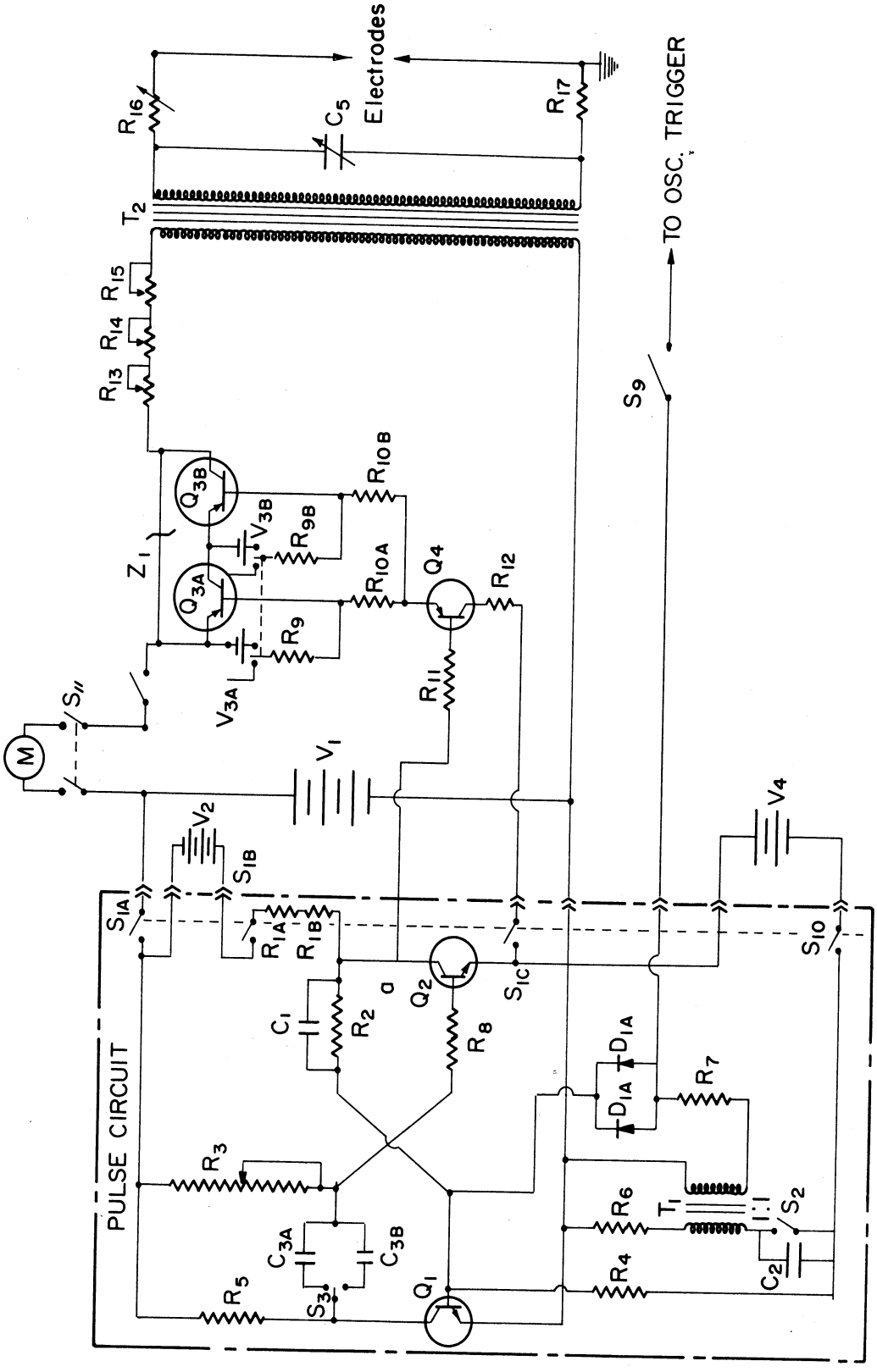

Figure 45. Spark control circuit.

APPENDIX B

RELAY CONTROL CIRCUIT

This circuit was used in conjunction with the balanced pressure diaphragm switch to open switch S-2 on the spark control panel, which fires the ignition spark.

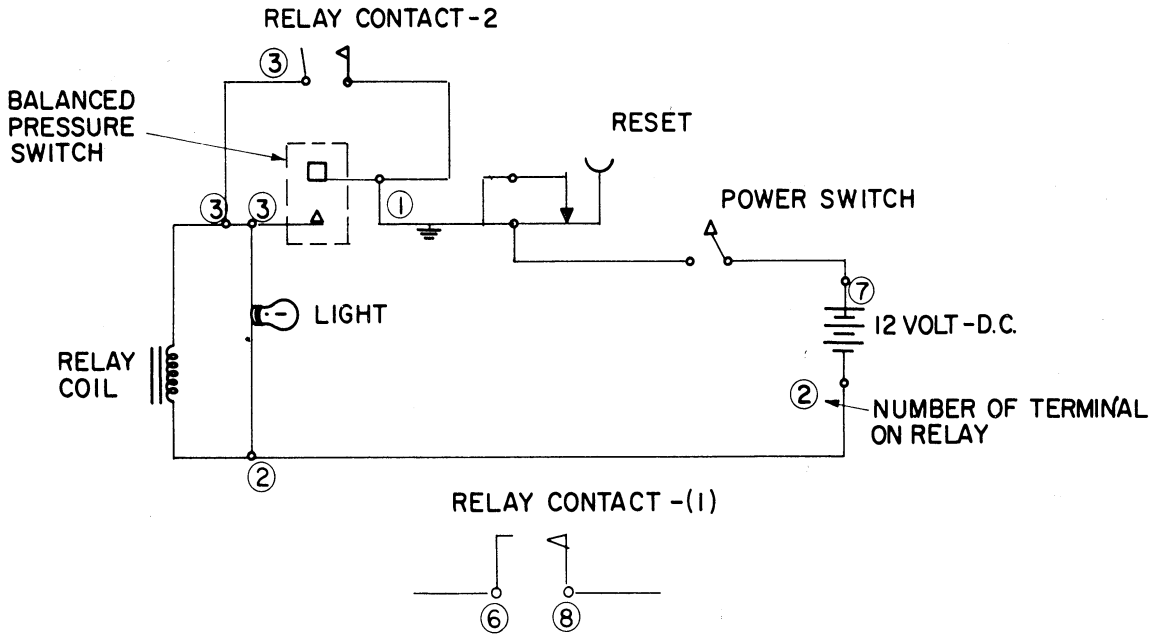

Relay contact (1) functions as S-2 in spark circuit. When balanced pressure switch closes, S-2 opens and spark occurs in bomb.

Figure 46. Balanced pressure switch circuit for bomb ignition.

APPENDIX C

PRESSURE RATE-DIFFERENTIATING CIRCUIT

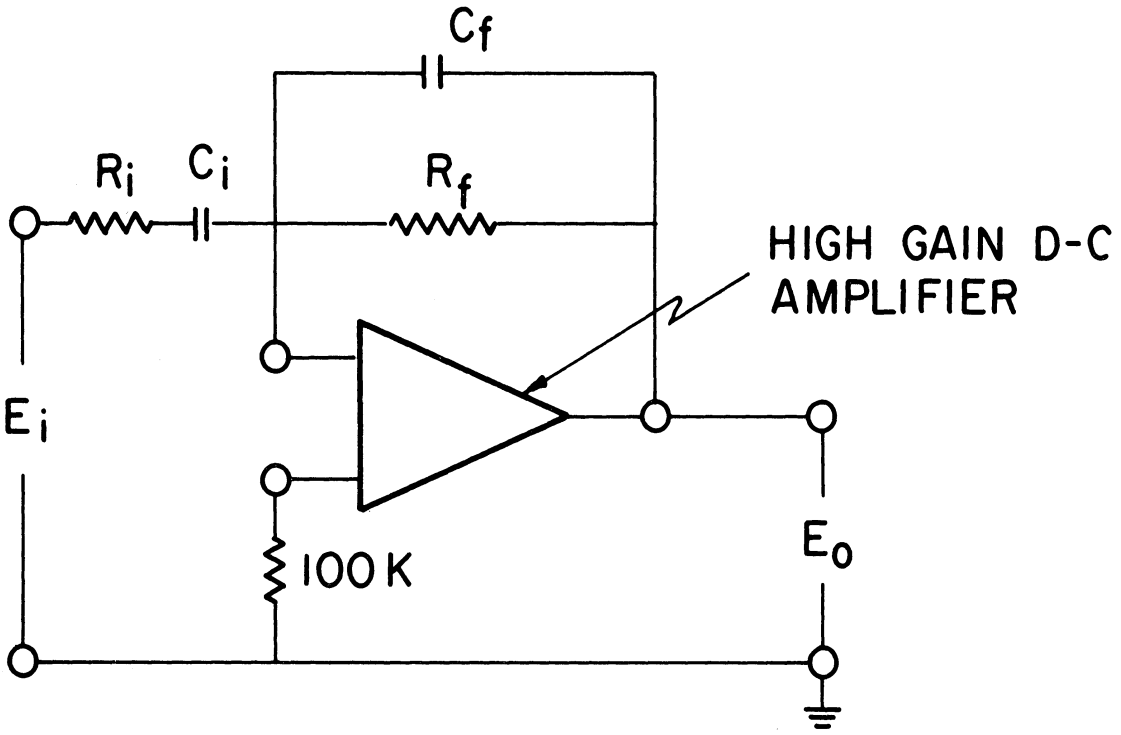

E_i = Input Voltage α Pressure (P)
E_o = Output Voltage α Pressure Rate (dP/dt)
R_i = Input Resistance
C_i = Input Capacitance
R_f = Feedback Resistance
C_f = Feedback Capacitance

Figure 47. Schematic diagram—differentiating circuit.

APPENDIX D

HOT-WIRE ANEMOMETER TRANSIENT VELOCITY-MEASURING CIRCUIT

This circuit was used to sense the unbalance of the hot-wire bridge circuit. The output signal was a measure of the transient character of the mixture-jet when it was switched into the bomb.

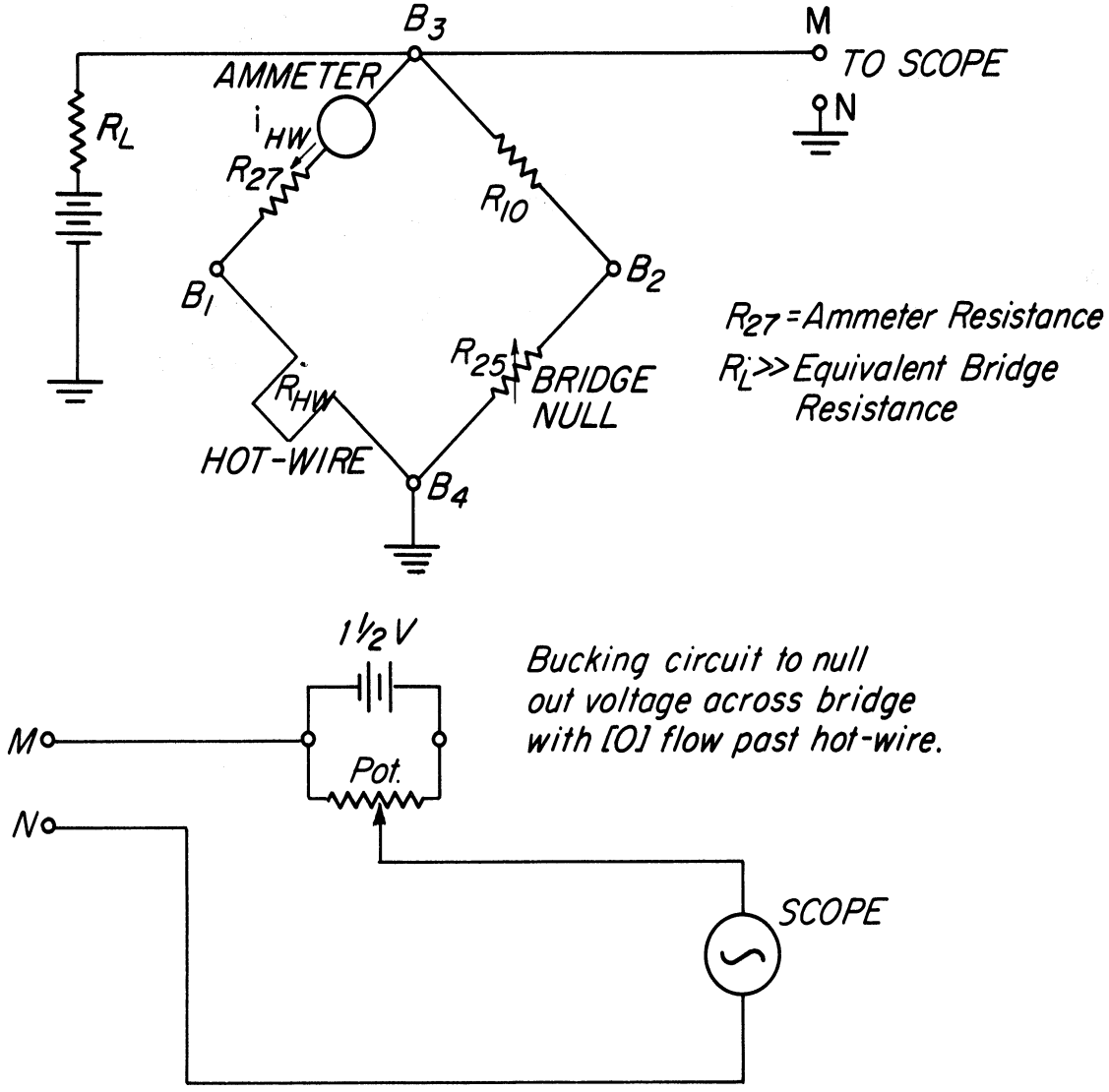

$V_{B_3B_4}$ is the voltage drop across the bridge circuit.

Figure 48. Schematic diagram—transient flow measurement circuit for the hot-wire anemometer.

APPENDIX E

COMPONENTS OF THE SCHLIEREN SYSTEM

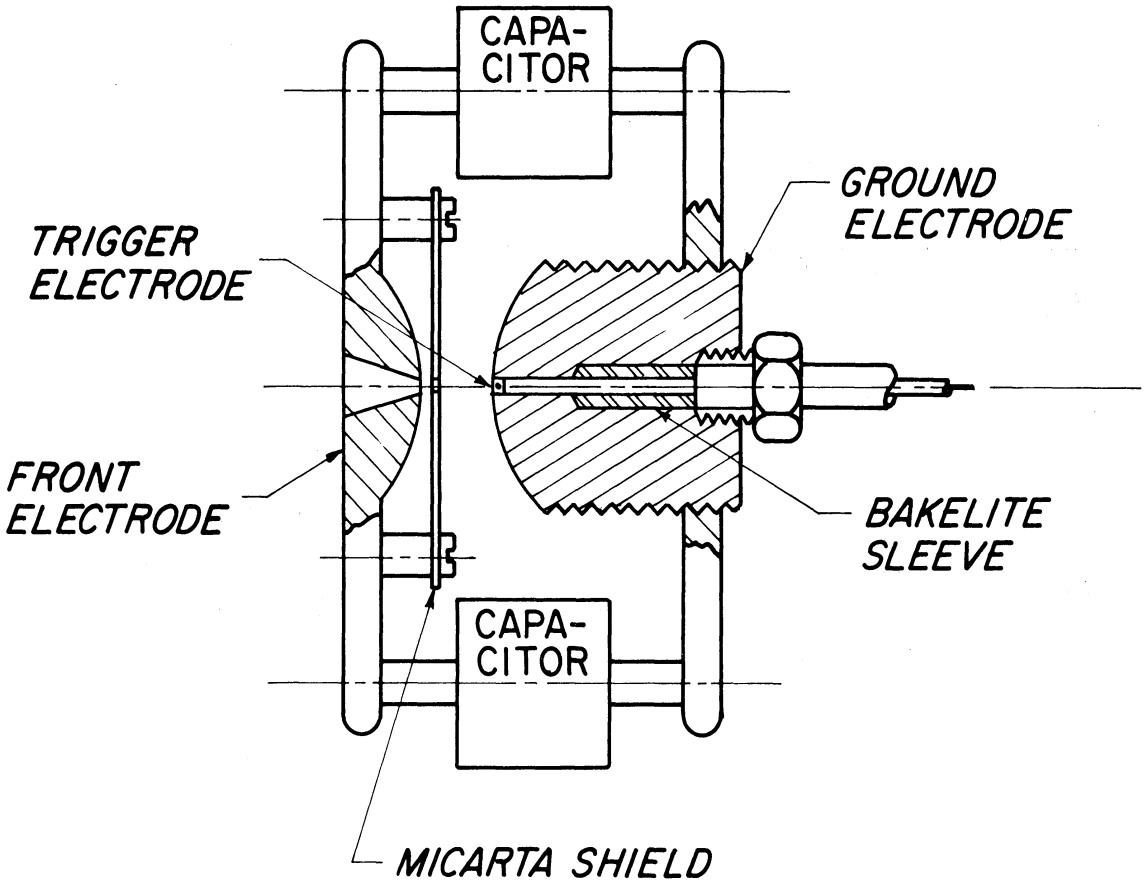

Figure 49. Section view—schlieren, spark light source.

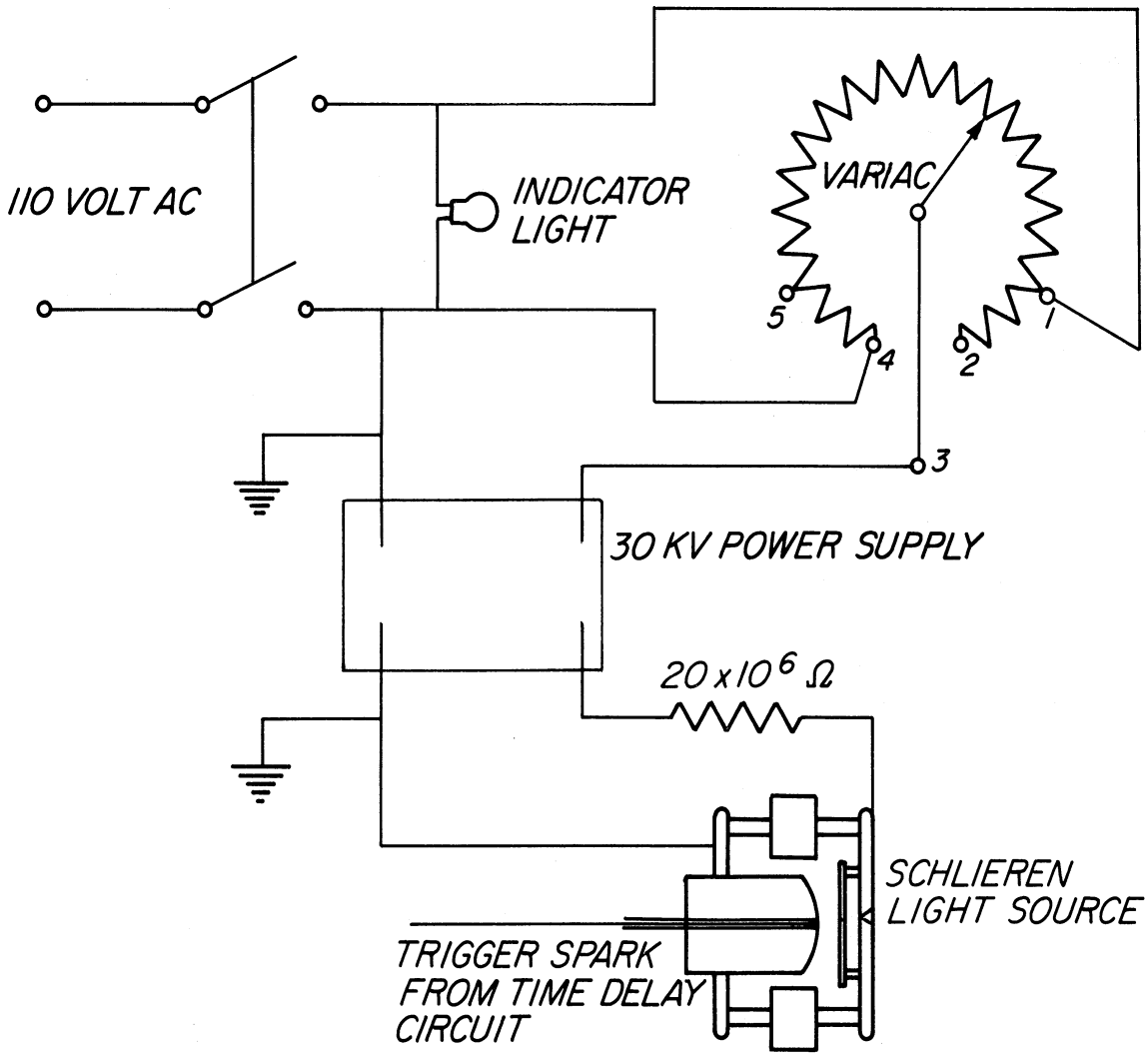

Figure 50. Circuit diagram—schlieren, spark light source.

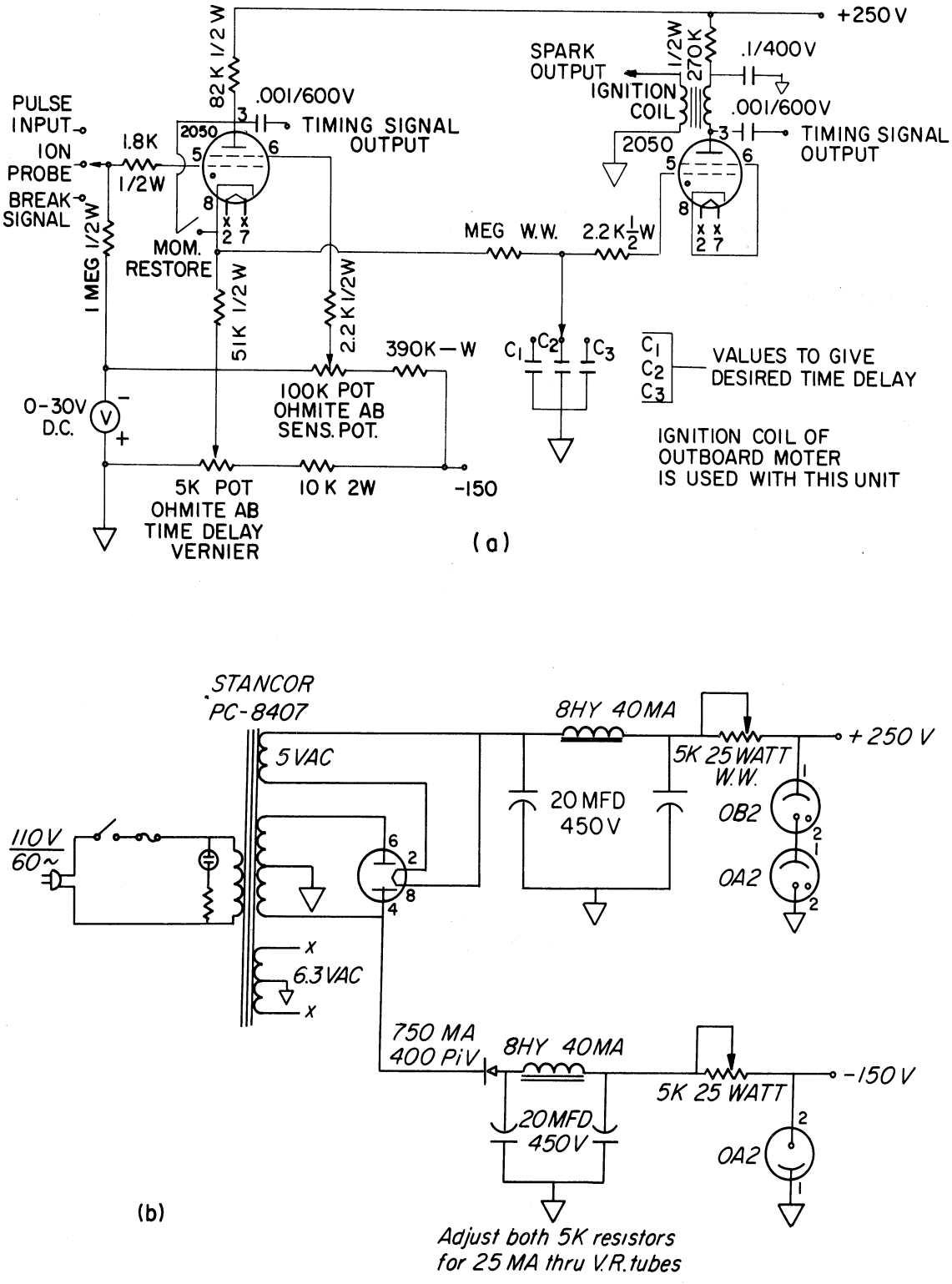

Figure 51. Schematic diagram of time delay circuit, (a) time delay section, and (b) power supply section.

APPENDIX F

CALIBRATION DATA

TABLE V

PRESSURE GAGE CALIBRATION DATA

Correct psi	Gage Reading - psi Pressure Increasing	Average Deviation psi (ΔP)
(a) C.L. 02, Lonergan Maximum Gauge, 0-300 psi		
15.0	16.0	+ 1.0
20.0	21.0	+ 1.0
30.0	30.0	0
40.0	39.0	- 1.0
50.0	49.0	- 1.0
60.0	58.5	- 1.5
70.0	68.0	- 2.0
80.0	78.5	- 1.5
90.0	88.5	- 1.5
100.0	98.0	- 2.0
110.0	107.5	- 2.5
120.0	117.5	- 2.5
130.0	127.5	- 2.5
140.0	137.0	- 3.0
150.0	147.0	- 3.0
160.0	157.5	- 2.5
170.0	167.5	- 2.5
180.0	177.0	- 3.0
190.0	187.0	- 3.0
200.0	197.0	- 3.0
210.0	207.5	- 2.5
220.0	217.5	- 2.5
230.0	228.0	- 2.0
240.0	238.0	- 2.0
250.0	248.0	- 2.0

TABLE V (Concluded)

Correct psi	Gage Reading - psi Pressure Increasing	Average Deviation psi (ΔP)
(b) C.L. 01, U.S. Gauge Co., 10861, Supergauge 0-100 psi		
0	0	0
5.0	5.0	0
10.0	9.7	- .3
15.0	14.6	- .4
20.0	19.7	- .3
25.0	24.5	- .5
30.0	29.7	- .3
35.0	34.7	- .3
40.0	39.7	- .3
45.0	44.8	- .2
50.0	49.8	- .2
55.0	54.8	- .2
60.0	59.8	- .2
65.0	64.8	- .2
70.0	69.8	- .2
75.0	74.8	- .2
80.0	79.8	- .2
85.0	84.7	- .3
90.0	89.7	- .3
95.0	94.7	- .3
100.0	99.7	- .3

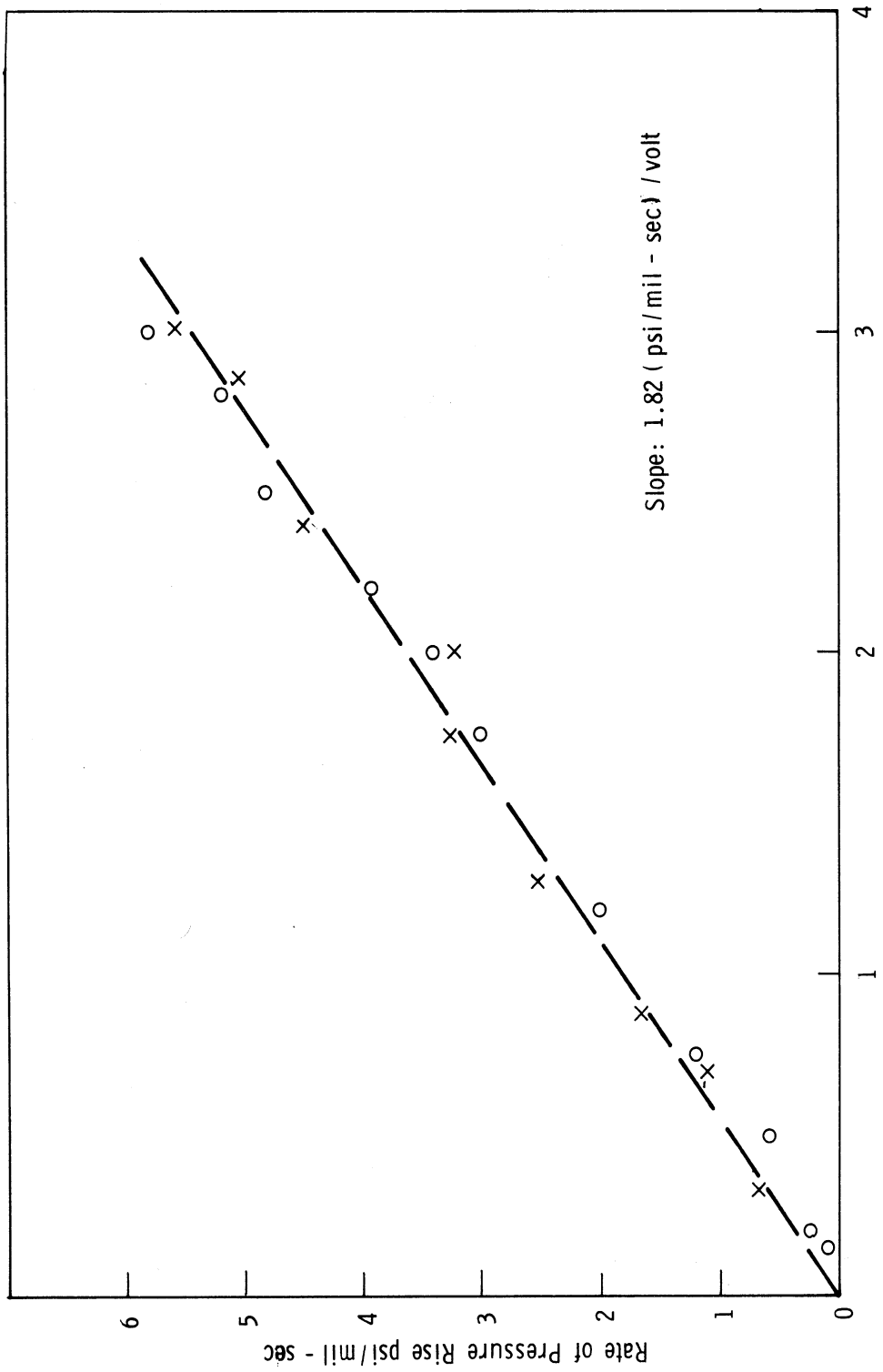

Figure 52. Calibration of pressure differentiating unit.

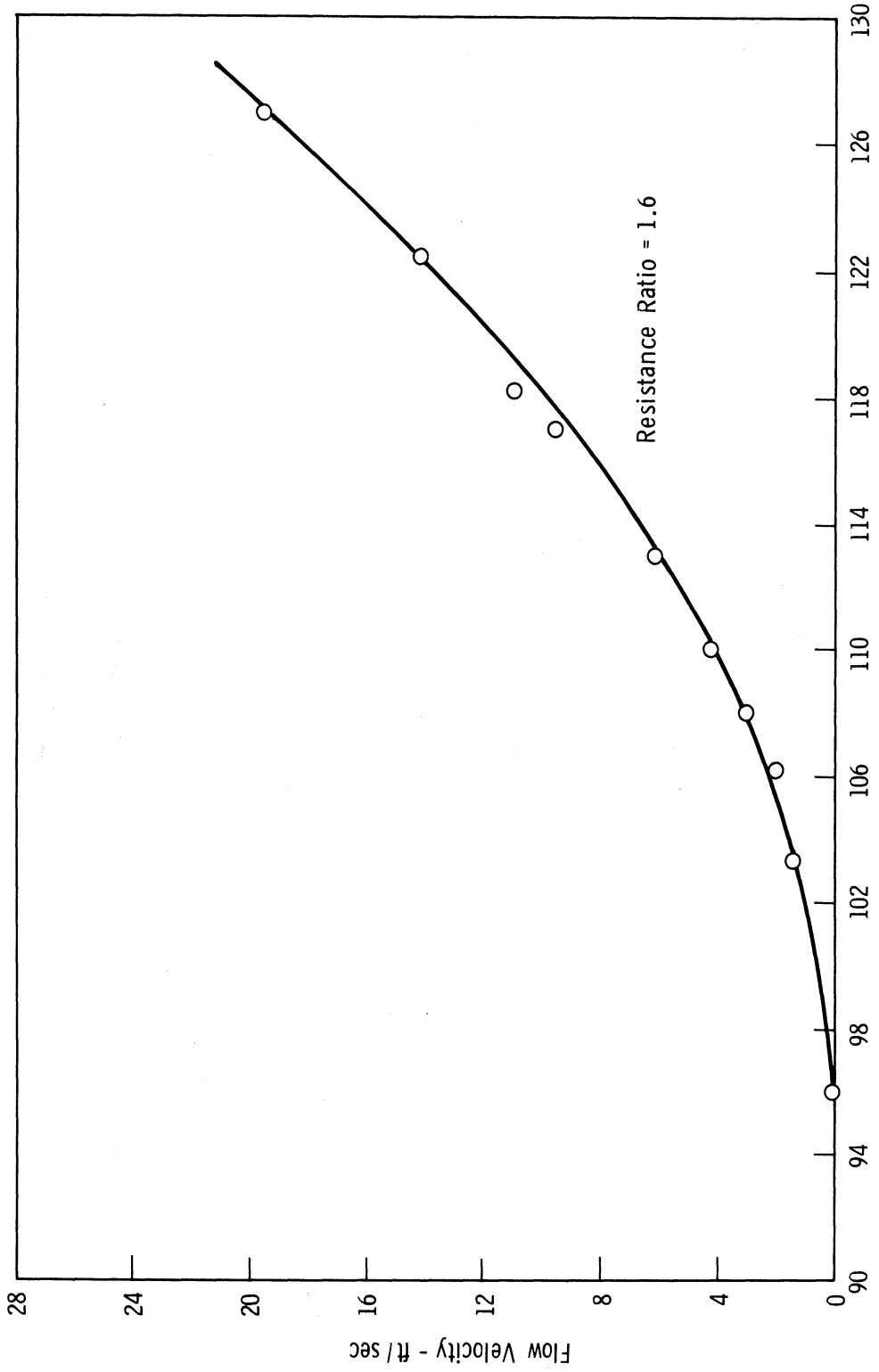

Figure 53. Calibration of hot-wire anemometer.

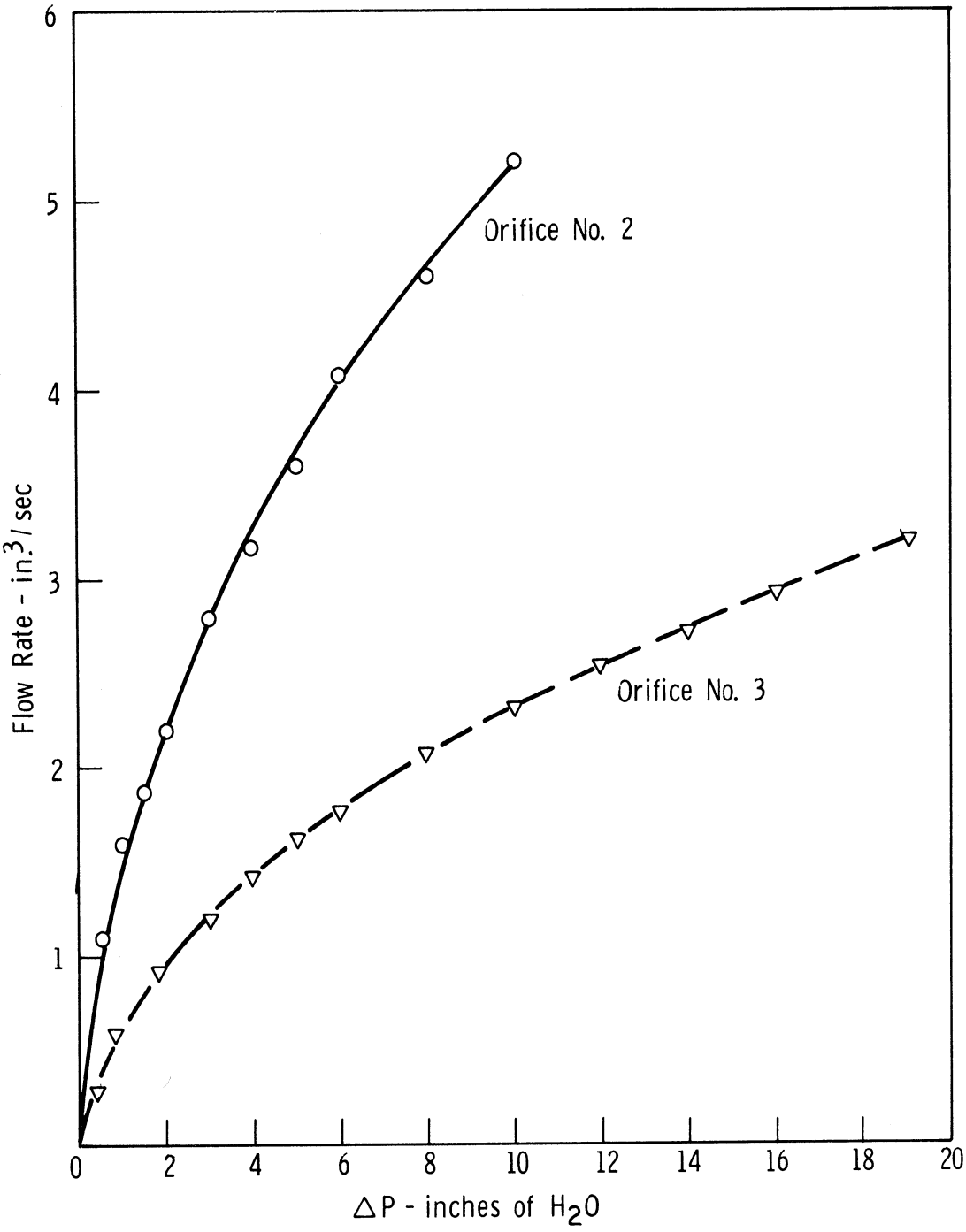

Figure 54. Calibration of mixture-jet metering orifices.

APPENDIX G

SAMPLE MIXTURE DATA

TABLE VI

SAMPLE MIXTURE DATA

Tank No.	ø	Barom. in. Hg.	Atmos. °F	Corr. Barom.	P_f in. Hg.	P_t psig	Tank Press. μ	Fuel °F	Mixture °F	P_t (corr.)	P_t (corr.) psia	ø Actual
C	1.0	29.95	80	29.11	18.3	208.5	120	79	80	210.5	224.8	.992
A	1.0	29.65	74	29.53	18.3	208.5	60	71	74	210.5	225.0	.991
C	1.0	29.40	71	29.29	18.3	208.5	50	68	72	210.5	224.9	.992
B	1.0	29.48	72	29.37	18.3	208.5	80	72	72	210.5	224.9	.992

APPENDIX H

REPRODUCIBILITY OF COMBUSTION IN A QUIESCENT MIXTURE—STATISTICAL ANALYSIS

Combustion in a quiescent mixture was studied 9.5 msec after ignition—ΣN = number of runs = 51.

Statistical Analysis

$X = \frac{dp}{dt}$ (cm)	N Occurrences	XN	X-M	$(X-M)^2$
4.2	1	4.2	.85	.7225
4.3	2	8.6	.75	.5625
4.6	1	4.6	.45	.2025
4.7	3	14.1	.35	.1225
4.8	3	14.4	.25	.0625
5.0	8	40.0	.05	.0025
5.1	16	81.6	.05	.0025
5.2	9	46.8	.15	.0225
5.3	4	21.2	.25	.0625
5.4	3	16.2	.35	.1225
5.7	1	5.7	.65	.4225
Totals	51	257.4		2.3075

$$\text{Mean (M)} = \frac{\Sigma XN}{\Sigma N} = \frac{257.4}{51} = \underline{\underline{5.05 \text{ cm}}}$$

$$\text{Standard Deviation } (\sigma) = \sqrt{\frac{\Sigma(X-M)^2}{\Sigma N}} = \sqrt{\frac{2.3075}{51}} = \underline{\underline{.213 \text{ cm}}}$$

In terms of psi/msec: M = .89 psi/msec

σ = .037 psi/msec

APPENDIX I

ORIGINAL DATA

TABLE VII

SAMPLE DATA SHEET

(Rate of Pressure Rise Data)

Jet Width: Medium d = .066
Jet Calibrated Flow Orifice: No. 3
Bomb Triggering Pressure: 29.5 in. Hg.
Bomb Initial Pressure before Jet Flow: 29.1 in. Hg.
Propane Relative Mixture Ratio: 1.0

Primary Spark Current: 5.0 amperes
Spark Gap: .050 in.
Scope Settings: (1) sensitivity volts/cm: .10
(2) sweep rate msec/cm: 1.0
Jet Nozzle Exit to Spark Gap: 3/16 in.

Run No.	Bomb Evacuation Pressure μ	Scope Deflection at 9.5 msec from Spark		Bomb Initial Temperature °F	Jet Flow ΔP in. H_2O Flow Orifice	Combustion Picture Schlieren System Time Delay From Ignition		
		cm	volts			μ_f (cap.)	Voltage	msec
1201	100	4.6	.46	80	0	.06	15.5	9.5
1202	120	5.2	.52	79	0	.06	15.5	9.5
1203	160	5.1	.51	80	0	.06	15.5	9.5
1204	120	5.2	.52	80	0	.06	15.5	9.5
1205	150	4.3	.43	81	0	.06	15.5	9.5
1206	100	5.1	.51	81	0	.06	15.5	9.5
1207	100	5.0	.50	80	0	.06	15.5	9.5
1208	120	5.1	.51	80	0	.06	15.5	9.5
1209	150	5.0	.50	80	0	.06	15.5	9.5
1210	150	5.2	.52	81	0	.06	15.5	9.5
1211	100	4.2	.42	81	0	.06	15.5	9.5
1212	120	5.4	.54	82	0	.06	15.5	9.5
1213	100	5.0	.50	81	0	.06	15.5	9.5
1214	60	5.3	.53	80	0	.06	15.5	9.5
1215	100	5.1	.51	79	0	.06	15.5	9.5
1216	150	5.1	.51	80	0	.06	15.5	9.5
1308	100	5.2	.52	78	0	.06	15.5	9.5
1401	150	5.2	.52	80	0	.06	15.5	9.5
1404	100	5.2	.52	80	0	.06	15.5	9.5
1405	120	5.1	.51	80	0	.06	15.5	9.5
1406	100	5.4	.54	81	0	.06	15.5	9.5

TABLE VIII

SUMMARY OF PRESSURE RATE DATA 9.5 MILLISECONDS AFTER IGNITION

V_J ft/sec	Nozzle Size					
	Small		Medium		Large	
	$\frac{dp}{dt}$ - "cm"	π_p-%	$\frac{dp}{dt}$ - "cm"	π_p-%	$\frac{dp}{dt}$ - "cm"	π_p-%
0	4.8	0	5.1	0	5.1	0
1	-	-	-	-	-	-
3	5.35	11.4	5.9	15.6	5.5	7.9
5	5.9	23.0	6.7	25.8	5.8	13.7
7	6.7	39.6	7.2	41.1	6.2	21.6

APPENDIX J

PROCEDURE, SAMPLE CALCULATIONS, AND DATA

1. CALCULATION OF FLAME FRONT AREAS

Procedure and Sample Calculation

The particular schlieren photograph measured in the sample calculations is shown in Figure 28 with V_J = 5 ft/sec. A line sketch of the flame front is shown below.

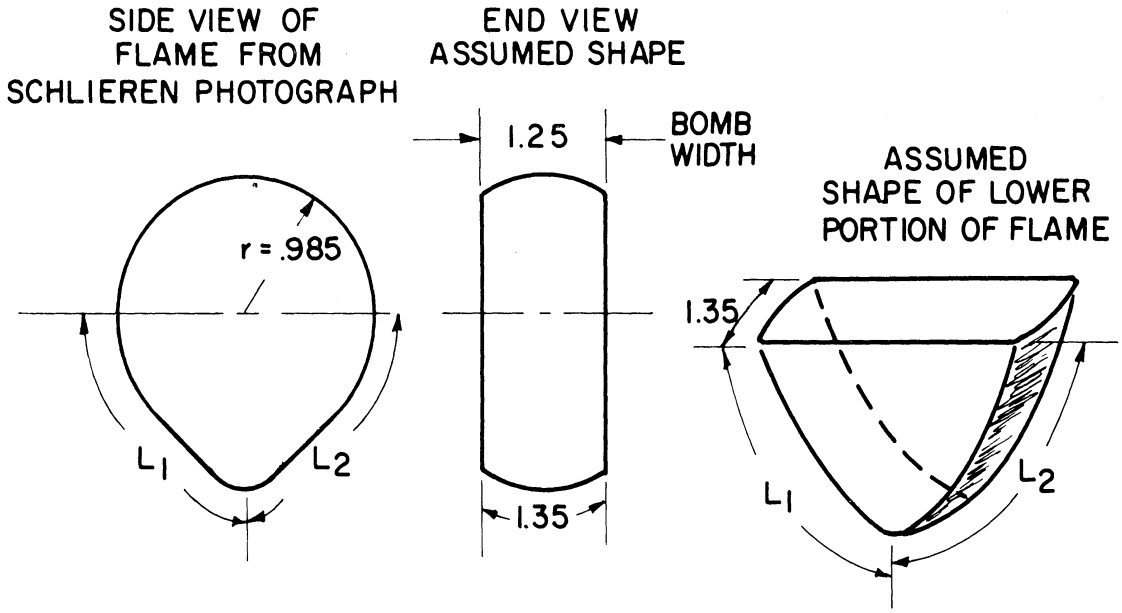

The area of the upper half of the flame kernel was determined by measuring its radius - r. The area is considered as a partial segment of a sphere. Its area is given by:

$$A_{f(upper)} = \pi \times r \times 1.25$$

for the sample, r = .985

$$\therefore A_{f(upper)} = \pi \times 1.25 \times .985 = 3.88 \text{ sq. in.}$$

The area of the lower portion of the flame kernel was determined by

assuming that it can be represented by a form of triangular prism shown at the right above. The width of the area, 1.35 in., was scaled from the end view of the assumed shape of the lower portion of the flame. This is slightly greater than the bomb width of 1.25 in. because the flame is assumed to be curved. The length of the sides of the prism, L_1 and L_2 was measured with a fine, soft wire fitted to the actual periphery of the flame. This was then scaled. The area is given by:

$$A_{f(lower)} = L_1 \times 1.35 + L_2 \times 1.35$$

for the sample $L_1 = 1.75$, $L_2 = 1.79$

$$A_{f(lower)} = 1.75 \times 1.35 + 1.79 \times 1.35 = \underline{\underline{4.77 \text{ sq. in.}}}$$

The total area was slightly less than the sum of $A_{f(upper)}$ and $A_{f(lower)}$ because the cross sectional area of the electrodes and the jet nozzle intersected the flame kernel. This cross-sectional area was .36 sq. in. The true flame area is given by:

$$A_{f(upper)} + A_{f(lower)} - .36$$

for the sample shown

$$A_f = 3.88 + 4.77 - .36 = \underline{\underline{8.29}} \text{ sq. in.}$$

The flame areas measured at each test condition were averaged and are presented in Table IX. At least four flame front photographs were studied at each condition.

The percent increase in the flame front area relative to the flame area measured in quiescent combustion is also indicated in Table IX.

TABLE IX

SUMMARY OF FLAME FRONT AREA CALCULATIONS

V_J-ft/sec.	Nozzle Size					
	Small		Medium		Large	
	Area	π_A%	Area	π_A%	Area	π_A%
0	6.19	0	7.17	0	7.09	0
1	--	--	--	--	--	--
3	6.58	6.3	7.73	8.0	7.52	6.1
5	7.22	16.2	8.29	16.5	7.68	8.3
7	7.63	23.4	8.54	21.1	7.89	11.5

2. CALCULATION OF MASS RATE OF COMBUSTION

Procedure and Sample Calculation

The mass rate of combustion, $\dot{m} = \rho_m A_f V_f$, was calculated by using the measured flame areas indicated in the preceding section and analytically determined mixture density and relative flame velocity. Sample calculations are based on combustion with the medium nozzle with V_J = 5 ft/sec.

a. The density, ρ_m, was calculated by assuming that the flame front compressed the unburned mixture in an isentropic manner and that there was no heat transfer from the burned to the unburned gas. The temperature of the unburned mixture, T_2, 9.5 msec. after ignition was then found by using the relation:

$$T_2 = T_1 \left(\frac{P_2}{P_1}\right)^{K_c - 1/K_c}$$

where

$T_1 = 540°R$ = mixture temperature before ignition

$P_1 = 29.5$ in. of Hg = 14.5 lb/in.^{2} = mixture pressure before ignition

P_2 = pressure 9.5 msec after ignition measured with the "Kistler" pickup

$K_c = C_P/C_V = 1.38$ for propane-air mixture

This equation reduces to:

$$T_2 = 540 \left(\frac{P_2}{14.5}\right)^{.275}$$

for the medium nozzle, $V_J = 5$ ft/sec

$$P_2 = 20 \text{ psia}$$

therefore $T_2 = 540(20/14.5)^{.275} = \underline{\underline{591°R}}$

By using the perfect gas relationship

$$\rho_m = \frac{P_2}{RT_2} ,$$

it was possible to determine the density of the mixture, ρ_m, just ahead of the flame.

$$R = 53.6 \frac{\text{ft lb.f.}}{\text{lb.m.}°R}$$

for the propane-air mixture, for the sample calculation—medium nozzle, $V_J = 5$ ft/sec

$$\rho_m = \frac{20.0 \times 144}{53.6 \times 591} = .0909 \text{ lb/ft}^3$$

The results of density calculations at all test points are shown in Table X.

b. The flame velocity relative to the unburned mixture, V_f was determined by using an equation for stoichiometric propane-air mixture taken from Reference (5). This equation, shown below, indicated V_f was a function of temperature, only.

$$V_f = 16.5 \frac{[25 + .00085\ T_2^2(°K)]}{100} \text{ in/sec.}$$

In terms of temperature in °R this equation takes the form:

$$V_f = 16.5 \frac{\left\{25 + .00085\left[273 + \frac{5}{9}(T_{2°F} - 32)\right]^2\right\}}{100} .$$

For the sample calculation

$$T_2 = 591°R = 131°F$$

and

$$V_f = \frac{16.5}{100}(25 + .00085 \times 330.1^2) = \underline{\underline{19.2}} \text{ in/sec}$$

c. The mass rate of combustion was then found by using the flame front area (A_f) from Section 1 of Appendix I.

$$\dot{m} = \rho_f A_f V_f$$

for the sample A_f = 8.29 sq. in. Thus

$$\dot{m} = \frac{.0909 \times 8.29 \times 19.2}{1728} = \underline{\underline{8.36}} \text{ lbm/sec.}$$

The results of the calculations are indicated in Table X for each test conditions.

The percent increase in mass rate of combustion, π_m, relative to combustion in a quiescent mixture is also tabulated in Table X.

TABLE X

SUMMARY OF MASS RATE OF COMBUSTION CALCULATIONS

V_J ft/sec	P_2 psia	T_2 °R	ρ_m lb/ft^3	V_f in/sec	A_f in^2	$\dot{m}$ lb/msec	π_m %
			A. Small Nozzle				
0	18.5	577	.086	18.6	6.19	5.82	0
3	19.5	586	.0893	19.0	6.58	6.40	10.0
5	20.0	591	.0909	19.2	7.22	7.28	24.6
7	20.5	595	.0926	19.4	7.63	7.92	36.8
			B. Medium Nozzle				
0	18.5	577	.086	18.6	7.17	6.65	0
3	19.5	586	.0895	19.0	7.73	7.58	14.1
5	20.0	591	.0909	19.2	8.29	8.36	25.8
7	20.5	595	.0926	19.4	8.54	8.89	34.0
			C. Large Nozzle				
0	18.2	575	.085	18.4	7.09	6.47	0
3	18.5	578	.086	18.5	7.52	6.94	7.9
5	19.0	582	.0878	18.8	7.68	7.30	13.7
7	19.5	586	.0893	19.1	7.89	7.73	21.6

3. CALCULATION OF THE FLAME SPATIAL VELOCITY (V_s) AND RELATIVE FLAME VELOCITY (V_f) THROUGH THE TOTAL COMBUSTION PROCESS IN A QUIESCENT MIXTURE

Procedure and Sample Calculations.

a. The spatial velocity (V_s) was measured from the sequential study shown in Figure 34 in Chapter V.

The lowest point on the flame kernel was used as a reference. The distance between consecutive positions of this point on the front was measured. The time between consecutive photographs was noted. The average velocity between the flame front positions was found by dividing the travel distance by the time interval, $\Delta L/\Delta t$. This average velocity is indicated at a point midway between the positions of the flame.

Considering photographs number 7 and 8 in Figure 34 the following was observed.

Distance between lower positions of the flame

$$\Delta L_{7-8} = 1.182 - .985 = \underline{\underline{.197}} \text{ in.}$$

Time interval between photographs

$$\Delta t_{7-8} = 11.2 - 9.6 = \underline{\underline{1.6}} \text{ msec.}$$

$$V_{s_{7-8}} = \frac{\Delta L_{7-8}}{\Delta t_{7-8}} = \frac{.197}{1.6} = \underline{\underline{123 \text{ in/sec.}}}$$

This velocity is assumed to occur at a distance from the spark gap of:

$$.985 + \frac{1.182-.985}{2} = \underline{\underline{1.085 \text{ in.}}}$$

and a time after ignition of:

$$9.6 + \frac{11.2-9.6}{2} = \underline{\underline{10.4 \text{ msec.}}}$$

The calculations are summarized in Table XI.

TABLE XI

SUMMARY OF FLAME SPATIAL VELOCITY AND APPARENT FLAME VELOCITY CALCULATIONS FROM THE SEQUENTIAL STUDY OF COMBUSTION IN A QUIESCENT MIXTURE

Distance From Spark Gap—in.	Time After Ignition—msec.	V_s in./sec.	V_f in./sec.
.240	2.4	85.0	16.6
.382	4.0	92.6	16.9
.524	5.6	85.5	17.1
.653	7.1	88.0	17.3
.725	7.9	125.0	17.3
.860	8.8	153.0	18.0
1.08	10.4	123.0	19.1
1.27	12.0	108.0	20.5
1.42	13.6	78.0	22.5
1.51	15.2	37.5	24.5
1.58	16.8	47.5	26.4
1.65	18.4	43.5	28.7
1.72	20.1	31.7	31.4
1.78	22.0	33.8	33.0
1.85	23.8	29.5	34.5
1.87	25.6	5.5	35.5

b. The relative flame velocity (V_f) is calculated by the technique indicated in part 2 of this appendix. The results of these calculations are also summarized in Table XI.

BIBLIOGRAPHY

1. Agnew, W. G., "The Effect of End Zone Fuel Injection on Combustion in a Spark-Ignition Engine," Ph.D. Thesis, Purdue University, 1952.

2. Bolz, R. E., Burlage, H., "Propagation of Free Flames in Laminar- and Turbulent-Flow Fields," NASA Technical Note D-551, 1960.

3. Curry, S., "A Three-Dimensional Study of Flame Propagation in a Spark-Ignition Engine," SAE paper No. 452P, 1962.

4. Dugger, G. L., Gerstein, M., "Turbulent Flames" NACA Report 1300, 1957, pp. 163-184.

5. Dugger, G. L., Simon, D. M., Gerstein, M., "Laminar Flame Propagation," NACA Report 1300, 1957, pp. 127-163.

6. Kumagai, S., Sakai, T., Kumura, I., "Effect of Ultrasonic Waves on Flame Propagation and Spark-Ignition," 4th Intl Symposium on Combustion, Williams and Wilkins, 1953, p. 148.

7. Marvin, C. F., Wharton, A., Roeder, C. H., "Further Studies of Flame Movements and Pressure Development in an Engine Cylinder," NACA TR 556, 1936.

8. Patterson, D. J., "Cylinder Pressure Variations, a Fundamental Combustion Problem," SAE paper No. 660129, 1966.

9. Rothrock, A. M., Spencer, R. C., "The Influence of Directed Air Flow on Combustion in a Spark-Ignition Engine," NACA Report No. 657.

10. Semenov, E. S., "Device for Measuring Turbulence in Piston Engines, "Inst. and Exp. Tech., Vol. 1, 1958.

11. Soltau, J. P., "Cylinder Pressure Variation in Petrol Engines," Inst. of Mech. Engr., Proceedings of Automotive Division, 1960-61.

12. Steiner, J. C., "The Effect of the Rate of Energy Input Upon the Minimum Spark-Ignition Energy of Lean Propane-Air Mixtures," Ph.D. Thesis, University of Michigan, 1963.

13. Swett, C. C., "Spark-Ignition of Flowing Gases IV Theory of Ignition in Nonturbulent and Turbulent Flow Using Long-Duration Discharges," NACA Research Memo RME 54F29a, 1954.

14. Taylor, C. F., Taylor, E. S., "The Internal Combustion Engine," Int'l Textbook Co., 1962, 2nd Edition, pp. 88-89.

15. Vichnievsky, R., "Combustion in Petrol Engines" Proceedings of the Joint Institute of Mech. Engineers and ASME Conference on Combustion, June and Oct. 1955, p. 288.